The Pennsylvania State University
The Graduate School
College of Engineering

LEVEL TRACKING IN THERMAL-HYDRAULIC SIMULATIONS OF NUCLEAR REACTORS

A Thesis in
Nuclear Engineering
by
Birol Aktas

Submitted in Partial Fulfillment
of the Requirements
for the Degree of

Doctor of Philosophy

May 2003

We approve the thesis of Birol Aktas

Date of Signature

John H. Mahaffy
Associate Professor of Nuclear Engineering
Thesis Advisor
Chair of Committee

Kostadin N. Ivanov
Associate Professor of Nuclear Engineering

Gordon Robinson
Professor Emeritus of Nuclear Engineering

Christopher J. Duffy
Professor of Civil Engineering

Jack Brenizer
Professor-in-Charge of Planning and
Administration/Program
Chair of Nuclear Engineering

ABSTRACT

The presence of stratified liquid-gas interfaces in vertical flows poses difficulties to most classes of solution methods for two-phase flows of practical interest in the field of reactor safety and thermal-hydraulics. These difficulties can plague the reactor simulations unless handled with proper care. To illustrate these difficulties, the US NRC Consolidated Thermal-hydraulics Code (TRAC-M) was exercised with selected numerical benchmark problems. These numerical benchmarks demonstrate that the use of an average void fraction for computational volumes simulating vertical flows is inadequate when these volumes consist of stratified liquid-gas interfaces. An accurate description of these computational volumes, which are divided into two regions with distinct flow topology, requires that separate void fractions be assigned to each region. This strategy requires that the liquid-gas interfaces be tracked in order to determine their location, the volumes of regions separated by the interface, and the void fractions in these regions.

Although the idea of tracking stratified liquid-gas interfaces is not new, its applications in the reactor safety codes in the past showed only limited success. Improper modifications to the field equations were mostly responsible for their failures. This thesis proposes a systematic approach to implement a method for tracking interfaces in the one- and three-dimensional field equations of TRAC-M. This approach is applicable to the solution methods of known thermal-hydraulic codes of the same class. The success of this approach was demonstrated by exercising TRAC-M with the same benchmark problems that were previously used to expose the difficulties of handling the liquid-gas interfaces.

TABLE OF CONTENTS

LIST OF FIGURES

LIST OF FIGURES (cont'd)

LIST OF FIGURES (cont'd)

LIST OF FIGURES (cont'd)

NOMENCLATURE

Acronyms

BWR : Boiling Water Reactor

CTFD : Computational Two-phase Fluid Dynamics

LOCA : Loss Of Coolant Accident

LWR : Light Water Reactor

RPV: Reactor Pressure Vessel

SETS: Stability Enhancing Two-Step

TH: Thermal-Hydraulic

Symbols

A : Flow area

α : Void fraction

β : Momentum flux time weighting factor

C_i : Interfacial drag coefficient

C_{wl} : Liquid wall drag coefficient

C_{wg} : Gas wall drag coefficient

γ : Mass, energy, and volume flux time weighting factor

Γ : Interfacial mass exchange term

Δh : Elevation change

Δt : Time step size

$\Delta\tau$: Critical time step size for boundary crossing

Δx : Cell height

Δz : Cell height in the Z-direction

e : Internal energy

ζ : Internal energy flux

f_i : Interfacial drag

f_{wl} : Liquid wall drag

f_{wg} : Gas wall drag

ϕ : Mass flux

Φ : Potential energy

g : Gravity vector

h_{fg} : Boiling enthalpy

K : Kinetic energy

L : Water level height

P : Pressure

q_{dl} : Flux of direct sensible heat to the liquid field

q_{il} : Heat flux from the saturation interface to the liquid field

q_{wl} : Wall heat flux to the liquid field

q_{dg} : Flux of direct sensible heat to the gas field

q_{ig} : Heat flux from the saturation interface to the gas field

q_{wg} : Wall heat flux to the gas field

ρ : Density

T : Temperature

t : Transient calculation time

V : Velocity

Vol : Volume

ω : Volume flux

Subscripts

a : Air

E : Edge variables

i, j, k : Discrete location indices

l : Liquid

g : Gas

R, Θ, Z : Spatial directions in cylindrical coordinates

Superscripts

- : Below the water level

+ : Above the water level

n : Time level n

n+1 : Time level n+1, i.e. unknowns

ACKNOWLEDGMENTS

Very few people have inspired and guided me throughout my education in the way my thesis advisor, Professor John Mahaffy, did. This dissertation was not completed by the time I took off from Penn State to join the work force. Professor Mahaffy's dedication, perseverance, and rigorous approach to solving problems have been shining examples which guided me during the years after I had left Penn State. I must also confess that I took advantage of his remarkable patience with me that far exceeded any reasonable standards. I consider myself fortunate to have the opportunity to collaborate with him.

I would like to thank to the members of my doctoral committee for their time, all of whom reviewed this thesis and made very useful suggestions. I also thank Dr. Glen Mortensen of Information Systems Laboratories, Inc. for his careful review and corrections to the three chapters of this thesis.

This work was made possible thanks to the generous support, directly at Penn State and indirectly afterwards, of the U.S. Nuclear Regulatory Commission. In particular, I thank Drs. Jennifer Uhle and Farouk Eltawila of the US Nuclear Regulatory Commission for their constant encouragement and support. I would also like to thank Dr. James Meyer for creating an environment in which I was able to finish this work while working at Information Systems Laboratories, Inc.

Special thanks go to my friends, Ada Kroll and Dr. Rex Shumway who never stopped reminding me the importance of finishing this thesis.

My parents Emen and Nuri Aktas had done all the things that parents do, and more. It was they who made personal sacrifices to provide me the freedom to think

freely and a good education that gave me the abilities necessary to complete this work. This work is dedicated to them.

And last but not least, I thank my wife, Feray, for her never ending understanding and patience as I struggled to finish this work. As for our daughter, Naz, who has endured her dad's preoccupation with *school work* as long as she can remember, I am sure she will still remember it when she grows up to have her own.

To my mother and the memory of my father
to whom I am forever indebted for their sacrifices.

CHAPTER 1

Thermal-Hydraulic Simulations of Nuclear Reactors

The purpose of this study is to develop a remedy for a deficiency known to exist in the state-of-the-art computational methods for simulating two-phase flows, and demonstrate that the computer simulations, a.k.a. "thermal-hydraulic" simulations, of light water nuclear reactors (LWRs) can be improved significantly by implementing this remedy.

The background information, the ideas behind the thesis and their implementation are presented in four chapters. In the first chapter, an introduction is made to the field of nuclear reactor safety and the concerns driving this field of nuclear engineering. This introduction emphasizes the importance of thermal-hydraulic simulations and the research done to improve these simulations in dealing with the issues pertinent to the safety of LWRs. This introduction will also help to understand my motivation behind pursuing this thesis that aims at improving these simulations. A limited review of the Computational Two-phase Fluid Dynamics (CTFD) will follow this introduction to prepare the reader for a detailed description of the core ideas and their implementation that form the basis of this thesis. In the second chapter, a set of benchmark tests are introduced. The purpose of these tests is to expose the known difficulties of handling water levels in thermal-hydraulic simulations. A method to overcome these diffi-

culties related to water levels or also known as "stratified liquid-gas interfaces" is described in the third chapter. While the method described in the third chapter is limited to the one-dimensional simulations of two-phase flows, the fourth chapter describes the extensions to this method in order to overcome the same difficulties related to water levels in three-dimensional simulations of two-phase flows.

Reactor Safety

LWRs are based on very simple concepts although today's power plants that generate electricity from nuclear energy are very advanced designs that incorporate complex and intricate systems. In LWRs, a reactor core generates the nuclear power, where the fission of heavy elements such as Uranium 235 is the source. Most reactor cores are formed by thousands of fuel rods. These rods are usually half an inch in diameter and twelve foot high, or maybe higher. While the numbers of these fuel rods can vary from one particular reactor type to another, the flow of water past these fuel rods is the common method among all LWR types used for extracting the heat generated within these fuel rods.

A steady generation of power and a steady cooling of the reactor core are the two essential elements for successful operation of an LWR. Large numbers of heavy elements like Uranium 235 simultaneously undergoing fission at a steady rate are the source of nuclear power. During each fission event, two or three high energy (fast) neutrons are released on the average following the split of heavy fissile nuclei. These high energy neutrons are eventually slowed down to lower energies in a series of collisions with the hydrogen atom of the water molecules. Eventually, these low energy (thermal) neutrons induce the next wave of fission events. For steady and self-sustained levels of reactor power, the neutron population must be controlled so that on the average only one neutron from each fission induces a new fission event. The neu-

tron population is controlled by neutron absorbing materials carefully placed around the fuel rods. These neutron absorbers can be solubles dissolved in the coolant water (e.g. boron) or pellets of absorbers stacked in rods (i.e. control rods). Here, it should be noted that the water inside the reactor core of most LWRs has multiple roles: 1) as coolant it extracts the heat generated within the fuel rods, 2) as moderator it slows down the fast neutrons to lower energy levels for self-sustained levels of fission, and 3) as host to soluble materials with high affinity to absorb neutrons, it helps to regulate the reactor power. These multiple roles of water inside LWRs and the strong interaction among these roles require that the flow of water inside the LWR cores be understood well in order to maintain a steady operation of these nuclear reactors and to maneuver them to desired flow rates and power levels. This requirement underscores the importance of computational tools for simulating coolant flow inside nuclear reactors.

The current generation of LWRs generates typically 3000MW, or more, of thermal power. Despite this tremendous power a typical reactor can generate, it occupies a very small space. For instance, the pressure vessel of a nuclear reactor usually fits onto a large trailer truck and it is generally towed to the construction site. Extracting the heat released inside this relatively small space therefore requires large quantities of water pumped through the reactor core at very high flow rates and very high pressures. There are two common types of LWRs based on their flow rates and operating pressures: 1) Pressurized Water Reactors (PWRs), and 2) Boiling Water Reactors (BWRs). In PWRs, the coolant flows inside two separate loops isolated from each other. The primary loop extracts the heat from the reactor core and transfers it to the secondary loop across a steam generator. Inside the secondary loop, the steam from the steam generators then drives the turbines powering the generators. To preclude the boiling of water inside the reactor core of PWRs, the primary loop is pressurized to about 2200 psia (i.e. 150 times the atmospheric pressure). To withstand this high

internal pressure, the reactor pressure vessel (RPV) of a PWR is manufactured from a 10 inch carbon-steel. On the other hand, BWRs operate at lower pressures at about 1000 psia (i.e. 70 times the atmospheric pressure) and allow the boiling of its coolant water inside the reactor core. The mixture of liquid and vapor water that exit the reactor core is forced into swirl-vane separators installed above the core. The water vapor separated from the liquid inside separators are then directed into the steam dryers high above the separator drums, where the remaining moisture is removed before the steam is delivered to the turbines. In BWRs, the coolant water flows inside a single loop which connects the RPV directly to the turbines eliminating the need for steam generators.

The above description of LWRs is sufficient to illustrate the complex interaction among different engineering disciplines involved in designing nuclear reactors capable of generating controlled-fission power, e.g. the theory of neutron kinetics and transport, coolant thermal-hydraulics, and material science. The interaction among these fields extends beyond simply meeting the goal of designing nuclear reactors. For instance, the flow rates inside BWRs and PWRs may exceed 150 million pounds per hour at pressures ranging from 1000 to 2200 psia. Any disruption in the flow of water through the reactor core or a breach in the boundaries of the coolant system can have undesired consequences. There is no doubt that the reactor fuel, highly radioactive due to fission products, inside a reactor core poses the greatest danger if released to the environment. Understanding the consequences of such hypothetical accident scenarios is the continuing goal of interaction among various engineering disciplines.

The better understanding of these postulated accidents, which a nuclear reactor may never experience in its lifetime, helps to design emergency systems that can mitigate their consequences, ensure public safety, and protect the environment if an accident ever happens. The single purpose of the emergency systems in nuclear reactors is

to prevent the release of highly radioactive fission products under any circumstance. Thus, gaining an in-depth understanding of accident scenarios at nuclear reactors is a paramount task. This difficult task has been a major thrust for advances made in the thermal-hydraulic research. Substantial resources are spent in two areas of the thermal-hydraulic research: 1) development and maintenance of thermal-hydraulic codes, 2) large- and small-scale experiments that support development of these codes.

The safety analysis of a postulated accident, in which the likelihood of radioactivity release to the environment is the greatest, identifies the events that may lead to the release so that strategies can be developed and implemented to prevent these events from occurring. In LWRs, there are four different barriers which must be breached before any radioactivity is released to the environment: 1) the ceramic fuel itself, 2) zircaloy fuel cladding, 3) the coolant system pressure envelope, and 4) the containment building. For most reactor designs, the worst case scenario is a Loss of Coolant Accident (LOCA). A LOCA is the discharge of coolant water into the containment atmosphere due to a breach in the coolant system such as a large pipe break followed by a sudden depressurization of the system. The entire system which includes the fuel rods, the RPV, and other components endures tremendous thermal and mechanical stresses induced by the violent depressurization as the water begins to turn into steam. To determine whether any fuel rod inside the reactor core will fail, the transient conditions that the fuel rods are exposed to must be determined by a safety analysis. If the analysis predicts any failure of fuel rods, the limiting conditions that the containment building can withstand must then be determined, and the potential pathways for the release of radioactivity to the environment must be identified. Otherwise, any fuel rod failure may lead to the release of the highly radioactive fission products to the coolant system, to the containment atmosphere, and thereafter to the environment. Predicting correctly the state of the coolant inside a nuclear reactor and its containment building is therefore very important to a safety analysis. Accurately

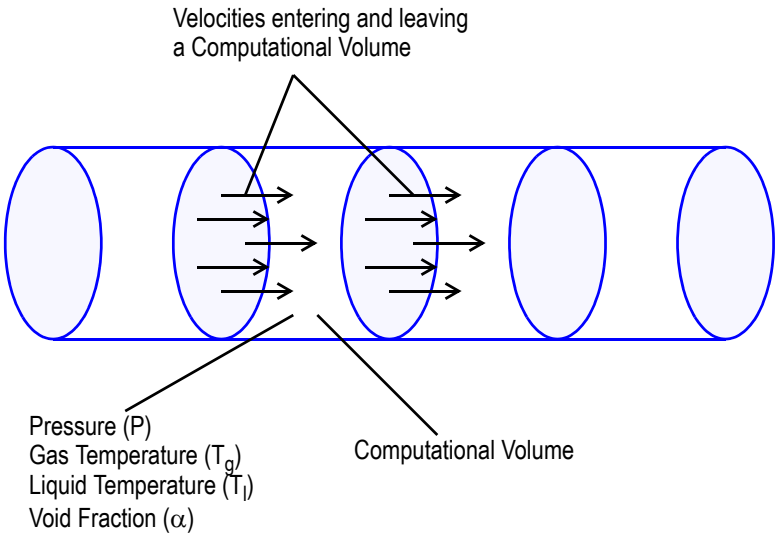

FIGURE 1-1. Section of a pipe broken down to computational volumes

predicting the transient conditions inside the reactor and the containment becomes especially important as the safety analysis is the only method used to demonstrate that the emergency systems implemented ensure the adequate cooling of the reactor core at all times during a LOCA.

A LOCA analysis requires that the coolant mass and energy flowing throughout the reactor system be simulated continuously and accurately, a task which demands the use of sophisticated computer programs. These computer programs are commonly known in the field of reactor safety as thermal-hydraulic (TH) codes. The TH codes break down the entire volume of a reactor system into smaller computational volumes. The TH codes then set up and solve the conservation equations that describe the balance of fluid mass, momentum and energy inside these computational volumes as the fluid is allowed to flow across their boundaries. Figure 1-1 shows the section of a pipe broken down into computational volumes. The velocities of fluid entering and leaving a computational volume are shown as vectors in this figure. In the example shown in Figure 1-1, the state of fluid inside computational volumes is

described as a function of fluid pressure and temperature. When separate conservation equations are set up for steam and water, the fraction of steam volume inside a computational volume is given by the void fraction. While most TH codes assume uniform pressure inside computational volumes, they use separate temperatures for steam and water to describe the state of a steam and water mixture. In most of the state-of-the-art TH codes, the conservation equations for each field, i.e. steam and water, also account for dynamic interactions at the interface between two phases of water such as drag and heat transfer.

A typical reactor safety analysis using TH codes begins with the system at an initial state precursor to the accident being simulated, usually a steady state. The transient is initiated by an event such as a pipe break, inadvertent opening of a relief valve, or pump trip, etc. The analysis then tracks the state of the fluid in all computational volumes which make up the entire system as the transient develops. The already non-trivial analysis due to the complex geometry of the reactor system becomes even more complicated due to the presence of complex interfaces between the liquid and vapor phases of water, and the transitions from one phase to another as the pressure in the system drops, e.g. bubbly flows, annular gas and liquid droplet flows, slug flows, etc. Predicting the thermal and mechanical conditions in and around the reactor therefore requires the use of (at least) two fluid models capable of simulating the flow of water in liquid and vapor phases. Therefore, not surprisingly, advances in computational modeling of multiphase flows have been driven mostly by the thermal-hydraulic research of nuclear reactors in its quest for more accurate and robust methods to simulate nuclear reactor accidents.

Computational Two-phase Fluid Dynamics

"Two-phase fluid dynamics has been described by several sets of equations ranging in complexity from a simple homogeneous equilibrium model to a very complicated two-fluid model involving a separate pressure for each phase" noted Liles and Reed[1-10] in reference to the works of Kojasoy[1-1] and Ishii.[1-2] Along with the publications of Kojasoy and Ishii, which have been cited for their pioneering work on formulating two-fluid flow equations, the publications by Stuhmiller,[1-3] Deemer and Slattery,[1-4] Drew and Lahey,[1-5] Addessio,[1-6] Stewart and Wendroff[1-7], Ransom and Hicks,[1-8] and numerous other articles in the literature not cited here present various formulations of two-fluid models and study their characteristics. While the intricacies of modeling two-phase flows will not be discussed here, a set of flow equations commonly known as the six-equation model, which is capable of describing two-phase flows of practical interest to the reactor safety, are presented here. Most of the state-of-the-art TH codes set up and solve the six-equation model to determine the state of fluid inside several hundreds of computational volumes combined together to simulate the fluid flow across complex networks of pipes in nuclear power plants. The TRAC† series (Transient Reactor Analysis Code) of thermal-hydraulic codes are well known in the industry for their state-of-the-art application of the six-equation model.[1-11] The remainder of discussions in this thesis will be presented in the context of this equation set and its implementation in TRAC.

†. The reactor safety code referred to as TRAC here is the US NRC Consolidated Thermal-hydraulics Code (a.k.a. TRAC-M).

The Six-Equation Model

The following equation set will form the basis for further discussion of two fluid models that will lead to the description of a deficiency in computational methods for two-phase flows and the remedy for it, which is the subject of this thesis.

Gas Momentum:

$$\alpha\rho_g\left(\frac{\partial \boldsymbol{V_g}}{\partial t} + \boldsymbol{V_g}\cdot\nabla\boldsymbol{V_g}\right) = -\alpha\nabla\boldsymbol{P} - \alpha\rho_g\boldsymbol{g} - \boldsymbol{f_i} + \boldsymbol{f_{wg}} \tag{1-1}$$

Liquid Momentum:

$$(1-\alpha)\rho_l\left(\frac{\partial \boldsymbol{V_l}}{\partial t} + \boldsymbol{V_l}\cdot\nabla\boldsymbol{V_l}\right) = -(1-\alpha)\nabla\boldsymbol{P} - (1-\alpha)\rho_l\boldsymbol{g} + \boldsymbol{f_i} + \boldsymbol{f_{wl}} \tag{1-2}$$

Gas Mass:

$$\frac{\partial}{\partial t}(\alpha\rho_g) + \nabla(\alpha\rho_g\boldsymbol{V_g}) = \Gamma_i \tag{1-3}$$

Liquid Mass:

$$\frac{\partial}{\partial t}[(1-\alpha)\rho_l] + \nabla[(1-\alpha)\rho_l\boldsymbol{V}_l] = -\Gamma_i \tag{1-4}$$

Gas Energy:

$$\frac{\partial}{\partial t}(\alpha\rho_g e_g) + \nabla(\alpha\rho_g e_g\boldsymbol{V_g}) = -P\left[\frac{\partial\alpha}{\partial t} + \nabla(\alpha\boldsymbol{V_g})\right] + \Gamma h_{fg} + q_{wg} + q_{ig} + q_{dg} \tag{1-5}$$

Mixture Energy:

$$\frac{\partial}{\partial t}[\alpha\rho_g e_g + (1-\alpha)\rho_l e_l] + \nabla[\alpha\rho_g e_g\boldsymbol{V_g} + (1-\alpha)\rho_l e_l\boldsymbol{V}_l] \tag{1-6}$$

$$= -P\nabla[\alpha\boldsymbol{V_g} + (1-\alpha)\boldsymbol{V}_l] + q_{wg} + q_{wl} + q_{dg} + q_{dl}$$

The above equation set is generally referred to as the six-equation model. It should be noted that while the appearance of these equations may vary from one implementation to another in the TH codes, the above equations are consistent with the equations solved by TRAC. Yet, some variations from the above set is expected even with TRAC. For example, Equation (1-4) may be replaced by (1-7), i.e. the mix-

ture mass equation, in order to avoid a singular solution as the flow becomes single phase.

$$\frac{\partial}{\partial t}[\alpha\rho_g + (1-\alpha)\rho_l] + \nabla[\alpha\rho_g \boldsymbol{V_g} + (1-\alpha)\rho_l \boldsymbol{V_l}] = 0 \qquad (1\text{-}7)$$

The solution to these equations requires additional information on the state of fluid, i.e. $\rho_g(P, T_g)$, $\rho_l(P, T_l)$, $e_g(P, T_g)$, and $e_l(P, T_l)$. Furthermore, the exchange of momentum and energy across the phase interface, and the exchange of momentum and energy with the surroundings (i.e. pipe walls or other enclosing structures) must be known as well for closure. The additional information which supplement the six-equation model are also known as the closure models.

The Semi-Implicit Method

The complex geometry of nuclear reactors and the degree of complexity due to the intricacies of two-phase flow make it impossible to obtain a closed form solution to any flow problem described by the six-equation model. Therefore, a practical computational approach had to be developed. In 1970s, Liles and Reed[1-10] presented "a technique for solving the equations of two-phase fluid dynamics." Named by these authors as the Semi-implicit Method, this technique had paved the way for today's TH codes that are applied in the field of reactor safety. In the field, these TH codes are also known widely as the "system codes."

A computational grid must be set up in order to develop an approximation to the system of Equations (1-1) thru (1-6). Figure 1-2 shows the so-called staggered grid which places the dynamic variables (i.e. fluid velocities) at the boundaries between computational volumes and the static variables (i.e. fluid temperatures, pressures, and void fractions) at the centers of computational volumes. The discrete equations of the

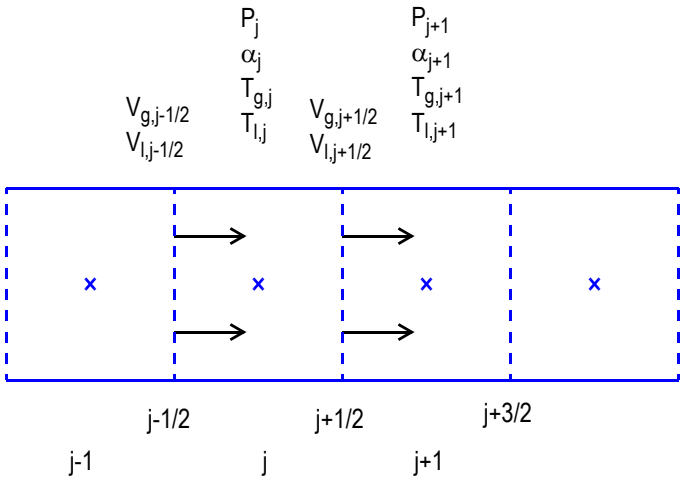

FIGURE 1-2. Computational grid for setting up the "discrete" field equations

semi-implicit method, which are approximations to Equations (1-1) thru (1-6), will be presented here using a fairly standard notation. In this notation, the subscripts provide information on spatial location. The centers of computational volumes are denoted by even integer subscripts (i.e. j-1, j). Similarly, the boundaries separating computational volumes are denoted by half integer subscripts (i.e. j-½, j+½).

First, the time derivative terms in the partial differential equations (PDEs), i.e. Equations (1-1) through (1-6), are approximated with the following equation

$$\frac{\partial \psi}{\partial t} = \frac{\psi^{n+1} - \psi^{n}}{\Delta t} \tag{1-8}$$

where the superscript n indicates the time level.†

†. In Eq. (1-8), the superscript n is an index variable which indicates the discrete time as the solution of discrete equations evolves in discrete time steps, i.e. t^0, t^1, t^2, ..., t^{n-1}, t^n, t^{n+1}, ..., t^{N-1}, t^N. In formulating the discrete approximations to Eqs. (1-1) thru (1-6), it is assumed that the current time step is n, and that the discrete equations are solved for the next time step which is n+1. Thus, the terms appearing with superscript n+1 in the system of discrete equations are treated as unknowns before the solution proceeds to the next time step.

In their discrete form, the convective transport terms in mass and energy in Equations (1-3) to (1-6), i.e. $\nabla(\psi \boldsymbol{V})$ terms, require that fluid quantities defined at the centers of computational volumes (shown in Figure 1-2) be made available at the boundaries separating these volumes using some form of an averaging scheme. The Semi-implicit method uses values from the volumes adjacent to any given boundary, so the averaging scheme in this method is always in the following form:

$$\langle \psi \rangle_{j+1/2} = w_{j+1/2}\psi_j + (1 - w_{j+1/2})\psi_{j+1} \tag{1-9}$$

The energy source terms in Equations (1-5) and (1-6), which describe the exchange of energy with the surroundings, are excluded later from the discussion of the discrete equations for the sake of simplicity since these terms are not significant to the thesis. The terms that describe the exchange of momentum and energy across the phase interface are included since the form of these terms needs to be understood well. The Semi-implicit method, and its implementation to TRAC is at the core of this thesis study — TRAC is one of well known state-of-the-art system codes. Therefore, the functional forms of the coefficients, which describe the momentum exchange at the phase interface and to the surroundings, as implemented in TRAC will be used in the discrete equations. In TRAC, the wall drag (f_{wg}, f_{wl}) and the interfacial drag (f_i) force terms in (1-1) and (1-2) are formulated into the equations of gas and liquid motion as follow:

$$f_{wl} = C_{wl}V_l|V_l| \tag{1-10}$$

$$f_{wg} = C_{wg}V_g|V_g| \tag{1-11}$$

$$f_i = C_i(V_g - V_l)|V_g - V_l| \tag{1-12}$$

Next, the discrete equations of the Semi-implicit method, which are approximations to the six-equation model, can be formulated in the following implicit form pre-

sented in Equations (1-13) to (1-18). The convective momentum transport term in these equations below are left in their differential form for the sake of simplicity. In Equations (1-19) to (1-20), these terms are formulated into a form approximating the gradient of velocity at the given cell boundary.

$$\frac{V_{g,j+1/2}^{n+1} - V_{g,j+1/2}^{n}}{\Delta t} + V_{g,j+1/2}^{n} \frac{\partial V_g}{\partial x}\bigg|_{j+1/2}^{n} + \frac{1}{\langle \rho_g \rangle_{j+1/2}^{n}} \frac{P_{j+1}^{n+1} - P_j^{n+1}}{\Delta x_{j+1/2}} \tag{1-13}$$

$$+ \frac{C_{wg}^{n}}{\langle \alpha \rho_g \rangle_{j+1/2}^{n}} (2V_{g,j+1/2}^{n+1} - V_{g,j+1/2}^{n}) \left| V_{g,j+1/2}^{n} \right|$$

$$+ \frac{C_i^{n}}{\langle \alpha \rho_g \rangle_{j+1/2}^{n}} (2V_{g,j+1/2}^{n+1} - V_{g,j+1/2}^{n} - 2V_{l,j+1/2}^{n+1} + V_{l,j+1/2}^{n}) \left| V_{g,j+1/2}^{n} - V_{l,j+1/2}^{n} \right|$$

$$+ g\Delta h = 0$$

$$\frac{V_{l,j+1/2}^{n+1} - V_{l,j+1/2}^{n}}{\Delta t} + V_{l,j+1/2}^{n} \frac{\partial V_l}{\partial x}\bigg|_{j+1/2}^{n} + \frac{1}{\langle \rho_l \rangle_{j+1/2}^{n}} \frac{P_{j+1}^{n+1} - P_j^{n+1}}{\Delta x_{j+1/2}} \tag{1-14}$$

$$+ \frac{C_{wl}^{n}}{\langle (1-\alpha) \rho_l \rangle_{j+1/2}^{n}} (2V_{l,j+1/2}^{n+1} - V_{l,j+1/2}^{n}) \left| V_{l,j+1/2}^{n} \right|$$

$$- \frac{C_i^{n}}{\langle (1-\alpha) \rho_l \rangle_{j+1/2}^{n}} (2V_{g,j+1/2}^{n+1} - V_{g,j+1/2}^{n} - 2V_{l,j+1/2}^{n+1} + V_{l,j+1/2}^{n}) \left| V_{g,j+1/2}^{n} - V_{l,j+1/2}^{n} \right|$$

$$+ g\Delta h = 0$$

$$\mathrm{Vol}_j \frac{\tilde{\alpha}_j^{n+1} \tilde{\rho}_{g,j}^{n+1} - \langle \alpha \rho_g \rangle_j^{n}}{\Delta t} + \sum \phi_g = \mathrm{Vol}_j \tilde{\Gamma}_{i,j}^{n+1} \tag{1-15}$$

$$\mathrm{Vol}_j \frac{(1-\tilde{\alpha}_j^{n+1})\tilde{\rho}_{l,j}^{n+1} - \langle (1-\alpha)\rho_l \rangle_j^n}{\Delta t} + \sum \phi_l = -\mathrm{Vol}_j \tilde{\Gamma}_{i,j}^{n+1} \tag{1-16}$$

$$\mathrm{Vol}_j \frac{\tilde{\alpha}_j^{n+1}\tilde{\rho}_{g,j}^{n+1}\tilde{e}_{g,j}^{n+1} - \langle \alpha\rho_g e_g \rangle_j^n}{\Delta t} + \sum \zeta_g + \mathrm{Vol}_j \tilde{P}_j^{n+1}\left[\frac{\tilde{\alpha}_j^{n+1} - \alpha_j^n}{\Delta t} + \sum \omega_g\right] = \mathrm{Vol}_j h_{fg} \tilde{\Gamma}_{i,j}^{n+1} \tag{1-17}$$

$$\mathrm{Vol}_j \left\{ \frac{\tilde{\alpha}_j^{n+1}\tilde{\rho}_{g,j}^{n+1}\tilde{e}_{g,j}^{n+1} - \langle \alpha\rho_g e_g \rangle_j^n}{\Delta t} + \frac{(1-\tilde{\alpha}_j^{n+1})\tilde{\rho}_{l,j}^{n+1}\tilde{e}_{l,j}^{n+1} - \langle (1-\alpha)\rho_l e_l \rangle_j^n}{\Delta t} \right\} + \sum \zeta_g + \sum \zeta_l + \mathrm{Vol}_j \tilde{P}_j^{n+1}\left[\sum \omega_g + \sum \omega_l\right] = 0 \tag{1-18}$$

where the momentum flux terms are:

$$V_{j+1/2} \left.\frac{\partial V}{\partial x}\right|_{j+1/2} = [\beta V_{j+1/2}^{n+1} + (1-\beta) V_{j+1/2}^n] \left.\frac{\partial V^n}{\partial x}\right|_{j+1/2} \tag{1-19}$$

$$\beta = \begin{cases} 1 & \text{when } \left.\dfrac{\partial V^n}{\partial x}\right|_{j+1/2} \geq 0 \\ 0 & \text{when } \left.\dfrac{\partial V^n}{\partial x}\right|_{j+1/2} < 0 \end{cases} \tag{1-20}$$

and the sum of flux terms for one-dimensional flows are defined as follow:

$$
\begin{aligned}
\sum \phi_g &= \phi_{g,j+1/2} - \phi_{g,j\text{-}1/2} \\
&= \langle \alpha \rho_g \rangle^n_{j+1/2} A_{j+1/2} V^{n+1}_{g,j+1/2} - \langle \alpha \rho_g \rangle^n_{j\text{-}1/2} A_{j\text{-}1/2} V^{n+1}_{g,j\text{-}1/2} \\
&= [w_{g,j+1/2} \langle \alpha \rho_g \rangle^n_j + (1 - w_{g,j+1/2}) \langle \alpha \rho_g \rangle^n_{j+1}] A_{j+1/2} V^{n+1}_{g,j+1/2} \\
&\quad -[w_{g,j\text{-}1/2} \langle \alpha \rho_g \rangle^n_{j\text{-}1/2} + (1 - w_{g,j\text{-}1/2}) \langle \alpha \rho_g \rangle^n_j] A_{j\text{-}1/2} V^{n+1}_{g,j\text{-}1/2}
\end{aligned}
\tag{1-21}
$$

$$
\begin{aligned}
\sum \phi_l &= \phi_{l,j+1/2} - \phi_{l,j\text{-}1/2} \\
&= \langle (1-\alpha) \rho_l \rangle^n_{j+1/2} A_{j+1/2} V^{n+1}_{l,j+1/2} - \langle (1-\alpha) \rho_l \rangle^n_{j\text{-}1/2} A_{j\text{-}1/2} V^{n+1}_{l,j\text{-}1/2} \\
&= [w_{l,j+1/2} \langle (1-\alpha) \rho_l \rangle^n_j + (1 - w_{l,j+1/2}) \langle (1-\alpha) \rho_l \rangle^n_{j+1}] A_{j+1/2} V^{n+1}_{l,j+1/2} \\
&\quad -[w_{l,j\text{-}1/2} \langle (1-\alpha) \rho_l \rangle^n_{j\text{-}1/2} + (1 - w_{l,j\text{-}1/2}) \langle (1-\alpha) \rho_l \rangle^n_j] A_{j\text{-}1/2} V^{n+1}_{l,j\text{-}1/2}
\end{aligned}
\tag{1-22}
$$

$$
\begin{aligned}
\sum \zeta_g &= \zeta_{g,j+1/2} - \zeta_{g,j\text{-}1/2} \\
&= \langle \alpha \rho_g e_g \rangle^n_{j+1/2} A_{j+1/2} V^{n+1}_{g,j+1/2} - \langle \alpha \rho_g e_g \rangle^n_{j\text{-}1/2} A_{j\text{-}1/2} V^{n+1}_{g,j\text{-}1/2} \\
&= [w_{g,j+1/2} \langle \alpha \rho_g e_g \rangle^n_j + (1 - w_{g,j+1/2}) \langle \alpha \rho_g e_g \rangle^n_{j+1}] A_{j+1/2} V^{n+1}_{g,j+1/2} \\
&\quad -[w_{g,j\text{-}1/2} \langle \alpha \rho_g e_g \rangle^n_{j\text{-}1/2} + (1 - w_{g,j\text{-}1/2}) \langle \alpha \rho_g e_g \rangle^n_j] A_{j\text{-}1/2} V^{n+1}_{g,j\text{-}1/2}
\end{aligned}
\tag{1-23}
$$

$$
\begin{aligned}
\sum \zeta_l &= \zeta_{l,j+1/2} - \zeta_{l,j\text{-}1/2} \\
&= \langle (1-\alpha) \rho_l e_l \rangle^n_{j+1/2} A_{j+1/2} V^{n+1}_{l,j+1/2} - \langle (1-\alpha) \rho_l e_l \rangle^n_{j\text{-}1/2} A_{j\text{-}1/2} V^{n+1}_{l,j\text{-}1/2} \\
&= [w_{l,j+1/2} \langle (1-\alpha) \rho_l e_l \rangle^n_j + (1 - w_{l,j+1/2}) \langle (1-\alpha) \rho_l e_l \rangle^n_{j+1}] A_{j+1/2} V^{n+1}_{l,j+1/2} \\
&\quad -[w_{l,j\text{-}1/2} \langle (1-\alpha) \rho_l e_l \rangle^n_{j\text{-}1/2} + (1 - w_{l,j\text{-}1/2}) \langle (1-\alpha) \rho_l e_l \rangle^n_j] A_{j\text{-}1/2} V^{n+1}_{l,j\text{-}1/2}
\end{aligned}
\tag{1-24}
$$

$$
\begin{aligned}
\sum \omega_g &= \omega_{g,j+1/2} - \omega_{g,j\text{-}1/2} \\
&= \langle \alpha \rangle^n_{j+1/2} A_{j+1/2} V^{n+1}_{g,j+1/2} - \langle \alpha \rangle^n_{j\text{-}1/2} A_{j\text{-}1/2} V^{n+1}_{g,j\text{-}1/2} \\
&= [w_{g,j+1/2} \langle \alpha \rangle^n_j + (1 - w_{g,j+1/2}) \langle \alpha \rangle^n_{j+1}] A_{j+1/2} V^{n+1}_{g,j+1/2} \\
&\quad -[w_{g,j\text{-}1/2} \langle \alpha \rangle^n_{j\text{-}1/2} + (1 - w_{g,j\text{-}1/2}) \langle \alpha \rangle^n_j] A_{j\text{-}1/2} V^{n+1}_{g,j\text{-}1/2}
\end{aligned}
\tag{1-25}
$$

$$
\begin{aligned}
\sum \omega_l &= \omega_{l,j+1/2} - \omega_{l,j\text{-}1/2} \\
&= \langle \alpha \rangle^n_{j\text{-}1/2} A_{j\text{-}1/2} V^{n+1}_{l,j\text{-}1/2} - \langle \alpha \rangle^n_{j+1/2} A_{j+1/2} V^{n+1}_{l,j+1/2} \\
&= [w_{l,j\text{-}1/2} \langle \alpha \rangle^n_{j\text{-}1/2} + (1 - w_{l,j\text{-}1/2}) \langle \alpha \rangle^n_j] A_{j\text{-}1/2} V^{n+1}_{l,j\text{-}1/2} \\
&\quad -[w_{l,j+1/2} \langle \alpha \rangle^n_j + (1 - w_{l,j+1/2}) \langle \alpha \rangle^n_{j+1}] A_{j+1/2} V^{n+1}_{l,j+1/2}
\end{aligned}
\tag{1-26}
$$

Equations (1-13) to (1-18) capture the Semi-implicit method in sufficient detail for the discussions of this thesis. An additional detail that is noteworthy to mention here is a special case when the void fraction approaches to zero or one. The semi-implicit method of TRAC requires that the gas mass and the liquid mass equations be replaced by the mixture mass and a void fraction equation, respectively.

Choosing a set of independent variables to formulate a solution to these equations is the first step towards solving these equations. Although the above equations suggest that fluid densities (ρ) and internal energy (e) along with fluid velocities (V) and the void fraction (α) are good candidates for being independent variables in a solution, the Semi-implicit method in TRAC chooses pressure (P) and temperature (T) in favor of density and internal energy for a more stable and simpler solution. Equations of state express fluid density and internal energy as functions of pressure and temperature, i.e. $\rho_g(P, T_g)$, $\rho_l(P, T_l)$, $e_g(P, T_g)$, and $e_l(P, T_l)$. Since these functions, which describe the relation of density and energy to pressure and temperature, are generally nonlinear, the system of equations formed by Equations (1-13) to (1-18)

combined with the state equations yield a coupled set of nonlinear equations. To obtain a solution for this equation set, the unknown terms (i.e. at time level n+1) are expressed as linear extrapolations of the known terms (i.e. at time level n). A key feature of TRAC is that a Newton iteration is used to obtain a solution to this set of nonlinear equations as opposed to a simpler approach which could merely replace the nonlinear equations by their linearized approximations.

The Semi-implicit method of TRAC begins the solution by formulating the unknown velocities as a linear function of changes in the pressure field, and thus, by treating the velocities as dependent variables in the mass and energy equations for the liquid and gas. First, the phase velocities at time level n+1 in (1-13) and (1-14) are expressed as linear functions of pressure changes at the adjacent computational volumes, i.e. (1-27) and (1-28) are substituted into (1-13) and (1-14):

$$V_{j+1/2}^{n+1} = \tilde{V}_{j+1/2}^{n+1} + \sum_{i} \left\{ \frac{\partial V_{j+1/2}^{n+1}}{\partial P_{j+1}^{n+1}} \delta P_{j+1}^{i} + \frac{\partial V_{j+1/2}^{n+1}}{\partial P_{j}^{n+1}} \delta P_{j}^{i} \right\} \tag{1-27}$$

$$V_{j-1/2}^{n+1} = \tilde{V}_{j-1/2}^{n+1} + \sum_{i} \left\{ \frac{\partial V_{j-1/2}^{n+1}}{\partial P_{j}^{n+1}} \delta P_{j}^{i} + \frac{\partial V_{j-1/2}^{n+1}}{\partial P_{j-1}^{n+1}} \delta P_{j-1}^{i} \right\} \tag{1-28}$$

The gas and liquid momentum equations, (1-13) and (1-14), are then solved for the tilde velocities by assuming that the pressures remain constant ($\delta P = 0$). Thus, the tilde velocities exclude the changes in fluid momentum due to pressure variations across computational volumes adjacent to any given boundary. The resulting momentum equations are coupled due to the interfacial drag component forming the linear

system in Equation (1-29) that can be solved directly for $\tilde{V}_{l,j+1/2}^{n+1}$, $\tilde{V}_{g,j+1/2}^{n+1}$, $\partial V_{l,j+1/2}^{n+1}/\partial P_j^{n+1}$ and $\partial V_{g,j+1/2}^{n+1}/\partial P_j^{n+1}$.

$$\begin{bmatrix} c_{V_g,1} & c_{V_l,1} \\ c_{V_g,2} & c_{V_l,2} \end{bmatrix} \cdot \begin{bmatrix} \tilde{V}_{g,j+1/2}^{n+1} \\ \tilde{V}_{l,j+1/2}^{n+1} \end{bmatrix} = \begin{bmatrix} rhs_g \\ rhs_l \end{bmatrix} \tag{1-29}$$

$$\begin{bmatrix} c_{V_g,1} & c_{V_l,1} \\ c_{V_g,2} & c_{V_l,2} \end{bmatrix} \cdot \begin{bmatrix} \partial V_{g,j+1/2}^{n+1}/\partial P_j^{n+1} \\ \partial V_{l,j+1/2}^{n+1}/\partial P_j^{n+1} \end{bmatrix} = \begin{bmatrix} \partial rhs_g/\partial P_j^{n+1} \\ \partial rhs_l/\partial P_j^{n+1} \end{bmatrix} \tag{1-30}$$

Next, (1-27) and (1-28) are substituted for phase velocities at time level n+1 in (1-15) to (1-18) eliminating the velocities as unknowns from these equations. Before Equations (1-15) to (1-18) can be solved by an iterative method, the nonlinear products in these equations, i.e. products of density and internal energy at time level n+1, are approximated by the following linear expressions.

$$\begin{aligned} \tilde{P}^{n+1} &= (\tilde{P}^{n+1})^i + \delta P^{i+1} \\ \tilde{\alpha}^{n+1} &= (\tilde{\alpha}^{n+1})^i + \delta \alpha^{i+1} \\ \tilde{T}_l^{n+1} &= (\tilde{T}_l^{n+1})^i + \delta T_l^{i+1} \\ \tilde{T}_g^{n+1} &= (\tilde{T}_g^{n+1})^i + \delta T_g^{i+1} \end{aligned} \tag{1-31}$$

$$\begin{aligned} \tilde{\alpha}^{n+1}\tilde{\rho}_g^{n+1} &= (\tilde{\alpha}^{n+1})^i(\tilde{\rho}_g^{n+1})^i + (\tilde{\rho}_g^{n+1})^i \delta\alpha^{i+1} \\ &\quad + (\tilde{\alpha}^{n+1})^i \frac{\partial \rho_g}{\partial P}\bigg|_{n+1}^i \delta P^{i+1} + (\tilde{\alpha}^{n+1})^i \frac{\partial \rho_g}{\partial T}\bigg|_{n+1}^i \delta T_g^{i+1} \end{aligned} \tag{1-32}$$

$$(1-\tilde{\alpha}_j^{n+1})\tilde{\rho}_{l,j}^{n+1} = \left[1-(\tilde{\alpha}^{n+1})^i\right](\tilde{\rho}_l^{n+1})^i - (\tilde{\rho}_l^{n+1})^i\,\delta\alpha^{i+1}$$
$$+\left[1-(\tilde{\alpha}^{n+1})^i\right]\left.\frac{\partial\rho_l}{\partial P}\right|_{n+1}^{i}\delta P^{i+1} + \left[1-(\tilde{\alpha}^{n+1})^i\right]\left.\frac{\partial\rho_l}{\partial T}\right|_{n+1}^{i}\delta T_l^{i+1} \qquad (1\text{-}33)$$

$$\tilde{\alpha}_j^{n+1}\tilde{\rho}_{g,j}^{n+1}\tilde{e}_{g,j}^{n+1} = (\tilde{\alpha}^{n+1})^i(\tilde{\rho}_g^{n+1})^i(\tilde{e}_g^{n+1})^i + (\tilde{\rho}_g^{n+1})^i(\tilde{e}_g^{n+1})^i\,\delta\alpha^{i+1}$$
$$+(\tilde{\alpha}^{n+1})^i(\tilde{e}_g^{n+1})^i\left[\left.\frac{\partial\rho_g}{\partial P}\right|_{n+1}^{i}\delta P^{i+1} + \left.\frac{\partial\rho_g}{\partial T}\right|_{n+1}^{i}\delta T_g^{i+1}\right] \qquad (1\text{-}34)$$
$$+(\tilde{\alpha}^{n+1})^i(\tilde{\rho}_g^{n+1})^i\left[\left.\frac{\partial e_g}{\partial P}\right|_{n+1}^{i}\delta P^{i+1} + \left.\frac{\partial e_g}{\partial T}\right|_{n+1}^{i}\delta T_g^{i+1}\right]$$

$$(1-\tilde{\alpha}_j^{n+1})\tilde{\rho}_{l,j}^{n+1}\tilde{e}_{l,j}^{n+1} = \left[1-(\tilde{\alpha}^{n+1})^i\right](\tilde{\rho}_l^{n+1})^i(\tilde{e}_l^{n+1})^i - (\tilde{\rho}_l^{n+1})^i(\tilde{e}_l^{n+1})^i\,\delta\alpha^{i+1}$$
$$+\left[1-(\tilde{\alpha}^{n+1})^i\right](\tilde{e}_l^{n+1})^i\left[\left.\frac{\partial\rho_l}{\partial P}\right|_{n+1}^{i}\delta P^{i+1} + \left.\frac{\partial\rho_l}{\partial T}\right|_{n+1}^{i}\delta T_l^{i+1}\right] \qquad (1\text{-}35)$$
$$+\left[1-(\tilde{\alpha}^{n+1})^i\right](\tilde{\rho}_l^{n+1})^i\left[\left.\frac{\partial e_l}{\partial P}\right|_{n+1}^{i}\delta P^{i+1} + \left.\frac{\partial e_l}{\partial T}\right|_{n+1}^{i}\delta T_l^{i+1}\right]$$

In the above equations, the superscript i is the iteration count of the iterative solution in TRAC, i.e. $(\psi^{n+1})^i$ is the value of ψ after the i-th iteration for time step n+1. Next, the linear approximations given in (1-27), (1-28), and (1-31) to (1-35), assuming the variations $(\delta\psi^i)$ are sufficiently small so that their products can be ignored, are substituted into (1-15) to (1-18), to form the following matrix equation.

$$\begin{bmatrix} a_{11} & a_{11} & a_{11} & a_{11} \\ a_{21} & a_{22} & a_{23} & a_{24} \\ a_{31} & a_{32} & a_{33} & a_{34} \\ a_{41} & a_{42} & a_{43} & a_{44} \end{bmatrix} \cdot \begin{bmatrix} \delta P_j \\ \delta \alpha_j \\ \delta T_{g,j} \\ \delta T_{l,j} \end{bmatrix}^{i+1} = \begin{bmatrix} b_1 \\ b_2 \\ b_3 \\ b_4 \end{bmatrix} + \begin{bmatrix} c_{1,2} \\ c_{2,2} \\ c_{3,2} \\ c_{4,2} \end{bmatrix} (\delta P_{j+1}^{i+1} - \delta P_j^{i+1}) + \begin{bmatrix} c_{1,1} \\ c_{2,1} \\ c_{3,1} \\ c_{4,1} \end{bmatrix} (\delta P_{j-1}^{i+1} - \delta P_j^{i+1}) \tag{1-36}$$

Equation (1-36) is then solved for the pressure, void fraction, and temperature variations in the following form:

$$\begin{bmatrix} \delta P_j \\ \delta \alpha_j \\ \delta T_{g,j} \\ \delta T_{l,j} \end{bmatrix}^{i+1} = \begin{bmatrix} b'_1 \\ b'_2 \\ b'_3 \\ b'_4 \end{bmatrix} + \begin{bmatrix} c'_{1,2} \\ c'_{2,2} \\ c'_{3,2} \\ c'_{4,2} \end{bmatrix} (\delta P_{j+1}^{i+1} - \delta P_j^{i+1}) + \begin{bmatrix} c'_{1,1} \\ c'_{2,1} \\ c'_{3,1} \\ c'_{4,1} \end{bmatrix} (\delta P_{j-1}^{i+1} - \delta P_j^{i+1}) \tag{1-37}$$

Equation (1-37) expresses the changes in void fraction and temperatures as linear functions of changes in fluid pressure reducing itself to a single equation that relates the pressure change in a computational volume to the pressure changes in its adjacent volumes.

$$-c'_{1,1}\delta P_{j-1}^{i+1} + (1 + c'_{1,1} + c'_{1,2})\delta P_j^{i+1} - c'_{1,2}\delta P_{j+1}^{i+1} = b'_1 \tag{1-38}$$

The coefficients of (1-38), which multiply fluid pressures, form a tridiagonal system when (1-38) is set up for a series computational volumes of an one-dimensional flow conduit. Once the solution for pressures is obtained, the changes in void fractions and temperatures, driven by changes in the pressure field, are predicted by substituting these changes in the remaining rows of (1-37). The predicted changes are

then substituted back into (1-31) to update the values of independent variables. At the end of a time step cycle, also updated are the end of time step phase velocities described by (1-27) and (1-28) as linear functions of pressure changes.

TRAC repeats this iterative cycle beginning with (1-31) until a desired convergence is achieved. For the sake of completeness, the basic step equations described here are reformulated using the variable names of TRAC and made available in Appendix A.

The Stability Enhancing Two-Step Method

In addition to the standard solution of the Semi-implicit method, where the maximum achievable time step size is bounded by the material Courant stability limit, TRAC provides a more implicit method known as SETS (Stability-Enhancing Two-Step).[1-12] As its name suggests, the SETS method constitutes a two step solution that allows it to advance the transient time using time step sizes that are not bounded by the material Courant stability limit. First, the semi-implicit solution (i.e. predictor step) converges to a new time velocity field as the velocities are updated by (1-27) and (1-28). A more implicit solution to the same equation set follows (i.e. corrector step), where the quantities convected across boundaries by Equations (1-21) to (1-26) are redefined at time level n+1, i.e. as unknowns. This additional equation set, also known as the stabilizer equations, is used to propagate the information on continuity waves more implicitly in order to eliminate the material Courant stability limit.

The SETS method of TRAC begins a time step by solving the following stabilizer equations for momentum. It should be noted that the order in which TRAC solved the predictor and corrector equations was chosen after performing rigorous numerical experiments to determine the most stable order.[1-13]

$$\frac{\tilde{V}_{g,j+1/2}^{n+1} - V_{g,j+1/2}^{n}}{\Delta t} + \tilde{V}_{g,j+1/2}^{n+1} \frac{\partial \tilde{V}_{g}^{n+1}}{\partial x}\bigg|_{j+1/2} + \frac{1}{\langle \rho_g \rangle_{j+1/2}^{n}} \frac{P_{j+1}^{n} - P_{j}^{n}}{\Delta x_{j+1/2}} \tag{1-39}$$

$$+ \frac{C_{wg}^{n}}{\langle \alpha \rho_g \rangle_{j+1/2}^{n}} (2\tilde{V}_{g,j+1/2}^{n+1} - V_{g,j+1/2}^{n}) \left| V_{g,j+1/2}^{n} \right|$$

$$+ \frac{C_{i}^{n}}{\langle \alpha \rho_g \rangle_{j+1/2}^{n}} (2\tilde{V}_{g,j+1/2}^{n+1} - V_{g,j+1/2}^{n} - 2\tilde{V}_{l,j+1/2}^{n+1} + V_{l,j+1/2}^{n}) \left| V_{g,j+1/2}^{n} - V_{l,j+1/2}^{n} \right|$$

$$+ g\Delta h = 0$$

$$\frac{\tilde{V}_{l,j+1/2}^{n+1} - V_{l,j+1/2}^{n}}{\Delta t} + \tilde{V}_{l,j+1/2}^{n+1} \frac{\partial \tilde{V}_{l}^{n+1}}{\partial x}\bigg|_{j+1/2} + \frac{1}{\langle \rho_l \rangle_{j+1/2}^{n}} \frac{P_{j+1}^{n} - P_{j}^{n}}{\Delta x_{j+1/2}} \tag{1-40}$$

$$+ \frac{C_{wl}^{n}}{\langle (1-\alpha) \rho_l \rangle_{j+1/2}^{n}} (2\tilde{V}_{l,j+1/2}^{n+1} - V_{l,j+1/2}^{n}) \left| V_{l,j+1/2}^{n} \right|$$

$$- \frac{C_{i}^{n}}{\langle (1-\alpha) \rho_l \rangle_{j+1/2}^{n}} (2\tilde{V}_{g,j+1/2}^{n+1} - V_{g,j+1/2}^{n} - 2\tilde{V}_{l,j+1/2}^{n+1} + V_{l,j+1/2}^{n}) \left| V_{g,j+1/2}^{n} - V_{l,j+1/2}^{n} \right|$$

$$+ g\Delta h = 0$$

where the momentum flux terms are redefined as follows:

$$\tilde{V}_{j+1/2}^{n+1} \frac{\partial \tilde{V}^{n+1}}{\partial x}\bigg|_{j+1/2} = V_{j+1/2}^{n} \frac{\partial \tilde{V}^{n+1}}{\partial x}\bigg|_{j+1/2} + \beta (\tilde{V}_{j+1/2}^{n+1} - V_{j+1/2}^{n}) \frac{\partial \tilde{V}^{n}}{\partial x}\bigg|_{j+1/2} \tag{1-41}$$

$$\beta = \begin{cases} 1 & \text{when } \dfrac{\partial V^{n}}{\partial x}\bigg|_{j+1/2} \geq 0 \quad \text{and} \quad V_{j+1/2}^{n} \tilde{V}_{j+1/2}^{n} > 0 \\ 0 & \text{when } \dfrac{\partial V^{n}}{\partial x}\bigg|_{j+1/2} < 0 \quad \text{or} \quad V_{j+1/2}^{n} \tilde{V}_{j+1/2}^{n} \leq 0 \end{cases} \tag{1-42}$$

As the stabilizer momentum equations of adjacent computational volumes are coupled due to term $\left.\frac{\partial \tilde{V}^{n+1}}{\partial x}\right|_{j+1/2}$ in (1-41), the coefficients of $\tilde{V}^{n+1}_{l,j+1/2}$ and $\tilde{V}^{n+1}_{g,j+1/2}$ in these equations form a tridiagonal matrix and the solution for these velocities therefore require a simultaneous solution of (1-39) and (1-40) for all computational volumes. Once $\tilde{V}^{n+1}_{l,j+1/2}$ and $\tilde{V}^{n+1}_{g,j+1/2}$ are obtained, the time step proceeds with the solution of Equations (1-13) and (1-14) where the momentum flux terms are modified to further enhance the stability of the method. The following equation replaces (1-19).

$$V_{j+1/2}\left.\frac{\partial V}{\partial x}\right|_{j+1/2} = V^{n}_{j+1/2}\left.\frac{\partial \tilde{V}^{n+1}}{\partial x}\right|_{j+1/2} + \beta(V^{n+1}_{j+1/2} - V^{n}_{j+1/2})\left.\frac{\partial \tilde{V}^{n}}{\partial x}\right|_{j+1/2} \tag{1-43}$$

The resulting velocities from the combined solution of stabilizer and basic step momentum equations are in better agreement with the expected variations in the pressure field than the velocities from a solution of the basic momentum equations alone.

The next step, also known as the basic step of the SETS method, obtains new time values of independent variables that describe the fluid flow, i.e. Equations (1-27), (1-28), and (1-31), by solving the Semi-Implicit equations as discussed in the previous section. To improve the robustness of the SETS method, the flux terms of the Semi-Implicit equations are redefined to use a mixture of old and new time values. The expressions in (1-44) to (1-47) are substituted into Equations (1-21) to (1-26) for the macroscopic quantities of the cells for which the balance equations are set up.

$$\langle \alpha\rho_g \rangle^{n}_{j} \rightarrow (1-\gamma)\langle \alpha\rho_g \rangle^{n}_{j} + \gamma \tilde{\alpha}^{n+1}_{j} \tilde{\rho}^{n+1}_{g,j} \tag{1-44}$$

$$\langle(1-\alpha)\rho_l\rangle_j^n \rightarrow (1-\gamma)\langle(1-\alpha)\rho_l\rangle_j^n + \gamma(1-\tilde{\alpha}_j^{n+1})\tilde{\rho}_{l,j}^{n+1} \tag{1-45}$$

$$\langle\alpha\rho_g e_g\rangle_j^n \rightarrow (1-\gamma)\langle\alpha\rho_g e_g\rangle_j^n + \gamma\tilde{\alpha}_j^{n+1}\tilde{\rho}_{g,j}^{n+1}\tilde{e}_{g,j}^{n+1} \tag{1-46}$$

$$\langle(1-\alpha)\rho_l e_l\rangle_j^n \rightarrow (1-\gamma)\langle(1-\alpha)\rho_l e_l\rangle_j^n + \gamma(1-\tilde{\alpha}_j^{n+1})\tilde{\rho}_{l,j}^{n+1}\tilde{e}_{l,j}^{n+1} \tag{1-47}$$

where γ is a weighting factor based on the phase change rate. It is set to zero for computational volumes where the fluid is single phase. It should be noted that while this modification to the flux terms is not a requirement of the SETS method, the modified flux terms improve the method's handling of situations where there is strong phase change such as boiling.

After the basic step, a fully implicit form of the mass and energy equations are solved to propagate the continuity waves across the solution domain more efficiently. The solution of the stabilizer mass and energy equations differ from their Semi-Implicit counterparts from the basic step not only in terms of their level of implicitness but also in terms of what they are solved for. The solution to these equations, (1-48) to (1-51), merely obtains the macroscopic densities of mass and energy.

$$\mathrm{Vol}_j\frac{\langle\alpha\rho_g\rangle_j^{n+1} - \langle\alpha\rho_g\rangle_j^n}{\Delta t} + \sum\phi_g = \mathrm{Vol}_j\Gamma_{i,j}^{n+1} \tag{1-48}$$

$$\mathrm{Vol}_j\frac{\langle(1-\alpha)\rho_l\rangle_j^{n+1} - \langle(1-\alpha)\rho_l\rangle_j^n}{\Delta t} + \sum\phi_l = -\mathrm{Vol}_j\Gamma_{i,j}^{n+1} \tag{1-49}$$

$$\mathrm{Vol}_j\frac{\langle\alpha\rho_g e_g\rangle_j^{n+1} - \langle\alpha\rho_g e_g\rangle_j^n}{\Delta t} + \sum\zeta_g + \mathrm{Vol}_j\tilde{P}_j^{n+1}\left[\frac{\tilde{\alpha}_j^{n+1} - \alpha_j^n}{\Delta t} + \sum\omega_g\right] = \mathrm{Vol}_j h_{fg}\tilde{\Gamma}_{i,j}^{n+1} \tag{1-50}$$

$$\mathrm{Vol}_j \frac{\langle(1-\alpha)\rho_l e_l\rangle_j^{n+1} - \langle(1-\alpha)\rho_l e_l\rangle_j^{n}}{\Delta t} + \sum \zeta_l + \mathrm{Vol}_j \tilde{P}_j^{n+1}\left[\frac{\alpha_j^n - \tilde{\alpha}_j^{n+1}}{\Delta t} + \sum \omega_l\right] = -\mathrm{Vol}_j h_{fg} \tilde{\Gamma}_{i,j}^{n+1} \tag{1-51}$$

where the flux terms are defined as follows:

$$\sum \phi_g = \left\{ w_{g,j+1/2} \langle \alpha\rho_g \rangle_j^{n+1} + (1 - w_{g,j+1/2}) \langle \alpha\rho_g \rangle_{j+1}^{n+1} \right\} A_{j+1/2} V_{g,j+1/2}^{n+1} + \left\{ w_{g,j-1/2} \langle \alpha\rho_g \rangle_{j-1}^{n+1} + (1 - w_{g,j-1/2}) \langle \alpha\rho_g \rangle_j^{n+1} \right\} A_{j-1/2} V_{g,j-1/2}^{n+1} \tag{1-52}$$

$$\sum \phi_l = \left\{ w_{l,j+1/2} \langle (1-\alpha)\rho_l \rangle_j^{n+1} + (1 - w_{l,j+1/2}) \langle (1-\alpha)\rho_l \rangle_{j+1}^{n+1} \right\} A_{j+1/2} V_{l,j+1/2}^{n+1} + \left\{ w_{l,j-1/2} \langle (1-\alpha)\rho_l \rangle_{j-1}^{n+1} + (1 - w_{l,j-1/2}) \langle (1-\alpha)\rho_l \rangle_j^{n+1} \right\} A_{j-1/2} V_{l,j-1/2}^{n+1} \tag{1-53}$$

$$\sum \zeta_g = \left\{ w_{g,j+1/2} \langle \alpha\rho_g e_g \rangle_j^{n+1} + (1 - w_{g,j+1/2}) \langle \alpha\rho_g e_g \rangle_{j+1}^{n+1} \right\} A_{j+1/2} V_{g,j+1/2}^{n+1} + \left\{ w_{g,j-1/2} \langle \alpha\rho_g e_g \rangle_{j-1}^{n+1} + (1 - w_{g,j-1/2}) \langle \alpha\rho_g e_g \rangle_j^{n+1} \right\} A_{j-1/2} V_{g,j-1/2}^{n+1} \tag{1-54}$$

$$\sum \zeta_l = \left\{ w_{l,j+1/2} \langle (1-\alpha)\rho_l e_l \rangle_j^{n+1} + (1 - w_{l,j+1/2}) \langle (1-\alpha)\rho_l e_l \rangle_{j+1}^{n+1} \right\} A_{j+1/2} V_{l,j+1/2}^{n+1} + \left\{ w_{l,j-1/2} \langle (1-\alpha)\rho_l e_l \rangle_{j-1}^{n+1} + (1 - w_{l,j-1/2}) \langle (1-\alpha)\rho_l e_l \rangle_j^{n+1} \right\} A_{j-1/2} V_{l,j-1/2}^{n+1} \tag{1-55}$$

$$\sum \omega_g = \left\{ w_{g,j+1/2} \tilde{\alpha}_j^{n+1} + (1 - w_{g,j+1/2}) \tilde{\alpha}_{j+1}^{n+1} \right\} A_{j+1/2} V_{g,j+1/2}^{n+1} + \left\{ w_{g,j-1/2} \tilde{\alpha}_{j-1}^{n+1} + (1 - w_{g,j-1/2}) \tilde{\alpha}_j^{n+1} \right\} A_{j-1/2} V_{g,j-1/2}^{n+1} \quad (1\text{-}56)$$

$$\sum \omega_l = \left\{ w_{l,j+1/2} (1 - \tilde{\alpha}_j^{n+1}) + (1 - w_{l,j+1/2}) (1 - \tilde{\alpha}_{j+1}^{n+1}) \right\} A_{j+1/2} V_{l,j+1/2}^{n+1} + \left\{ w_{l,j-1/2} (1 - \tilde{\alpha}_{j-1}^{n+1}) + (1 - w_{l,j-1/2}) (1 - \tilde{\alpha}_j^{n+1}) \right\} A_{j-1/2} V_{l,j-1/2}^{n+1} \quad (1\text{-}57)$$

It should be noted that the left hand sides of (1-15) to (1-17) and the liquid energy equations are substituted for the phase change terms on the right hand sides of Equations (1-48) to (1-51). When Equations (1-48) to (1-51) are set up for a series of computational volumes, the coefficients of unknowns, i.e. $\langle \alpha \rho_g \rangle^{n+1}$, $\langle (1-\alpha) \rho_l \rangle^{n+1}$, $\langle \alpha \rho_g e_g \rangle^{n+1}$, and $\langle (1-\alpha) \rho_l e_l \rangle^{n+1}$, form a tridiagonal matrix for each equation that can be solved independently.

While it is recognized that the pressures, temperatures, and void fractions from the basic step are no longer consistent with the macroscopic densities from the stabilizer step, the experience with TRAC has shown that the use of these pressures and temperatures in the next time step is adequate. However, the experience has also shown that the SETS method in TRAC is more robust if a new a void fraction consistent with terms $\langle \alpha \rho_g \rangle^{n+1}$, $\langle (1-\alpha) \rho_l \rangle^{n+1}$, $\langle \alpha \rho_g e_g \rangle^{n+1}$, and $\langle (1-\alpha) \rho_l e_l \rangle^{n+1}$ from the solution of (1-48) to (1-51), not $\tilde{\alpha}^{n+1}$ from the basic step, is used. First, the macroscopic densities from the stabilizer step are expressed in terms of final values of pressures, temperatures, and void fractions for every computational volume.

$$
\begin{aligned}
\langle \alpha \rho_g \rangle_j^n &= \alpha_j^{n+1} \rho_{g,j}^{n+1} \\
\langle (1-\alpha) \rho_l \rangle_j^n &= (1-\alpha_j^{n+1}) \rho_{l,j}^{n+1} \\
\langle \alpha \rho_g e_g \rangle_j^n &= \alpha_j^{n+1} \rho_{g,j}^{n+1} e_{g,j}^{n+1} \\
\langle (1-\alpha) \rho_l e_l \rangle_j^n &= (1-\alpha_j^{n+1}) \rho_{l,j}^{n+1} e_{l,j}^{n+1}
\end{aligned}
\tag{1-58}
$$

The left hand sides of (1-58) are the macroscopic quantities known from the solution of the stabilizer equations. When the right hand sides of (1-58) are linearized following Equations (1-31) to (1-35), the resulting equations form a 4x4 linear system that can be solved for δP_j, $\delta T_{l,j}$, $\delta T_{g,j}$, and $\delta \alpha_j$ in every computational volume. The SETS method in TRAC keeps only the void fraction from this solution and discards the other variables.

Simulation of Two-Phase Flows in Three-Dimensional Cylindrical Coordinates

TRAC is one of very few TH codes that include the capability to solve the six-equation model fully in three-dimensional cylindrical and cartesian coordinates. This capability is especially important in LOCA simulations where one-dimensional models of the reactor pressure vessel are not adequate to determine how much of the emergency coolant reaches into the reactor core. The one- and three-dimensional finite volume formulations of the six-equation model are identical in terms of their resolution of time and length scales of the flow phenomena considered by them, i.e. both approaches employ similar size computational volumes and similar time step sizes. The two approaches differ mainly due to the extra flow directions considered by the three-dimensional field equations. Figure 1-3 shows the three-dimensional computational grid in cylindrical coordinates. Similar to the computational grid set up for the one-dimensional field equations, the three-dimensional grid places the dynamic variables (i.e. fluid velocities) the boundaries between computational volumes, and the

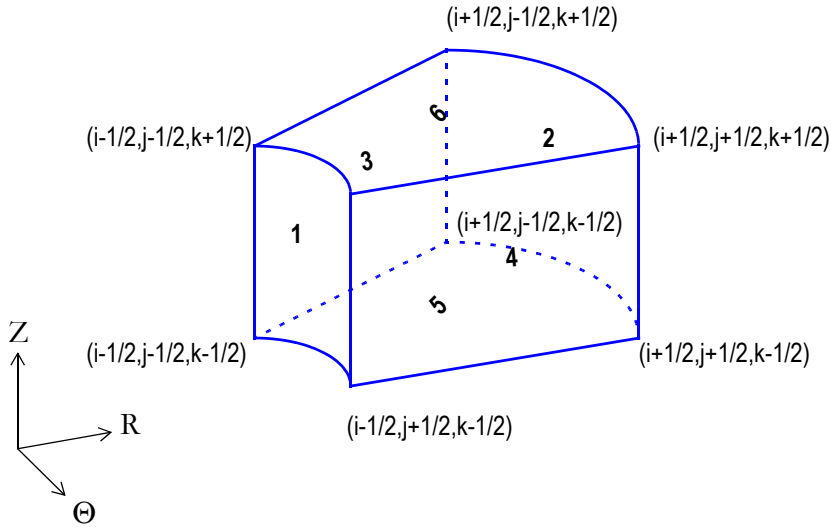

FIGURE 1-3. A three-dimensional computational volume

static variables (i.e. fluid temperatures, pressures, and void fractions) at the centers of computational volumes. Similar to the notation used to present the one-dimensional field equations, the subscripts are used to provide information on spatial location. The centers of computational volumes are denoted by three subscripts where a separate subscript is used for each direction. Figure 1-3 illustrates the use of the subscripts in three-dimensional grid by marking the eight corners of a three-dimensional volume with half integer subscripts. In addition to the use of these subscripts, each of the six faces on a computational volume are assigned an integer number for a simpler notation.

Rather than offering a full description of the three-dimensional field equations, only the differences between them and the one-dimensional field equations are emphasized here to avoid lengthy equations. The differences between the one- and three-dimensional field equations originate from the vector quantities, which appear in boldface, in Equations (1-1) to (1-6).

The momentum equations are split into each orthogonal component of the liquid and gas vector momentum.

$$\alpha\rho_g\left(\frac{\partial V_{gz}}{\partial t}+V_{gr}\frac{\partial V_{gz}}{\partial r}+\frac{V_{g\theta}}{r}\frac{\partial V_{gz}}{\partial \theta}+V_{gz}\frac{\partial V_{gz}}{\partial z}\right)=-\alpha\frac{\partial P}{\partial z}-\alpha\rho_g g_z-f_{iz}+f_{wgz} \tag{1-59}$$

$$\begin{aligned}\alpha\rho_g\left(\frac{\partial V_{gr}}{\partial t}+V_{gr}\frac{\partial V_{gr}}{\partial r}+\frac{V_{g\theta}}{r}\frac{\partial V_{gr}}{\partial \theta}-\frac{V_{g\theta}^2}{r}+V_{gz}\frac{\partial V_{gr}}{\partial z}\right)\\ =-\alpha\frac{\partial P}{\partial r}-\alpha\rho_g g_r-f_{ir}+f_{wgr}\end{aligned} \tag{1-60}$$

$$\begin{aligned}\alpha\rho_g\left(\frac{\partial V_{g\theta}}{\partial t}+V_{gr}\frac{\partial V_{g\theta}}{\partial r}+\frac{V_{g\theta}}{r}\frac{\partial V_{g\theta}}{\partial \theta}+\frac{V_{gr}V_{g\theta}}{r}+V_{gz}\frac{\partial V_{g\theta}}{\partial z}\right)\\ =-\alpha\frac{\partial P}{\partial \theta}-\alpha\rho_g g_\theta-f_{i\theta}+f_{wg\theta}\end{aligned} \tag{1-61}$$

$$\begin{aligned}(1-\alpha)\rho_l\left(\frac{\partial V_{lz}}{\partial t}+V_{lr}\frac{\partial V_{lz}}{\partial r}+\frac{V_{l\theta}}{r}\frac{\partial V_{lz}}{\partial \theta}+V_{lz}\frac{\partial V_{lz}}{\partial z}\right)\\ =-(1-\alpha)\frac{\partial P}{\partial z}-(1-\alpha)\rho_l g_z+f_{iz}+f_{wlz}\end{aligned} \tag{1-62}$$

$$\begin{aligned}(1-\alpha)\rho_l\left(\frac{\partial V_{lr}}{\partial t}+V_{lr}\frac{\partial V_{lr}}{\partial r}+\frac{V_{l\theta}}{r}\frac{\partial V_{lr}}{\partial \theta}+V_{lz}\frac{\partial V_{lr}}{\partial z}\right)\\ =-(1-\alpha)\frac{\partial P}{\partial r}-(1-\alpha)\rho_l g_r+f_{ir}+f_{wlr}\end{aligned} \tag{1-63}$$

$$\begin{aligned}(1-\alpha)\rho_l\left(\frac{\partial V_{l\theta}}{\partial t}+V_{lr}\frac{\partial V_{l\theta}}{\partial r}+\frac{V_{l\theta}}{r}\frac{\partial V_{l\theta}}{\partial \theta}+V_{lz}\frac{\partial V_{l\theta}}{\partial z}\right)\\ =-(1-\alpha)\frac{\partial P}{\partial \theta}-(1-\alpha)\rho_l g_\theta+f_{i\theta}+f_{wl\theta}\end{aligned} \tag{1-64}$$

In the above equations, the wall and interfacial drag force terms are simply denoted with directional subscripts while no further discussion on how these force terms are determined will be given here. The discrete forms of the momentum equations in three-orthogonal directions are lengthy because of the cross-derivative terms. Therefore, to illustrate the procedure to evaluate these terms, only the in R- and Z-directional components of the gas momentum equation are presented here.

$$\frac{V_{g6}^{n+1} - V_{g6}^{n}}{\Delta t} + \left(V_{gr}\frac{\partial V_{gz}}{\partial r} + V_{g\theta}\frac{\partial V_{gz}}{\partial \theta} + V_{gz}\frac{\partial V_{gz}}{\partial z} \right)\Bigg|_{i,j,k+1/2} = -\frac{1}{\langle \rho_g \rangle_6^n}\frac{P_{i,j,k+1}^{n+1} - P_{i,j,k}^{n+1}}{\Delta z_6} + \frac{1}{\langle \alpha \rho_g \rangle_6^n}(f_{iz} - f_{wgz}) - g_z \Delta h_6 \tag{1-65}$$

$$\frac{V_{g2}^{n+1} - V_{g2}^{n}}{\Delta t} + \left(V_{gr}\frac{\partial V_{gr}}{\partial r} + \frac{V_{g\theta}}{r}\frac{\partial V_{gr}}{\partial \theta} - \frac{V_{g\theta}^2}{r} + V_{gz}\frac{\partial V_{gr}}{\partial z} \right)\Bigg|_{i+1/2,j,k} = -\frac{1}{\langle \rho_g \rangle_2^n}\frac{P_{i+1,j,k}^{n+1} - P_{i,j,k}^{n+1}}{\Delta r_2} + \frac{1}{\langle \alpha \rho_g \rangle_2^n}(f_{ir} - f_{wgr}) - g_r \Delta h_2 \tag{1-66}$$

where the cross-derivative terms of the Z-direction gas momentum are given by the following equations. To maintain a simple notation, the subscripts in the following equations are omitted unless the subscript points to a cell other than Cell (i, j, k).

$$V_{gr}\frac{\partial V_{gz}}{\partial r}\Bigg|_{i,j,k+1/2} = \mathrm{Min}\left[\frac{V_{g2}\Delta z + V_{g2,k+1}\Delta z_{k+1}}{\Delta z + \Delta z_{k+1}}, 0 \right]\frac{V_{g6,i+1} - V_{g6}}{\Delta r_2} + \mathrm{Max}\left[\frac{V_{g1}\Delta z + V_{g1,k+1}\Delta z_{k+1}}{\Delta z + \Delta z_{k+1}}, 0 \right]\frac{V_{g6} - V_{g6,i\text{-}1}}{\Delta r_1} \tag{1-67}$$

$$V_{g\theta}\frac{\partial V_{gz}}{\partial \theta}\bigg|_{i,j,k+1/2} = \mathrm{Min}\left[\frac{V_{g4}\Delta z + V_{g4,k+1}\Delta z_{k+1}}{\Delta z + \Delta z_{k+1}}, 0\right]\frac{V_{g6,j+1} - V_{g6}}{\Delta\theta_4} + \mathrm{Max}\left[\frac{V_{g3}\Delta z + V_{g3,k+1}\Delta z_{k+1}}{\Delta z + \Delta z_{k+1}}, 0\right]\frac{V_{g6} - V_{g6,j-1}}{\Delta\theta_3} \quad (1\text{-}68)$$

In Equations (1-67) and (1-68), Min and Max are the mathematical functions of minimum and maximum values of the terms inside the brackets. Analogous expressions hold for the other cross-derivative terms. The derivative terms in the direction of flow continue to be defined by Equations (1-19) and (1-20).

The next significant difference between the one- and three-dimensional field equations of TRAC is in the sum terms which signify the net flow of quantities across a computational volume. As the number of faces increase from two to six, the terms which were previously defined by Equations (1-20) to (1-26) must be redefined to include the flow through Faces 1 to 4 shown in Figure 1-3 (i.e. radial and azimuthal flows). Using the face number notation from Figure 1-3, the flux sum terms are redefined as follows.

$$\sum \phi_g = \phi_{g2} - \phi_{g1} + \phi_{g4} - \phi_{g3} + \phi_{g6} - \phi_{g2} \quad (1\text{-}69)$$

$$\sum \phi_l = \phi_{l2} - \phi_{l1} + \phi_{l4} - \phi_{l3} + \phi_{l6} - \phi_{l2} \quad (1\text{-}70)$$

$$\sum \zeta_g = \zeta_{g2} - \zeta_{g1} + \zeta_{g4} - \zeta_{g3} + \zeta_{g6} - \zeta_{g2} \quad (1\text{-}71)$$

$$\sum \zeta_l = \zeta_{l2} - \zeta_{l1} + \zeta_{l4} - \zeta_{l3} + \zeta_{l6} - \zeta_{l2} \quad (1\text{-}72)$$

$$\sum \omega_g = \omega_{g2} - \omega_{g1} + \omega_{g4} - \omega_{g3} + \omega_{g6} - \omega_{g2} \quad (1\text{-}73)$$

$$\sum \omega_l = \omega_{l2} - \omega_{l1} + \omega_{l4} - \omega_{l3} + \omega_{l6} - \omega_{l2} \tag{1-74}$$

where the flux terms are defined using the same face number notation.

$$\begin{aligned}
\phi_{gm} &= \langle \alpha \rho_g \rangle_m^n A_m V_{gm}^{n+1} \\
\phi_{lm} &= \langle (1-\alpha) \rho_l \rangle_m^n A_m V_{lm}^{n+1} \\
\zeta_{gm} &= \langle \alpha \rho_g e_g \rangle_m^n A_m V_{gm}^{n+1} \\
\zeta_{lm} &= \langle (1-\alpha) \rho_l e_l \rangle_m^n A_m V_{lm}^{n+1} \\
\omega_{gm} &= \langle \alpha \rangle_m^n A_m V_{gm}^{n+1} \\
\omega_{lm} &= \langle 1-\alpha \rangle_m^n A_m V_{lm}^{n+1}
\end{aligned} \tag{1-75}$$

where m =1,2,...,6. Just as for the one-dimensional field equations, the velocities in the above equation are eliminated in favor of the change in cell pressures (i.e. δP) using equations analogous to Equation (1-28). Next, Equations (1-31) to (1-35) are substituted into the mass and energy equations to obtain a linearized set of equations, which then can be solved iteratively following the same steps already described for the one-dimensional equations.

The Continuing Role of Thermal-Hydraulic Codes in Reactor Safety

One of the most debated issues in the field of reactor safety is the continued use of the three decade old TH codes. Developed in the late 70's, these codes continue to be the work horse of the industry and the regulatory agencies around the world. For instance, the US Nuclear Regulatory is currently consolidating its suite of thermal-hydraulic codes into a single code.[1-14] Although significant leaps are made in simulation technology in various industries, the nuclear industry remains behind these advances. While there are less limitations imposed by today's computing technology, the thermal-hydraulic simulations of the nuclear reactors remain as one of very chal-

lenging computing tasks. For example, the simulation of a nuclear reactor requires that the complex feedback mechanisms among different processes whose time and length scales differ by several orders of magnitude be handled very accurately, i.e. fluid flow, conduction and radiation heat transfer, and nuclear reactions. Further, there is an added complexity due to the control system mechanisms of the reactors such as emergency procedures, shut down mechanisms, valve operations, etc. The codes capable of simulating reactors with all of these details are continuously maintained and improved by the industry to handle more and more sophisticated designs of the new generation nuclear reactors. For example, the thermal-hydraulic model in Figure 1-4 is for one of the recent reactor designs. This model includes the reactor pressure vessel and its internals, valves of several different types, a steam generator, tanks holding emergency coolant supplies, etc.

It is extremely difficult for the industry to drop a proven (and tested) capability and switch to a revolutionary new approach. The best analogy can be made to the heavy bombers of the air force still in service. Some of these planes are flown by pilots who are several generations younger than their planes. While the fuselage of these planes have been the same shape since their inception, these planes did undergo significant upgrades including new flight controls, improved aerodynamic surfaces, and more powerful engines. The TH codes are the "heavy bombers" of the nuclear industry. Many analysts using these codes to simulate nuclear reactors are at least a generation or two younger than their computer codes. Just as the heavy bombers of the air force, the TH codes have been continuously maintained and upgraded to avoid falling behind the advances in computing technology. Some of the deficiencies described in this study and the remedies developed to cure these deficiencies may be a non-issue for more advanced computational methods for fluid flow. However, these new methods have not been applied to meet the needs of the nuclear industry and these deficiencies continue to have serious consequences in simulations of nuclear reactors.

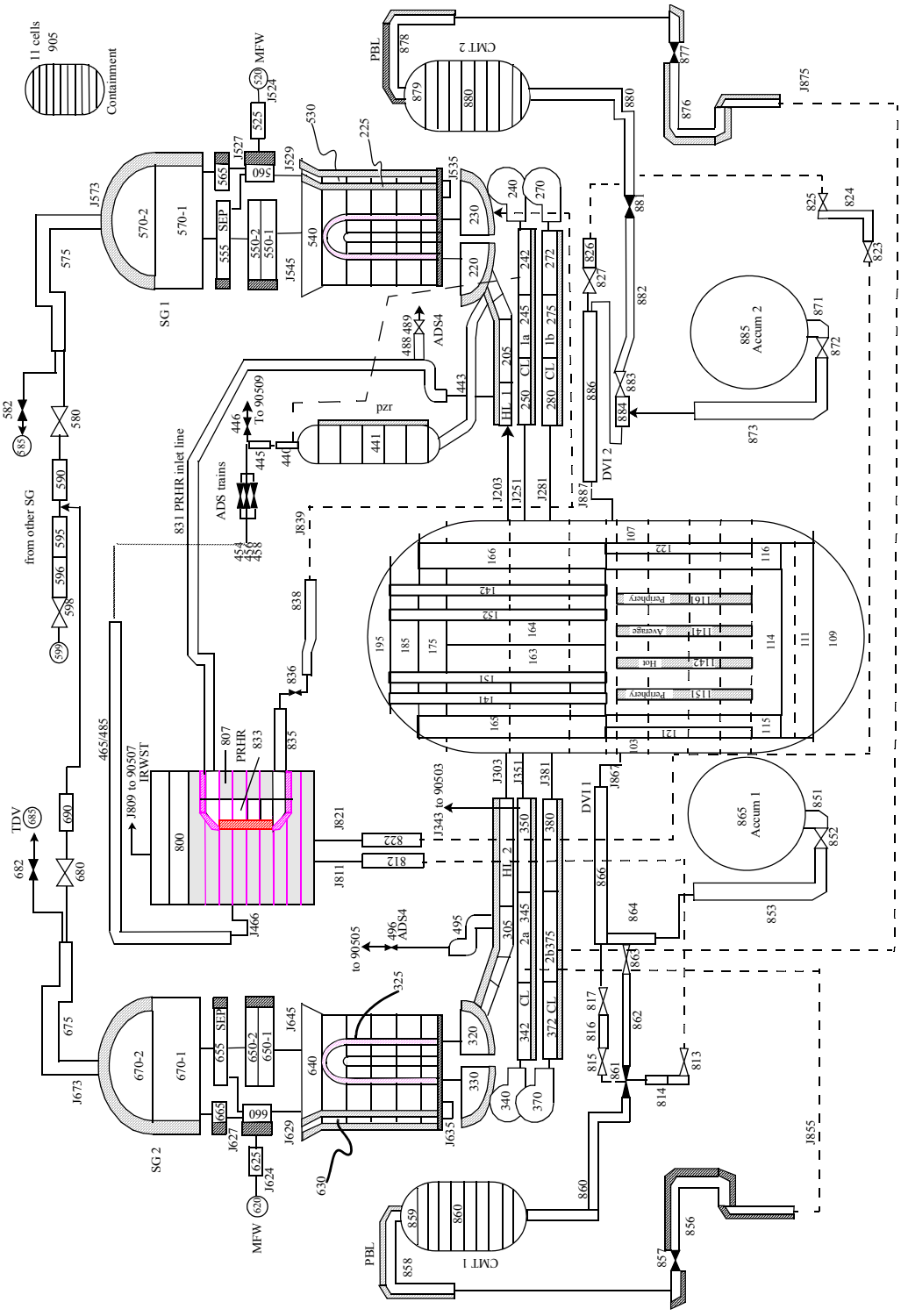

FIGURE 1-4. A thermal-hydraulic model of a nuclear plant (Courtesy of Rex Shumway)

References

1-1. Kojasoy, G., "Thermo-Fluid Dynamics of Separated Two-Phase Flow," Ph.D. Thesis, School of Mechanical Engineering, Georgia Institute of Technology (1971)

1-2. Ishii, M., "Thermo-Fluid Dynamic Theory of Two-Phase Flow," Eyrolles, Paris (1975)

1-3. Stuhmiller, J. H., "The Influence of Interfacial Pressure Forces on The Character of Two-phase Flow Model Equations," International Journal of Multiphase Flow, **3**, 551-560 (1977)

1-4. Deemer, A.R. and Slattery, J.C., "Balance Equations and Structural Models for Phase Interfaces," International Journal of Multiphase Flow, **4**, 171-192 (1978)

1-5. Drew, D. and Lahey, R., "Application of General Constitutive Principles to the Derivation of Multidimensional Two-phase Flow Equations," International Journal of Multiphase Flow, **5**, 243-264 (1979)

1-6. Addessio, F.L., "A Review of the Development of Two-Fluid Models," NUREG/CR-2146 (1981)

1-7. Steward, H.B. and Wendroff, B., "Two Phase Flow: Models and Methods," Journal of Computational Physics, **56**, 363-409 (1984)

1-8. Ransom, V. H. and Hicks, D. L., "Hyperbolic Two-Pressure Models for Two-Phase Flow," Journal of Computational Physics, **53**, 124 (1984)

1-9. Harlow, F.H. and Amsden, A.A., "A Numerical Fluid Dynamics Calculation Method for All Flow Speeds,"Journal of Computational Physics, **8**, 197-213 (1971)

1-10. Liles, D.R. and Reed, W. H., "A Semi-Implicit Method for Two-Phase Fluid Dynamics," Journal of Computational Physics, **26**, 390-407 (1978)

1-11. Spore et al., "TRAC-PF1/MOD2 Volume I. Theory Manual," NUREG/CR-5673 (1993)

1-12. Mahaffy, J.H, "A Stability-Enhancing Two Step Method For Fluid Flow Calculations," Journal of Computational Physics, **46**, 329-441 (1982)

1-13. Mahaffy, J. H., personal communication.

1-14. B. Aktas and J. Uhle, "USNRC Code Consolidation and Development Effort," Proceedings of the OECD-CSNI Workshop on Advanced Thermal-Hydraulic and Neutronic Codes: Current and Future Applications, Barcelona, Spain, (2000)

CHAPTER 2

Numerical Experiments With Moving Water Levels

Ensuring the stability and accuracy of the computational methods for simulating two-phase flows is relatively more difficult than it is for the methods for single-phase flows. There are numerous studies available in the literature which focus on the stability and accuracy of computational methods for two-phase flows. While the conventional forms of stability analysis highly abundant in these studies help to understand better the characteristics of computational methods, they are not sufficient to determine the overall stability of a method over a wide range of two-phase flow conditions expected during thermal-hydraulic simulations of nuclear reactors. Only the carefully constructed numerical experiments can provide such insight into the stability of these methods over the expected wide range of conditions.[2-1,2-2] One particular example is the concern over the stability and accuracy of a method when water levels are present in thermal-hydraulic simulations of nuclear reactors. The experience with the popular methods shows that the difficulties posed by water levels can plague a simulation unless the water levels are handled by a computational method with proper care.

This chapter presents a series of numerical experiments which put the spot light on areas where computational methods for solving the six-equation model exhibit serious failures when water levels are present in simulations. Also included

in this chapter are the results of simulations performed with TRAC that demonstrate the kinds of troubles suffered by most methods similar to the Semi-implicit/SETS method of TRAC.

Fill and Drain Test

A schematic diagram of the test problem is shown in Figure 2-2. The model consists of a vertical pipe with 1.0 m^2 axial flow area and 10.0 m height. A "T" branch with 0.5 m^2 axial flow area and 3.0 m height is connected to the bottom of the test pipe. There are two variations to this test problem. In the first case, liquid water is injected, at the side entry of the "T" branch, to raise the level of the liquid column and then withdrawn to let the level drop back to its starting location. In the second case, air is injected, at the bottom entry of the "T" branch, to maintain a steady mixture of liquid water and air under the standard room temperature and pressure conditions. Again, liquid water is first injected to raise the level of the mixture, and then withdrawn to let the level drop back to its starting location. The injection and withdrawal of liquid water in both cases at 1.0 m^3/s moves the level across one computational volume in every second.[2-3,2-4]

Conditions are subcooled and isothermal to remove any complications that may result from failures of interfacial heat transfer packages to account properly for the level. Gravity and interfacial drag between air bubbles and liquid water are the only forces that act on the fluid. The wall friction is suppressed in the test so that pressure below the level is due to the hydrostatic gravity head only. Moreover, the isothermal and subcooled conditions at the standard room temperature and pressure conditions force all interfacial mass transfer terms to zero. Hence the solution depends only on the terms of the six-equation model that describe the exchange of fluid by convection

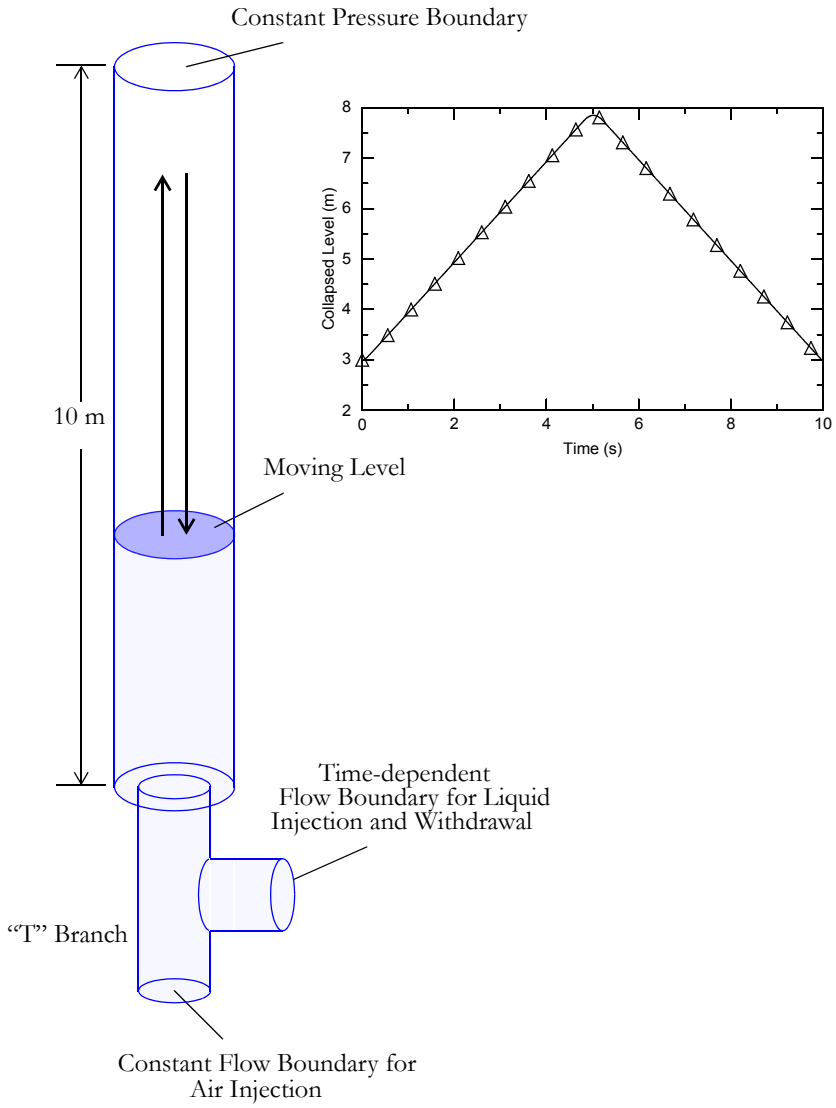

FIGURE 2-1. Schematic of the fill and drain test

across the boundaries of computational volumes and the momentum flux due to convection, interfacial drag, and gravity. The TRAC simulations of the fill and drain test are discussed below.

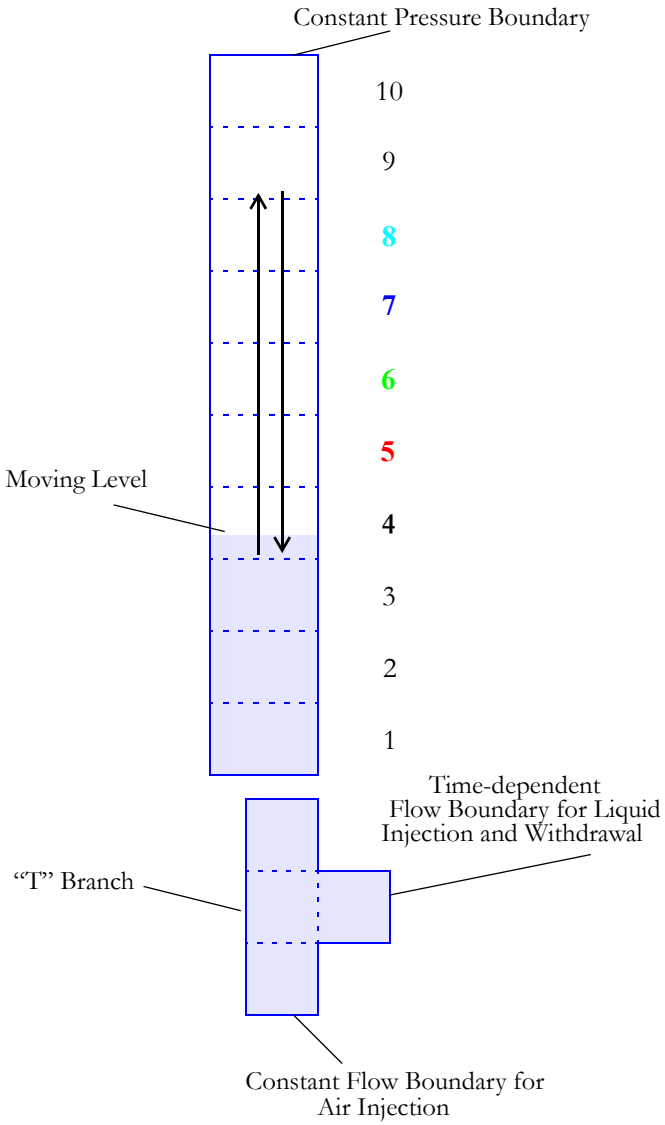

FIGURE 2-2. Schematic of the fill and drain test simulated using one-dimensional equations

Shown in Figure 2-2 is the computational model that represents the test pipe, made of ten equal computational volumes. Henceforth, the computational volumes will also be referred to as "cells."

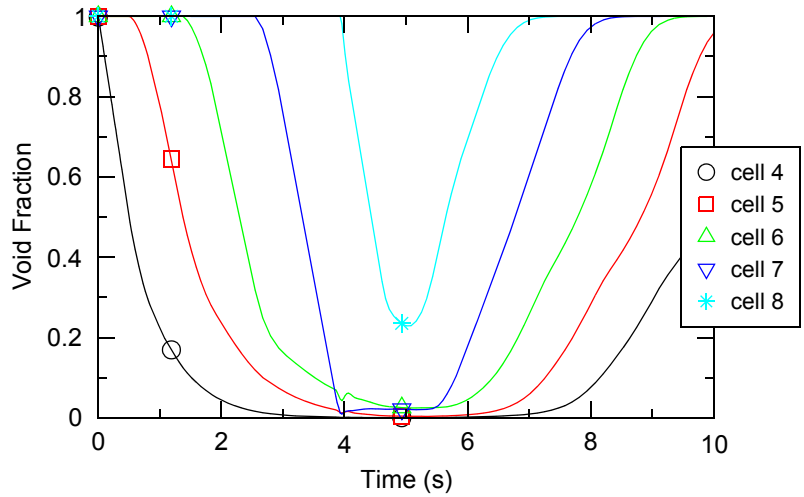

FIGURE 2-3. Void fractions of the single-phase fill and drain test (simulated with the standard method of solution)

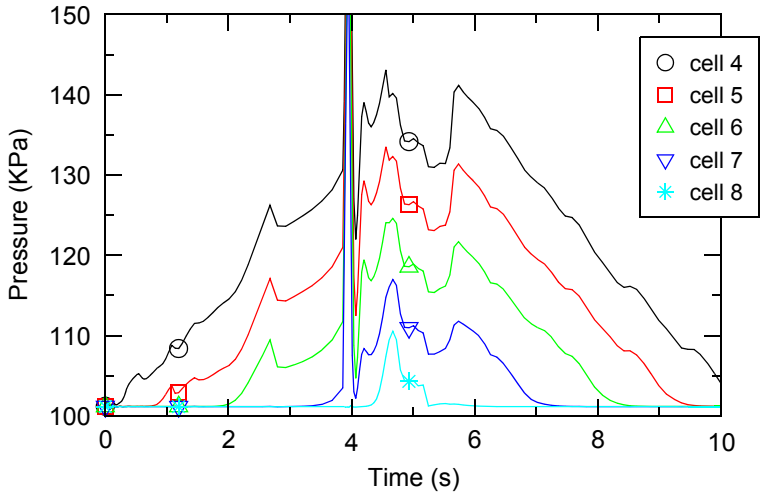

FIGURE 2-4. Pressures of the single-phase fill and drain test (simulated with the standard method of solution)

This test problem was simulated using the SETS method of TRAC with the standard upstream donor method. As shown in Figure 2-2, the collapsed water level given by $H_C(t) = \sum[1-\alpha_i(t)]\Delta x_i$, is rising and falling back to its starting location at a steady rate. The rising front is expected to fill the computational volumes at a steady rate starting from the bottom of the pipe and move to the next volume above once

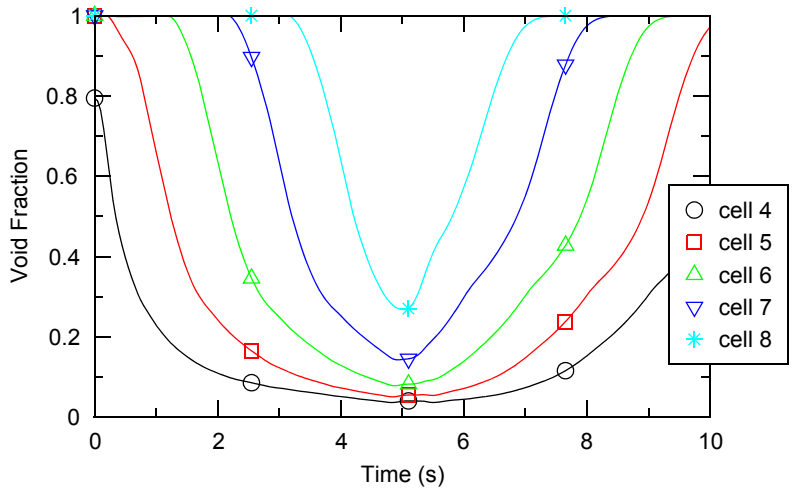

FIGURE 2-5. Void fractions of the two-phase fill and drain test (simulated with the standard method of solution)

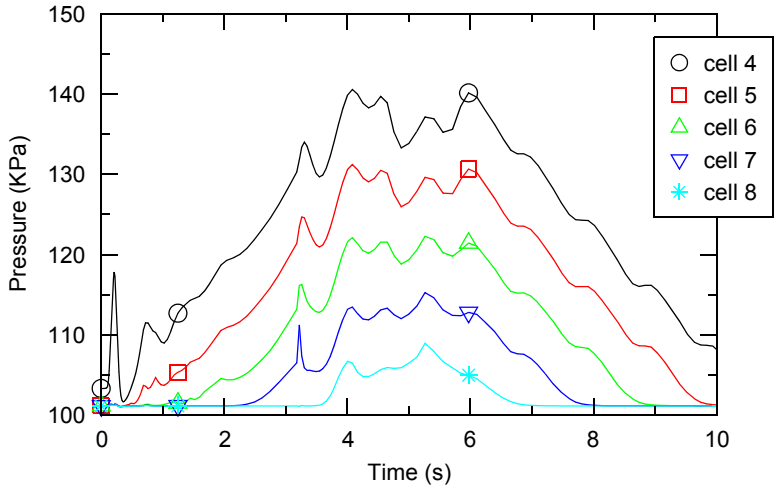

FIGURE 2-6. Pressures of the two-phase fill and drain test (simulated with the standard method of solution)

the volume being filled is full of liquid water. The SETS solution of TRAC with the standard upstream donor method fails to predict this expected behavior of cell void fractions as the water level rises. A plot of void fractions in Figure 2-3 shows that the liquid front moves to the next volume above, before the volume is fully liquid water, trapping a gas bubble behind. This distorted picture of the rising liquid front repeats itself as the water is drained from the test pipe and the water level drops back to its

starting location. The liquid front is smeared over several volumes as the descending liquid front leaves significant amount of liquid left behind in its tail. Due to smearing of the liquid front, the "predicted" cell pressures below the moving liquid front do not exhibit the expected behavior as well, i.e. a steady change proportional to the height of the rising and falling water level. Instead, the cell pressures below the water level increase and decrease sporadically indicating sudden acceleration and deceleration of the fluid, a behavior which is absolutely numerical in nature. Figure 2-5 and Figure 2-6 show that the SETS method with the standard donor method continues to suffer severely from similar difficulties when the fluid below the moving liquid front is a mixture of air and liquid water.

The fill and drain test in Figure 2-2 exercises the one-dimensional flow equations of TRAC. To exercise the three-dimensional flow equations in cylindrical coordinates, the fill and drain test was repeated using the VESSEL component of TRAC to simulate the vertical pipe in Figure 2-1. The VESSEL component in TRAC is nothing but a cylindrical tank that can consist of computational cells in three orthogonal directions of the cylindrical coordinate system. Figure 2-7 shows the two- and three-dimensional versions of the fill and drain test designed to exercise the three-dimensional field equations of TRAC. The two-dimensional version of the test pipe is divided into two "equal volume" cells in the R direction and ten "equal height" cells in the Z direction, and it consists a total of 20 computational cells. The two-dimensional pipe exercises the R- and Z-direction components of the field equations. The three-dimensional version of the test pipe is divided into eight "equal volumes" in the R-Θ plane and ten "equal height" levels in the Z direction, and it consists a total of 80 computational cells. The three-dimensional pipe exercises all of the directional components of the field equations making the test a very challenging one. As with the one-dimensional version of the test, the two- and three-dimensional versions of the test were repeated with the air-water mixture below the water level.

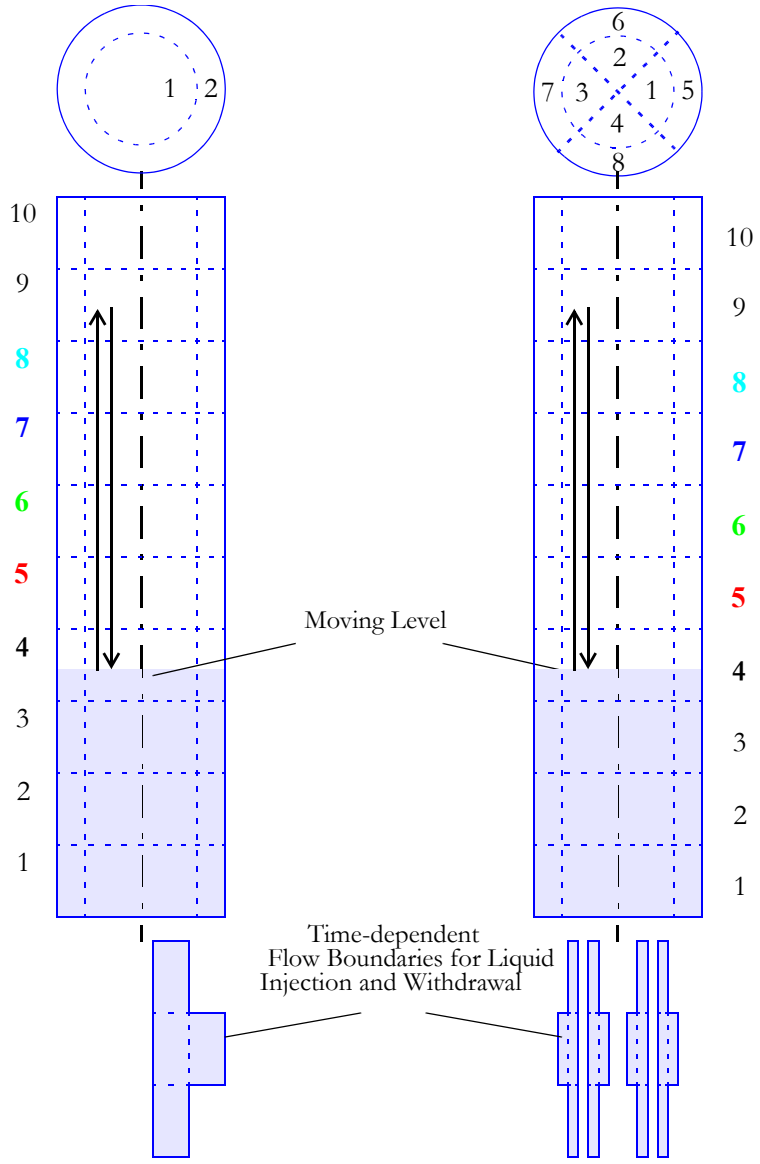

FIGURE 2-7. Schematic of the fill and drain tests that exercise the 2D and 3D field equations

It should be noted that the use of two- and three-dimensional computational cells allows more accurate modelling of expanding flow area from the "T" branch into the vertical test pipe. Certainly, this added detail increases the level of difficulty in simulating the fill and drain test.

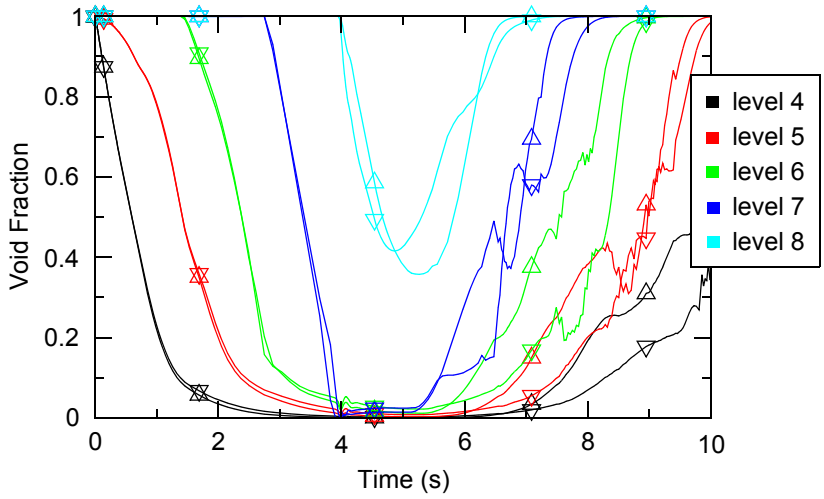

FIGURE 2-8. Void fractions of the 2D single-phase fill and drain test (simulated with the standard method of solution)

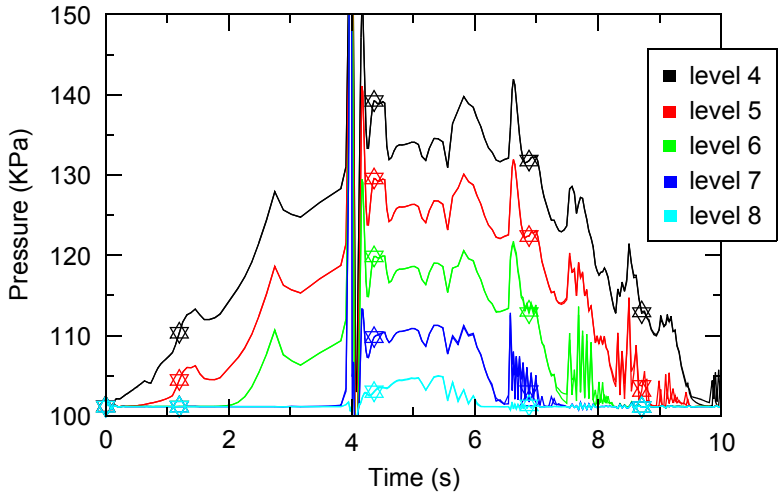

FIGURE 2-9. Pressures of the 2D single-phase fill and drain test (simulated with the standard method of solution)

The increased level of irregularities in the simulation results reveal that the Semi-Implicit/SETS method of TRAC, and the standard solution methods in general, suffer more severely when simulating the two- and three-dimensional versions of the fill and drain test. The signs of trouble are obvious in Figure 2-8 and Figure 2-10. The void fractions in the latter figure belong to the simulation repeated with the gas injection that created a steady mixture of liquid water and air bubbles inside the vertical

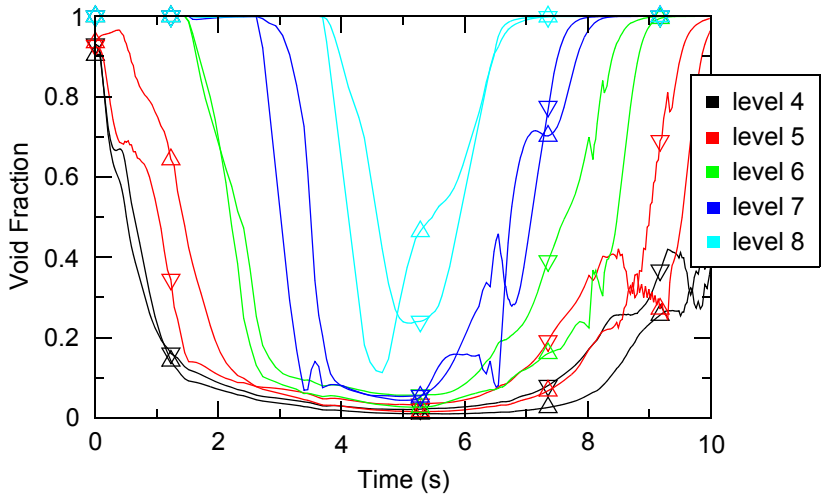

FIGURE 2-10. Void fractions of the 2D two-phase fill and drain test (simulated with the standard method of solution)

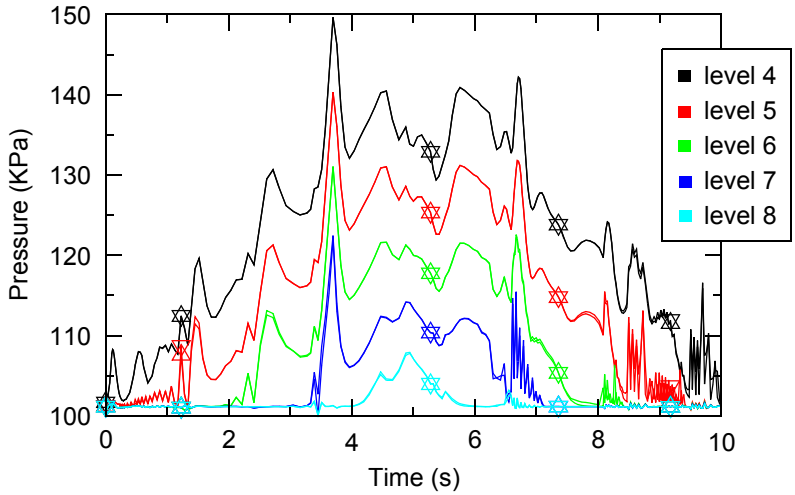

FIGURE 2-11. Pressures of the 2D two-phase fill and drain test (simulated with the standard method of solution)

pipe. In addition to the diffusive behavior already seen in the one-dimensional version of the test (Figure 2-3), the moving water level in the two-dimensional test is no longer stratified spreading over several cells in the lateral and vertical planes. Moreover, the void fractions predicted for the drain phase of the test indicate a break up of the liquid phase that results in pancaking of high and low void fraction regions near the water level. The spread of the water front is also apparent in the three-dimen-

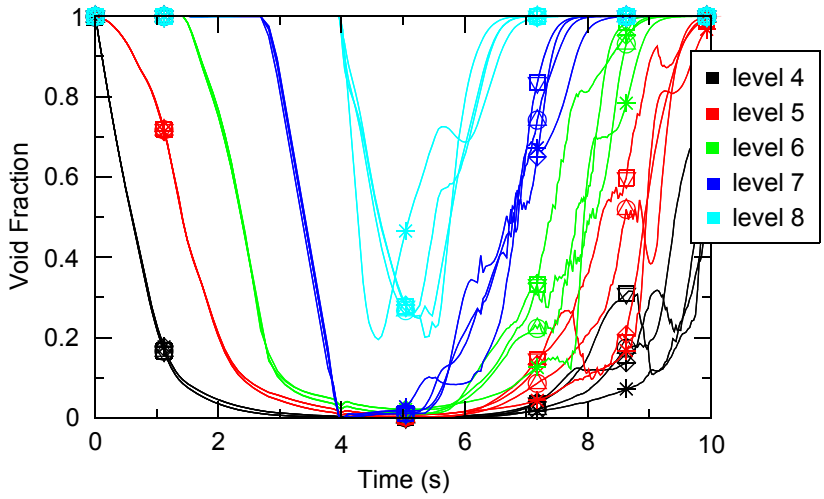

FIGURE 2-12. Void fractions of the 3D single-phase fill and drain test (simulated with the standard method of solution)

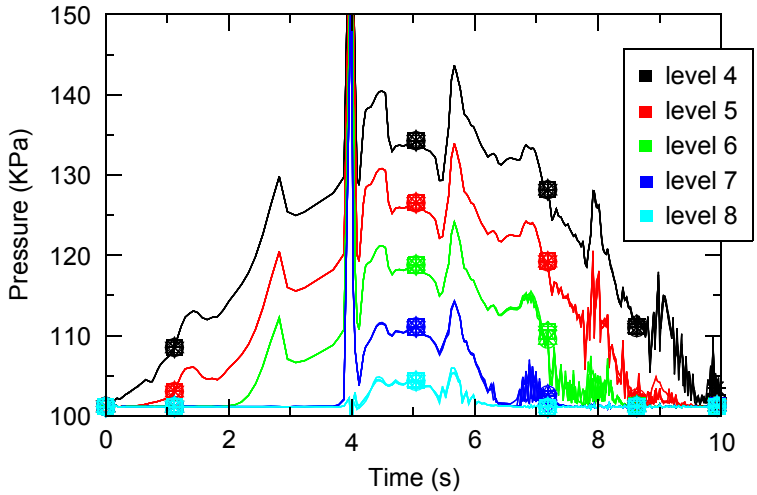

FIGURE 2-13. Pressures of the 3D single-phase fill and drain test (simulated with the standard method of solution)

sional version of the fill and drain test that exercises the Θ-direction field equations. As a consequence to these reversals in void fraction distribution in the axial and lateral planes, the simulations exhibit bounded oscillations in cell pressures as seen in Figure 2-9 and Figure 2-13.

The most challenging of all benchmarks presented here is perhaps the two-phase version of the three-dimensional fill and drain test. The void fractions of 40 cells, i.e.

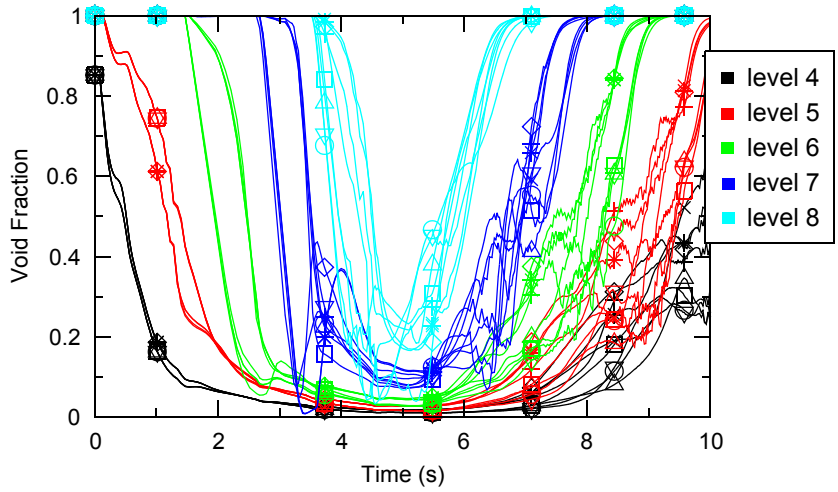

FIGURE 2-14. Void fractions of the 3D two-phase fill and drain test (simulated with the standard method of solution)

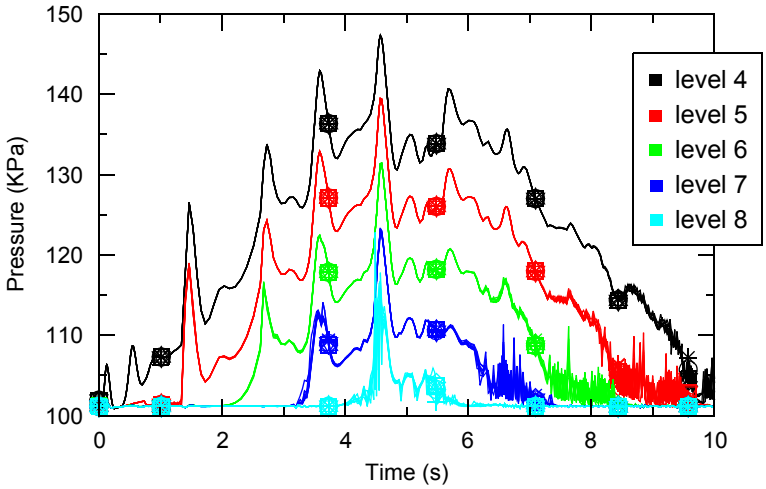

FIGURE 2-15. Pressures of the 3D two-phase fill and drain test (simulated with the standard method of solution)

eight cells per level, plotted in Figure 2-14 exhibit a very "chaotic" behavior. Unlike any of the previous simulations of the fill and drain test, the liquid-gas interface is smeared across several cells in the axial and lateral directions. The pressures of the same cells are plotted in Figure 2-15 exhibiting spike changes and oscillations. This test clearly demonstrate the need for improvement in TRAC to simulate the water levels more accurately.

Oscillating Manometer

The U-tube manometer in this test consists of gas and liquid with the liquid forming equal collapsed water levels in each arm. Initially, the liquid slug has a uniform velocity and no acceleration. The top of manometer arms are open to the standard room temperature and pressure conditions — it should be noted that the original benchmark problem connects the manometer arms at the top, forming a closed system. The schematic of the oscillating manometer test is given in Figure 2-16. Ransom specifies the problem,[2-6] "The initial conditions for the problem are: isothermal throughout at 50^{o}C temperature, pressure at the interfaces between the vapor and liquid equal to 1.01x10^{5} Pa, and corresponding hydrostatic pressures at all other points in the system, ... The initial position of the liquid-vapor interface is 5.0 m from the bottom of each manometer leg and all fluid initially has a velocity of 2.1 m/s. This initial velocity will cause the interface to oscillate approximately 1.5 m in height from the initial location... The system is adiabatic so that the thermal boundary condition is zero flux at the wall." Ransom further explains the objective of the problem is modeling the period of oscillation, which is analytically known; and evaluating the capability of the numerical discretization scheme to retain the liquid-gas interface.

An analytic solution for the water levels and the pressures at any location inside the two manometer arms can be obtained by applying a mechanical energy balance to the oscillating water slug. In the absence of any losses, the mechanical energy balance dictates that the gain of total potential energy is always equal to the loss of total kinetic energy and vice versa.[2-5]

$$\frac{dK}{dt} + \frac{d\Phi}{dt} = 0 \qquad (2\text{-}1)$$

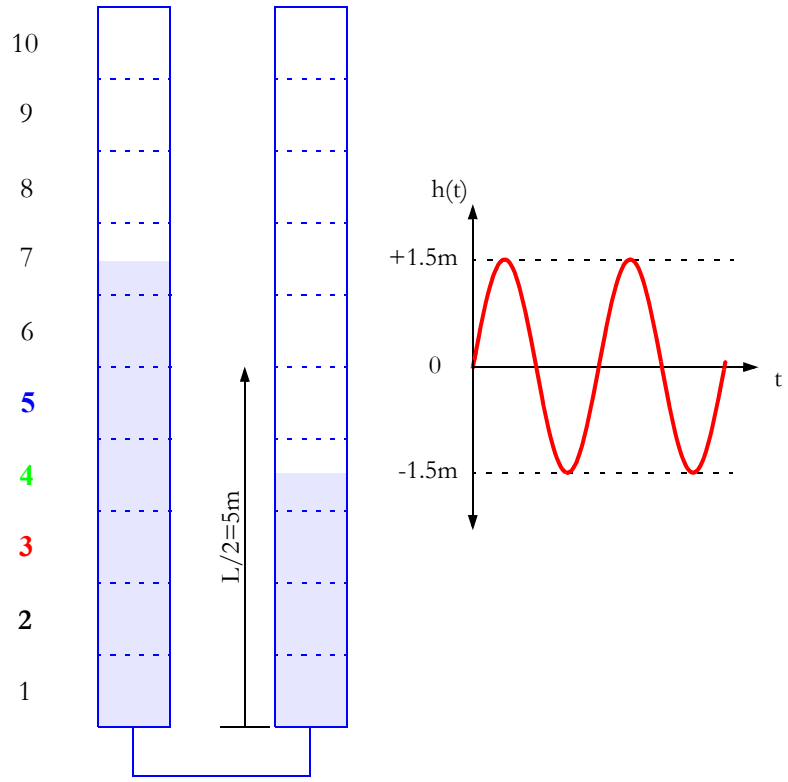

FIGURE 2-16. Schematic of the oscillating manometer test

Defining the length of the oscillating slug L, and the cross sectional area of the manometer arm S, the distance between the water level at any time to its initial position with H(t), and the velocity of the oscillating slug with V(t), the change of kinetic energy and potential energy with respect to time can be expressed as follows:

$$\frac{d}{dt}\left(\frac{1}{2}\rho V^2(t)SL\right) + \frac{d}{dt}\left(\int_0^{H(t)} \rho g S z dz + \int_{-H(t)}^{0} \rho g S z dz\right) = 0 \qquad (2\text{-}2)$$

$$LV(t)\frac{d}{dt}V(t) + 2gH(t)\frac{d}{dt}H(t) = 0 \qquad (2\text{-}3)$$

$$\frac{d^2}{dt}H(t) + \left(\frac{2g}{L}\right)H(t) = 0 \tag{2-4}$$

Equation (2-4) can be solved for the location of the manometer water level as function of time, i.e. *H(t)*, with the initial conditions that specify the initial position of the oscillating slug and its velocity:

$$H(t) = 0 \quad , \quad \left.\frac{dH}{dt}\right|_{t=0} = V_0 \tag{2-5}$$

The solution of Equation (2-4) yields the distance between the surface of the oscillating water levels and their starting location inside the left and right manometer arms:

$$H_L(t) = \frac{V_0 T}{2\pi}\sin\left(\frac{2\pi t}{T}\right) \text{ and } \quad H_R(t) = -H_L(t) \tag{2-6}$$

where the period of the oscillating manometer is found to be

$$T = 2\pi\sqrt{\frac{L}{2g}}. \tag{2-7}$$

Once the location of the oscillating manometer water level is known as a function of time, pressures at any point along the manometer arm can be determined from a simple force balance between the point of interest and the surface of the oscillating water level. The force balance should include the terms due to fluid acceleration and gravity.

$$\frac{\partial}{\partial t}V(x,t) = -\frac{1}{\rho}\frac{P_s - P(x,t)}{\xi(x,t)} - g \tag{2-8}$$

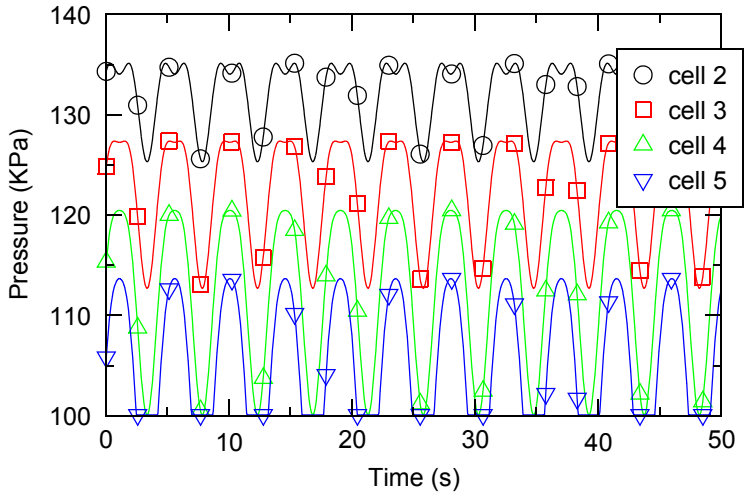

FIGURE 2-17. Manometer pressures predicted by a closed form solution

In the above equation, the length of the water slug between the surface of the oscillating water level and the point of interest is defined as follows:

$$\xi(x,t) = \begin{cases} \frac{L}{2} + H(t) - x & \text{, for } x < \frac{L}{2} + H(t) \\ 0 & \text{, for } x > \frac{L}{2} + H(t) \end{cases} \tag{2-9}$$

In Equation (2-9), variable x is the distance from the point of interest to the bottom of the manometer arm. The solution of Equation (2-8) for the locations below the oscillating water level then be becomes:

$$P(x,t) = P_S + \left[\frac{L}{2} + H(t) - x\right]\left[1 - \frac{2H(t)}{L}\right]\rho g \quad \text{for } x < \frac{L}{2} + H(t) \tag{2-10}$$

Equation (2-10) can be used to compute the cell pressures and then be compared to the TRAC solution. Figure 2-17 shows the resulting pressures from applying Equa-

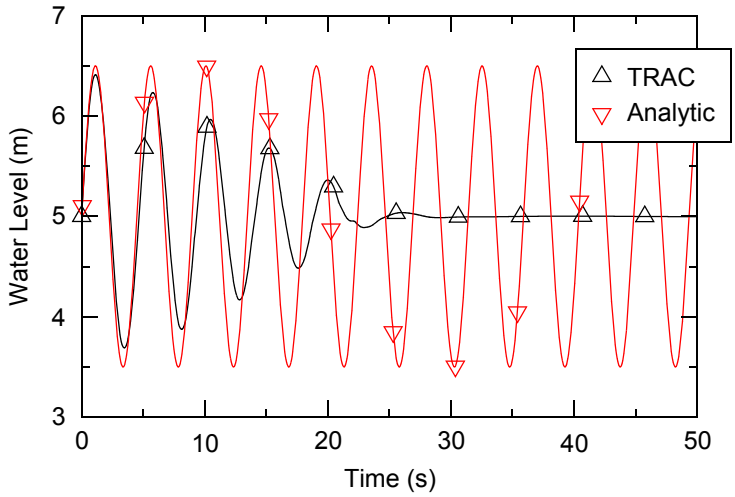

FIGURE 2-18. Water level of the oscillating manometer (simulated with the standard method of solution)

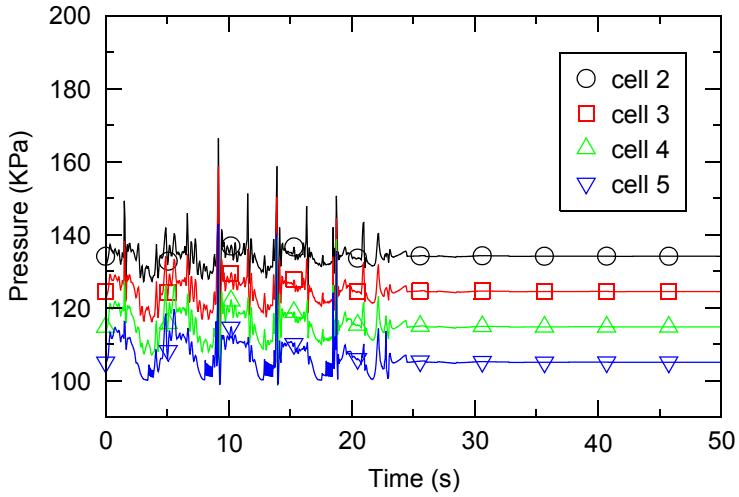

FIGURE 2-19. Pressures along the oscillating manometer arm (simulated with the standard method of solution)

tion (2-10) to the oscillating manometer test. A related variable which provides insight to the manometer test is the difference between the pressures at the same elevation of the two manometer arms. This variable, given in Equation (2-11), simply defines the net force acting on the segment of the manometer fluid between the two locations at the same elevation of the opposing arms. A program written in Fortran that computes the manometer pressures and the oscillating water level is provided in Appendix B.

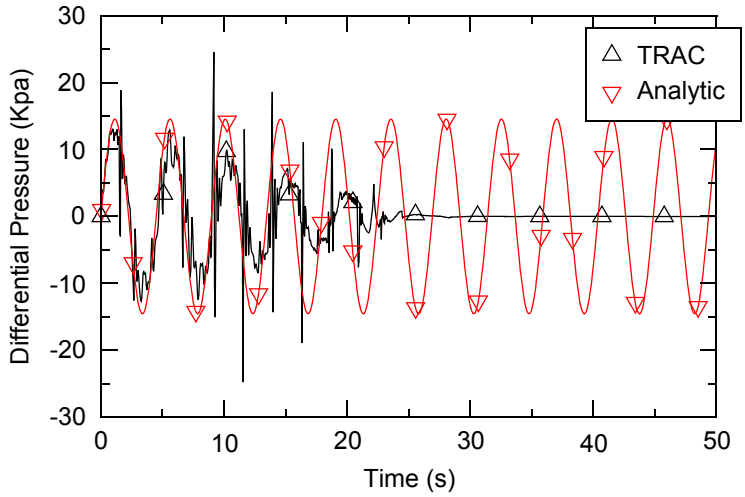

FIGURE 2-20. The net force on the fluid segment below 2.5m elevation of the manometer arms (simulated with the standard method of solution)

$$P_L(x,t) - P_R(x,t) = \frac{4x}{L}H(t) \tag{2-11}$$

For a manometer with 10m long oscillating water slug and 2.1m/s initial velocity, Equation (2-6) gives an oscillation amplitude of 1.5m measured from its starting location. Based on Equation (2-7), the period of these oscillations should be 4.48 seconds.

This test problem was simulated using the Semi-Implicit method of TRAC. The results show that the standard solution method fails to simulate the manometer oscillations. Figure 2-18 compares the collapsed water level predicted by TRAC to the oscillating water level predicted by Equation (2-6). A comparison of the pressures along the manometer arm predicted by TRAC (Figure 2-19) and predicted by Equation (2-10) (Figure 2-17) reveals that the standard solution method of TRAC dissipates the kinetic energy of the oscillating fluid very quickly. This conclusion is more obvious when the net force acting on a given segment of the oscillating fluid described by Equation (2-11) is considered. Figure 2-20 compares the net force acting on a segment of oscillating fluid contained between 2.5m elevation in one manometer

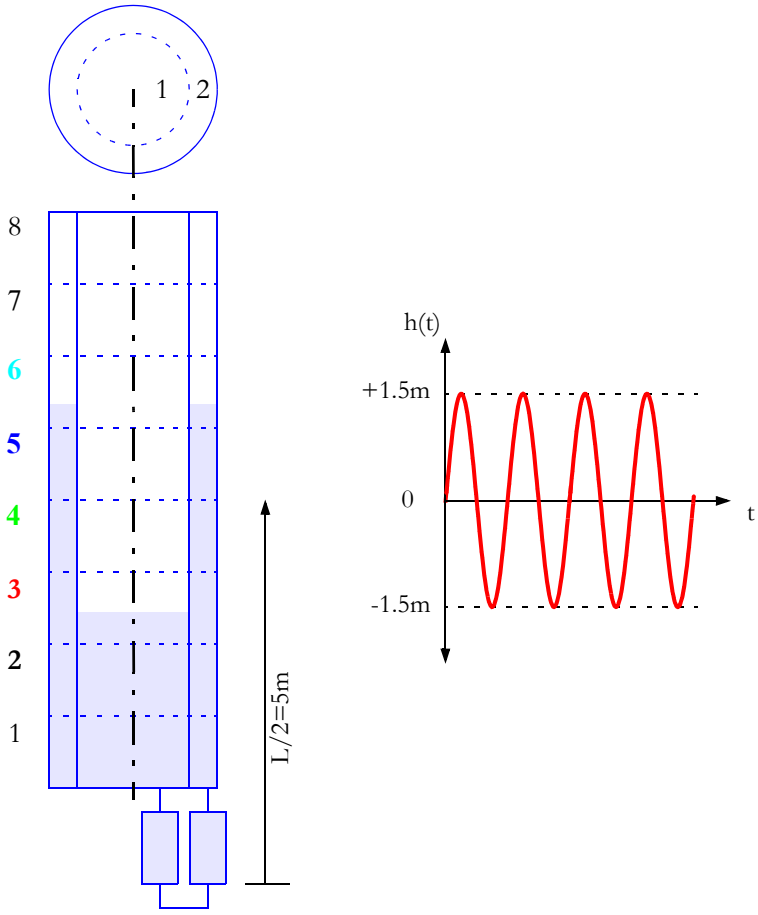

FIGURE 2-21. Schematic of the oscillating manometer formed by two 2D concentric cylinders

arm to 2.5m elevation in the opposing arm. This comparison concurs that the solution with the upwind donor method quickly dissipates the kinetic energy of the oscillating fluid. It is therefore concluded that the standard solution method of TRAC, i.e. Semi-Implicit method, fails to simulate the oscillating manometer test.

Next, the oscillating manometer is modified to exercise the Z-direction component of the three-dimensional field equations in cylindrical coordinates. In the repeat simulation, the manometer arms are formed by two concentric cylinders. The flow

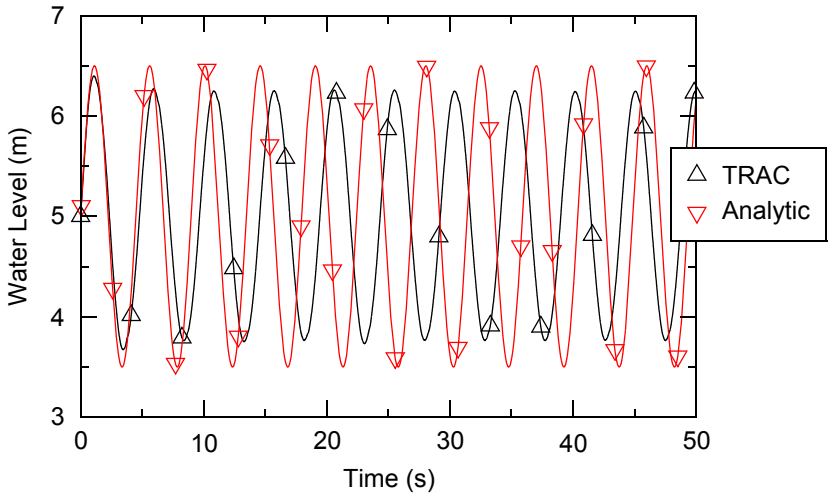

FIGURE 2-22. Collapsed levels of the 2D oscillating manometer test (simulated with the standard method of solution)

areas of the annulus region and the inside cylinder are kept identical. The length of the oscillating liquid slug is kept at 10 m by modeling the 1 m section at the bottom with two separate one-dimensional volumes as the frequency of manometer oscillations is a function of the slug length. The initial and boundary conditions for the problem remain identical to the conditions of one-dimensional manometer test.

The Semi-implicit method, i.e. the standard method of solving the field equations in TRAC, was used to simulate this two-dimensional version of the oscillating manometer. Figure 2-22 compares the collapsed water level predicted by the TRAC solution to the level obtained analytically from (2-6). While Figure 2-22 can be used to argue that the three-dimensional field equations had some limited success in simulating the oscillating manometer, the deviations from the frequency and amplitude of the expected oscillations is a source of concern. In Figure 2-23, the pressures of computational volumes inside the annulus region reveals that the fluid experiences bounded oscillations in pressure dissipating its momentum. However, the fluid also experiences occasional spike changes in pressure adding to its momentum. The comparison of the differential pressure between fluid inside and outside the inner cylinder

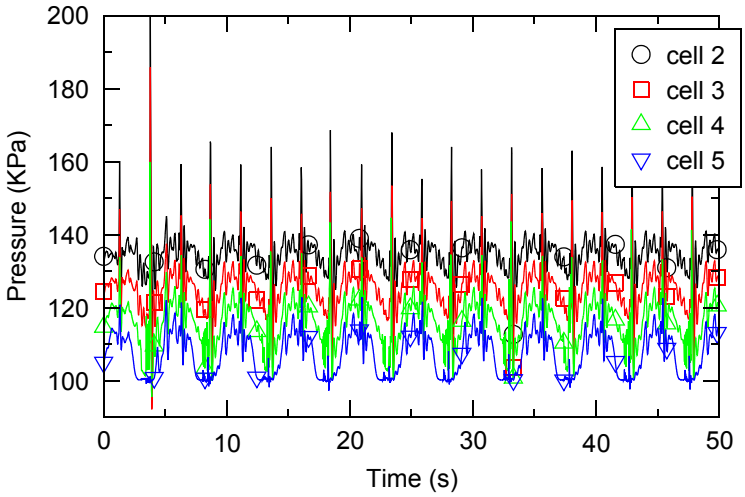

FIGURE 2-23. Pressures along the 2D oscillating manometer arm (simulated with the standard method of solution)

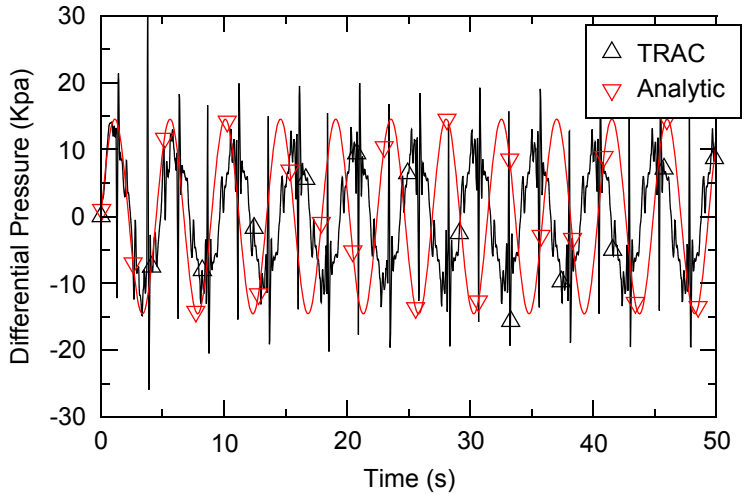

FIGURE 2-24. The net force on the fluid segment below 2.5 elevation of the manometer arms (simulated with the standard method of solution)

at 2.5 m elevation further supports this analysis. Figure 2-22 is therefore a good example why one should not judge a method for its ability to simulate the oscillating manometer by simply tracing the location of the water level.

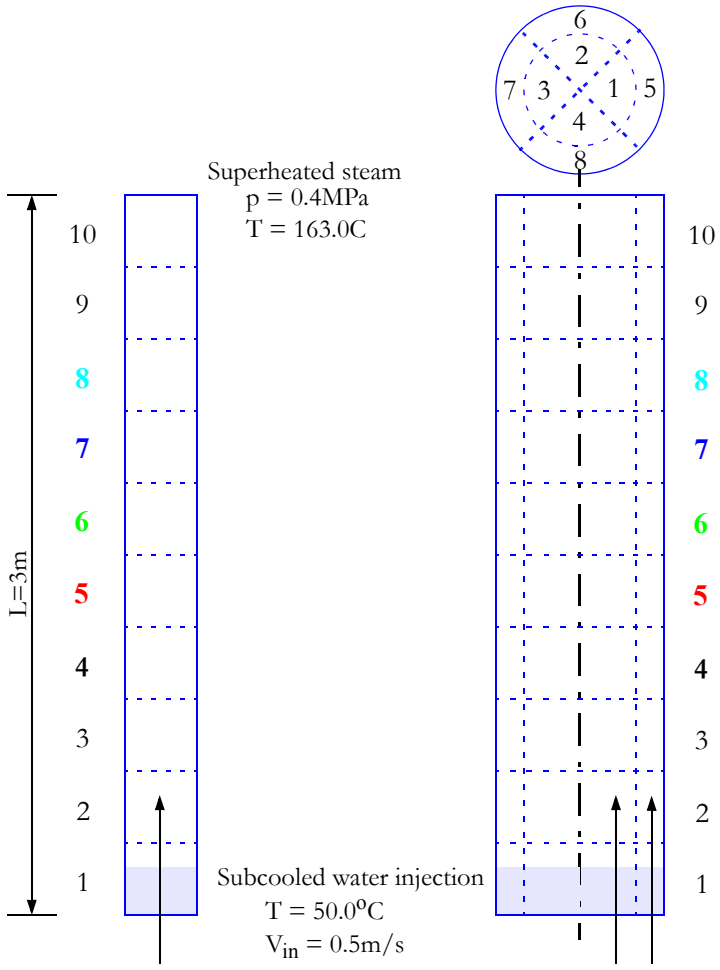

FIGURE 2-25. Schematic of the 1D and 3D condensation tests

Expulsion of Superheated Steam by Subcooled Water

The purpose of this test problem is to study the complications in the solution to the six-equation model resulting from failures of the interfacial heat transfer model to account properly for the water levels. The problem, which will be referred to as the "condensation test" from hereon, consists of a vertical pipe, 3m in height and 1m in diameter, initially filled with superheated steam at constant temperature and pressure

of 163^{o}C and 0.4MPa respectively. The vertical pipe is connected to a very large reservoir of steam. The computational model divides the vertical pipe into ten equal computational volumes. A schematic diagram of the test problem is shown in Figure 2-25. Also shown in Figure 2-25 is the three-dimensional version of the same test that divides the vertical pipe into 80 equal computational volumes. During the test, liquid water subcooled at 50^{o}C is injected with 0.5 m/s velocity at the bottom inlet of the pipe until it fills the pipe completely.[2-7]

This test problem was designed to measure the ability of a solution method to cope with the difficulties which arise from inaccurate modelling of the computational volumes as they are filled by the rising liquid front. Predicting the interfacial heat transfer rate in these volumes, and thereof, the condensation of superheated steam in contact with the very subcooled water is very critical to the successful simulation of this test. There is also an added complexity as a saturated layer of liquid builds up in the tail of the rising front that should continuously decrease the condensation rate. A solution method without proper care for these details is expected to suffer severely as a cell becomes "packed" with liquid water when the method fails to turn off the condensation behind the rising liquid front.

The recommended maximum time step size for the simulation of this test is 0.05 seconds.

The standard solution method of TRAC displays the expected difficulties due to water packing and inaccurate modeling of the condensation at the rising liquid front. Figure 2-26 shows the pressures at each computation volume along the pipe as the subcooled water is injected. The presence of the water packing phenomenon is apparent in this figure. The magnitude of the resulting compression waves from the "numerical" water hammer reaches to 2.5 MPa rendering the TRAC solution unus-

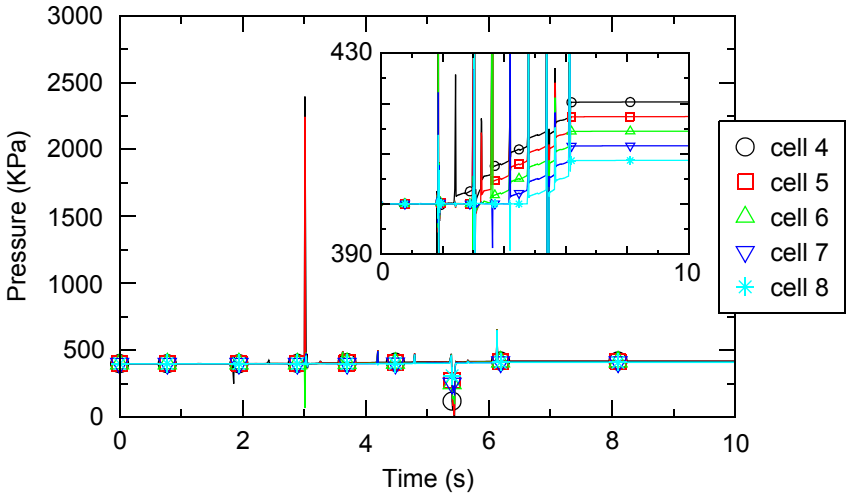

FIGURE 2-26. Pressures along the condensation test pipe (simulated with the standard method of solution)

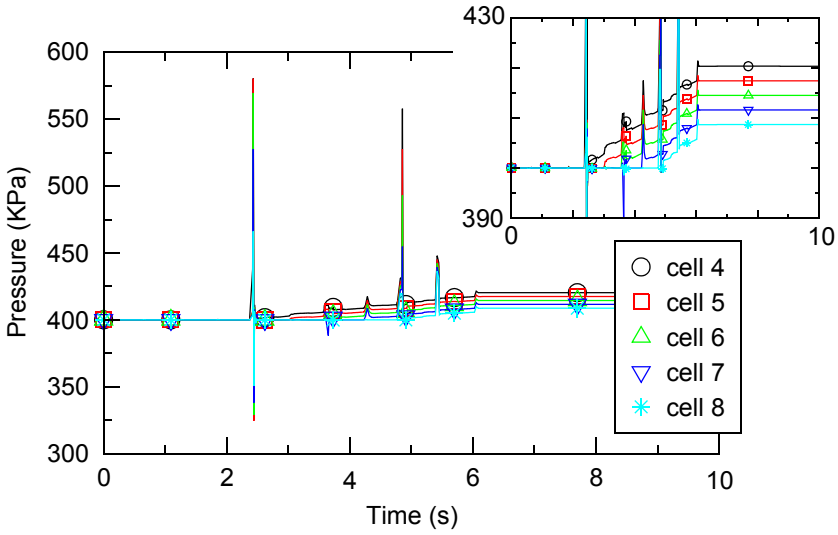

FIGURE 2-27. Pressures along the condensation test pipe (simulated with the standard option for water packing treatment)

able. Before drawing a conclusion on the performance of TRAC, the water packing option, an optional method that overcomes the fluid packing problem by dampening the pressure field, must be engaged in the simulation of the condensation test. Figure 2-27 shows the pressures along the test pipe recomputed by TRAC with the water packing option. Although the amplitude of pressure spikes are several times smaller, their mere presence is sufficient to prove that the standard method of solution even

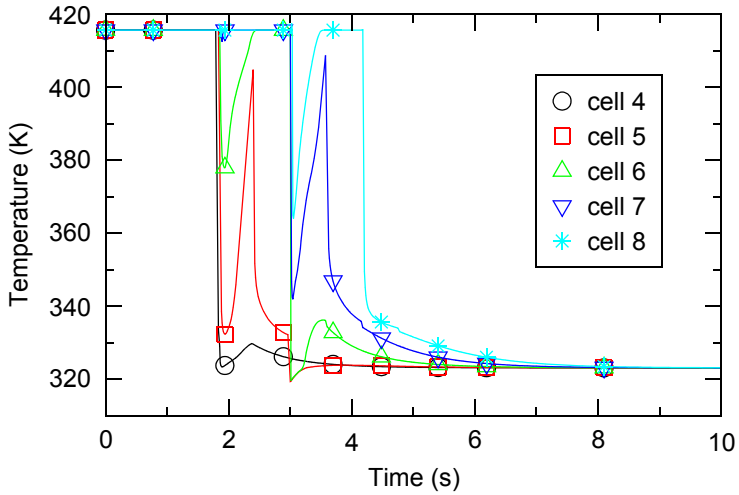

FIGURE 2-28. Liquid temperatures along the condensation test pipe (simulated with the standard method of solution)

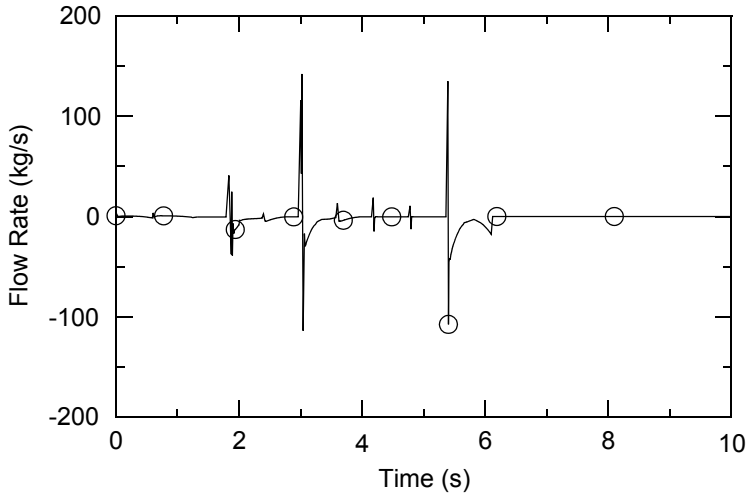

FIGURE 2-29. Steam flow at the top of the condensation test pipe (simulated with the standard method of solution)

with the help from a special method is still unable to properly handle the steam condensation at the rising liquid front.

Another variable of equal interest is the liquid temperature along the pipe which is expected to indicate the build up of a saturated liquid layer behind the rising front. Figure 2-28 shows that the liquid temperatures rather closely follow the sub-cooled temperature with occasional jumps to the saturation temperature in the vicinity of the

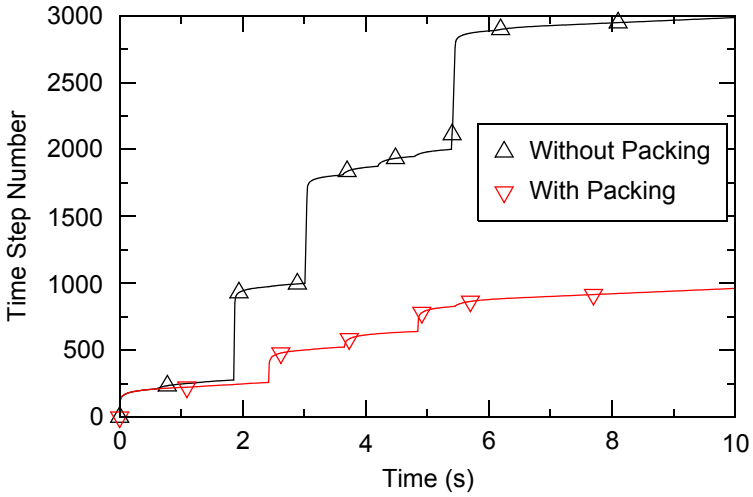

FIGURE 2-30. Comparison of total time step numbers of condensation test simulations (with and without the option for water packing treatment)

rising front. As sub-cooled water is injected at the bottom, superheated steam is withdrawn into the pipe at the top replenishing the steam being condensed at such extreme rates. Normally, the direction of steam flow should be an outcome of a balance between the volume rate at which liquid displaces steam and the volume rate at which steam is being condensed at the front. However, the compression waves induced by the fluid packing dominates the TRAC solution causing high bursts of steam flowing out of the test pipe as seen in Figure 2-29.

It should also be noted here that the water packing option of TRAC, at least, achieves a limited success by reducing the severity of the failures mentioned above. This limited success is evident in Figure 2-30 that compares the timesteps number as function of the simulation time for the two cases: 1) without the water packing option, 2) with the water packing option.

The test simulations repeated using a three-dimensional computational mesh exhibited similar troubles. First, the standard solution method of TRAC was exercised. Pressures from this exercise are shown in Figure 2-31. The severity of spike

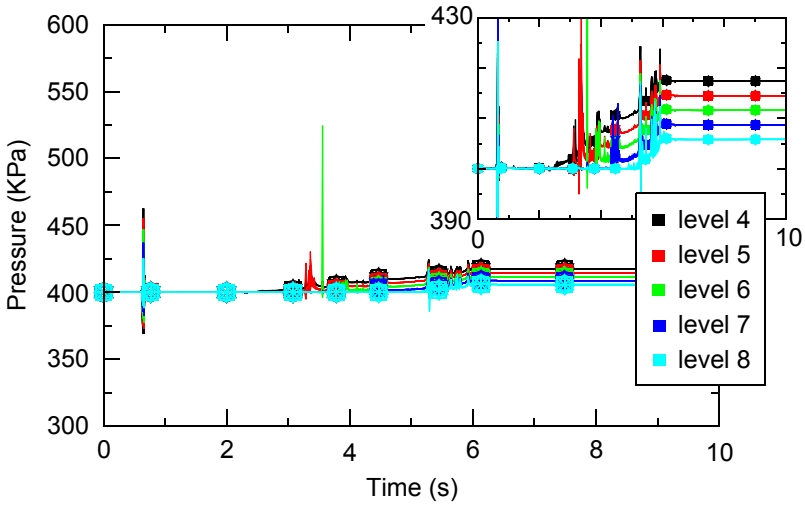

FIGURE 2-31. Pressures along the 3D condensation test pipe (simulated with the standard method of solution)

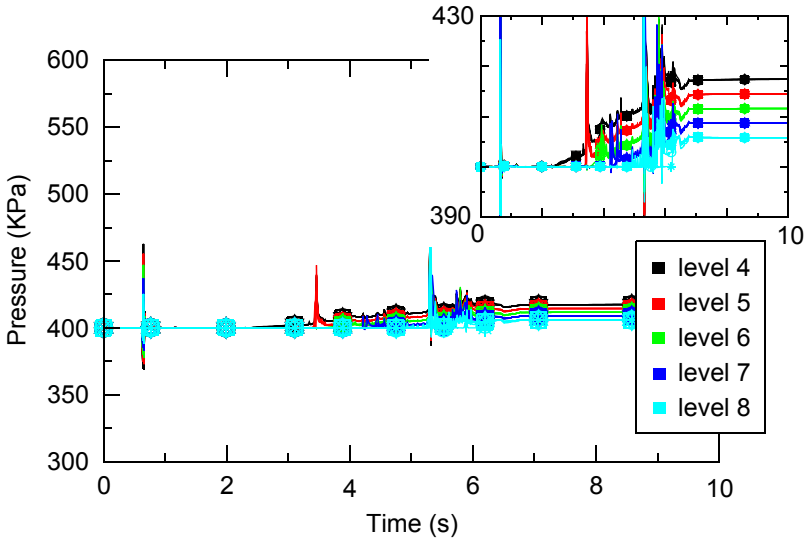

FIGURE 2-32. Pressures along the 3D condensation test pipe (simulated with the standard option for water packing treatment)

changes in cell pressures is at a minimum in comparison to the one-dimensional version of the same test (see Figure 2-26). Water packing does not dominate the simulation of the three-dimensional condensation test because it is a phenomenon mainly one-dimensional in nature. Unlike a one-dimensional volume with only two faces, a three-dimensional volume has six faces and it hardly becomes "packed." The pressures shown in Figure 2-32, which are the result of a TRAC simulation repeated with

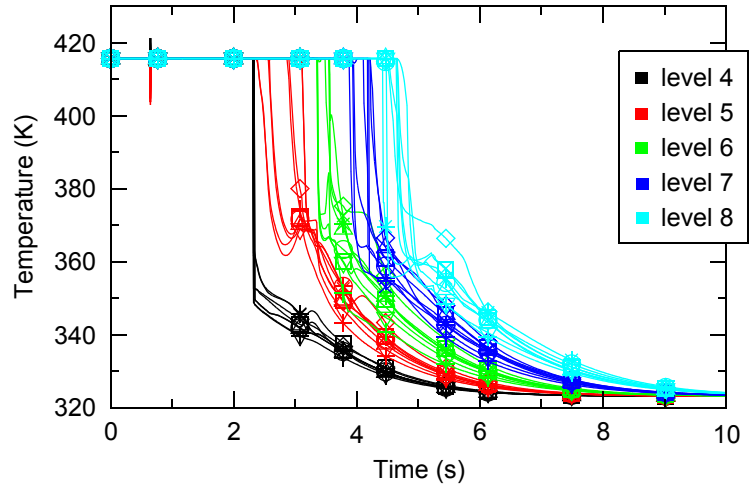

FIGURE 2-33. Liquid temperatures along the 3D condensation test pipe (simulated with the standard method of solution)

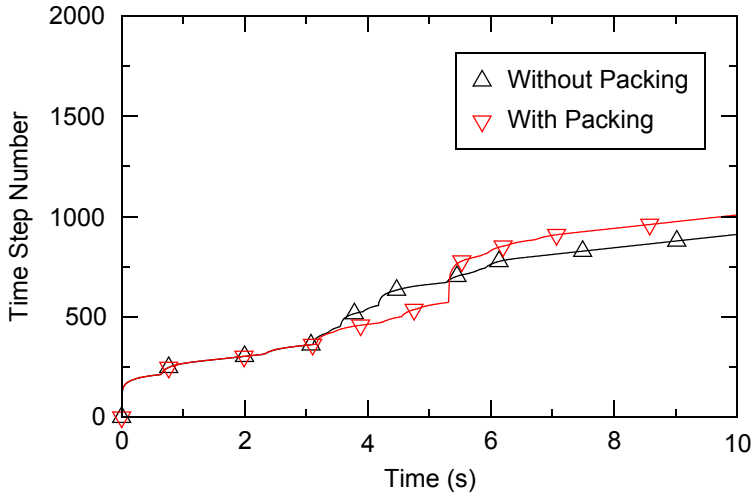

FIGURE 2-34. Comparison of total time step numbers of the 3D condensation test simulations (with and without the option for water packing treatment)

the water packing option, support this conclusion as there is very little difference between them and the pressures in Figure 2-31. The close-up in Figure 2-32 even suggests that the simulation with the water packing option suffers from more numerical troubles which are hinted by the increased level of bounded oscillations. Furthermore, the liquid temperatures shown in Figure 2-33 illustrate how the failure of TRAC to capture the rising cold front in three dimensions add to the complexity of the simula-

tion. For some of the axial levels in Figure 2-33, the adjacent cells registered liquid temperatures which were at least 50^{o}C apart behind the rising front. Figure 2-34 compares the number of time steps required to simulate the condensation test with the standard solution and with the solution aided by the water packing model. Clearly, the water packing model has very little effect on the solution.

In conclusion, TRAC fails to predict the constant rate of condensation along the test pipe. As the rising front passes through a cell, the condensation reaches extremely high rates due to apparent problems with the interfacial heat transfer between liquid and gas fields. The root cause of this failure should be sought in the interfacial heat transfer model and its inability to properly describe cells that consist of phases separated by a moving phase front.

A Summary of the Simulations with TRAC's Standard Method of Solution

All of the test problems discussed in this chapter are designed to measure the performance of the semi-implicit method of solution to the six-equation model in the presence of moving water levels. However, it should also be emphasized that these problems are designed to reveal the difficulties of a method and magnify them as much as possible, so that these difficulties can be identified and studied further.

The results of the numerical experiments presented in this chapter can summarized as follows:

- All of the tests reveal that the solution method in TRAC fails to predict accurately the acceleration of liquid and gas fields in vertical paths when both fields are separated by a stratified liquid-gas interface. This failure is evident from the figures that show the transient behavior of fluid pressure in all tests.

- The solution methods like the Semi-implicit method, which are equipped with the standard upstream donor method in general, are unable to retain the liquid-gas interface. The figures that show the void fraction along the test pipes suggest that numerical diffusion of fluid mass is very high in the presence of stratified liquid-gas interface. Unlike the diffusion due to the discrete nature of the solution, the root cause of this failure is hidden behind the inability of the upstream donor method to recognize that a computational volume consists of two sub-volumes separated by a liquid-gas interface.
- The mixture of steam and water poses added complexities due to the inability of the interfacial heat transfer model to distinguish the two sub-volumes, which are topologically different, separated by the liquid-gas interface. As the interfacial heat transfer model determines the heat transfer coefficients based on volume average void fraction, the interfacial heat transfer between the two fields is over or under predicted for the computational volume that consists of the liquid-gas interface.
- The current measures built into the solution method, e.g. the water packing option, have limited success in mitigating the consequences of numerical water hammer when the sudden condensation is initiated by moving liquid-gas interfaces.

References

2-1. Mahaffy, J.H., "Numerics of Codes: Stability, Diffusion, and Convergence," Nuclear Engineering and Design, **145**, 131-145 (1993)

2-2. Shieh, A.S., Krishnamurthy, R., and Ransom, V.H., "Stability, Accuracy, and Convergence of the Numerical Methods in RELAP5/MOD3," Nuclear Science and Engineering, **116**, 227-244 (1994)

2-3. Aktas, B. and Mahaffy, J.H., "Level Tracking in Detailed Reactor Simulations," Proceedings of the 7th International Meeting on Nuclear Reactor Thermal-hydraulics, New York, 2035-2044 (1995)

2-4. Aktas, B. and Mahaffy, J.H., "A Two-phase Level Tracking Method," Nuclear Engineering and Design, **162**, 271-280 (1996)

2-5. Aktas, B. and Mahaffy, J.H. "Enhanced Numerical Modeling of Manometer Based Oscillations by Discontinuity Tracking," Eleventh Proceedings of Nuclear Reactor Thermal Hydraulics, American Nuclear Society, San Francisko CA 101-109 (1995)

2-6. Ransom, V., "Numerical Benchmark Test No. 2.2: Oscillating Manometer," Multiphase Science and Technology, **6**, Hemisphere Publishing, New York, 591-609 (1992)

2-7. Ransom, V., "Numerical Benchmark Test No. 2.3: Expulsion of Steam by Subcooled Water," **6**, Hemisphere Publishing, New York, 611-621 (1992)

2-8. Mahaffy, J.H. and Liles, D.R., "Numerically Induced Pressure Excursions in Two-Phase Flow Calculations," Proceedings of the Second International Topical Meeting on Nuclear Reactor Thermal-Hydraulics, Santa Barbara CA (1983)

CHAPTER 3

Tracking Water Levels in One-Dimensional Flows

The numerical experiments presented in CHAPTER 2 reveal that the presence of water levels can severely plague the standard methods of solution to the six-equation model. These "thought" experiments also demonstrate that the use of an average void fraction for a computational volume can lead to erroneous description of a computational volume when it contains of a water level. A short analysis of the initial TRAC simulations of these tests reached a conclusion that such computational volumes indeed had two sub-volumes separated by the interface and each of these sub-volumes had their own distinct flow topology, e.g. the dispersed liquid droplets above the interface and the gas bubbles below. A further conclusion was drawn that for more accurate description of these divided computational volumes, regions above and below the interface ought to be treated separately requiring the use of separate void fractions inside each region as the outcome of closure models strongly depended on the flow regime and the flow regimes were strong functions of the "cell" void fraction.

Not only the void fractions must be known for the regions above and below the interface, but also the volumes of each region and the rate at which they change. Only when this additional information is known, can one modify a standard method of solution for the six-equation model such as Semi-Implicit or

SETS to accomplish a more accurate description of computational volumes with water levels inside them. This strategy of "tracking" to deal with water levels requires that the location of a water level, the volumes of regions above and below it, and the void fractions inside these regions be known at all times.

The idea of tracking water levels is not new. An example is the method which had been developed for the BWR version of TRAC to track water levels in BWR simulations. This method in TRAC-BWR, which had been applied to the transient simulations of BWRs with some limited success, permitted the use of very large volumes in building computational models of BWR pressure vessels. While tracking water levels had increased the solution method's resolution to locate the vessel penetrations within very large computational volumes, the users of TRAC-BWR had to be warned against potential flow oscillations, conflicting water levels, and pressure disturbances which could result from employing the level tracking method itself. For instance, the simulation of a natural circulation test (6PNC1-6) conducted at the Full Integral Scale Test (FIST) facility was cited in one of TRAC-BWR manuals for the problems with the level tracking.[3-1] Flow instabilities of purely numerical nature caused by the level tracking method were reported. In addition to the flow oscillations, spike changes were observed in cell pressures each time after a water level crossed across the boundaries between computational volumes. The use of level tracking in BWR simulations therefore required extreme care to ensure the fidelity of the reactor simulations.

Recently, this level tracking method of TRAC-BWR was incorporated into TRAC† as part of a larger effort to consolidate the capabilities of TRAC-BWR to simulate BWRs.[3-2] The numerical experiments presented in CHAPTER 2 were also repeated to test this level tracking method in TRAC. Results from some of these simulations

†. The reactor safety code referred to as TRAC here is the US NRC Consolidated Thermal-hydraulics Code (a.k.a. TRAC-M), and the code referred to as TRAC-BWR is TRAC-BF1/MOD1 of US NRC.

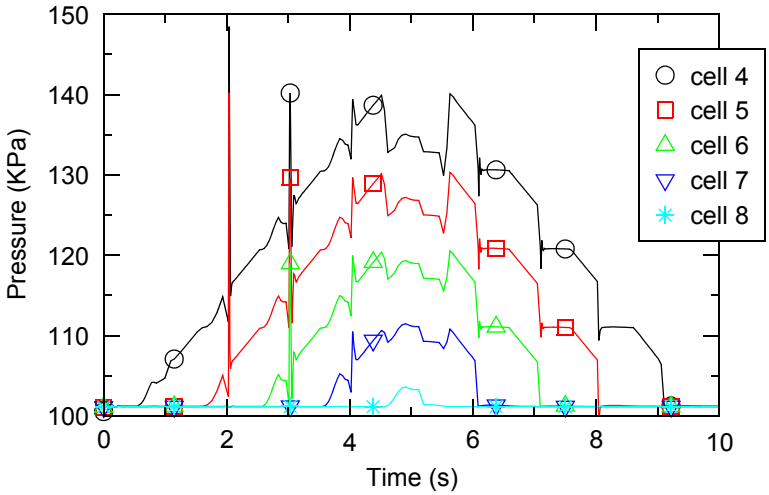

FIGURE 3-1. Pressures of the single-phase fill and drain test (simulated with the original level tracking method of TRAC-BWR)

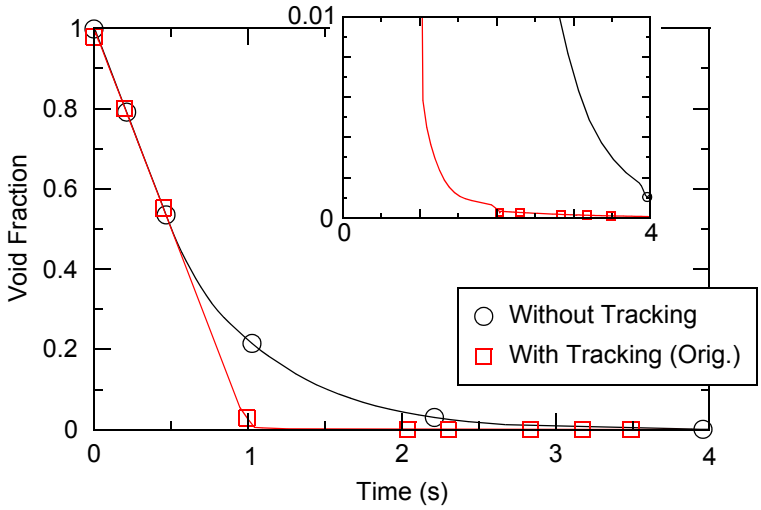

FIGURE 3-2. A comparison of void fractions in Cell 4 of the single-phase fill and drain test (simulated with and without the original level tracking method of TRAC-BWR)

are included here to illustrate that half measures do not produce satisfactory results and that one must consider a full range of issues for a successful level tracking method. Figure 3-1 shows the cell pressures predicted by TRAC as it simulated the single-phase version of the fill and drain test while the original method of tracking in TRAC-BWR was engaged. The figure exhibits spikes and step changes in pressures of Cells 4 to 8 along the vertical test pipe as the single-phase column of water rises and

returns to its starting location. The root cause of these pressure spikes is the failure of the original tracking method to propagate the water level properly across the cell boundaries. For instance, the void fraction history of Cell 4 (shown in Figure 3-2) reveals that a small pocket of gas is trapped in a cell when the level moves across a boundary between two cells. The void fraction of Cell 4 is expected to be zero after the water level leaves Cell 4.

Simulations of the remaining "thought" experiments exhibit similar troubles caused by the original method of level tracking. TRAC fails to simulate the oscillating manometer when the level tracking method is switched on inside the manometer arms. It also predicts unreasonably high pressures due to the water packing phenomenon for the condensation test when the original method of level tracking is engaged. While the original method of level tracking was tested only against some laboratory experiments, the troubles discussed above were overlooked. For instance, the early assessment of the method only evaluated the void fraction data and made no reference to the pressures predicted by TRAC except noting that there were occasional pressure spikes as the water levels crossed the cell boundaries. In contrast, the numerical experiments presented in CHAPTER 2 put the failures of the level tracking method under a spot light.

The level tracking method of TRAC-BWR, and thereof TRAC, consists of two parts: 1) a decision making step to locate and follow the water levels, 2) modifications to the field equations to account for the presence of a water level. The presentation in this chapter is organized around these two parts. First, the method of locating the water levels is presented. Modifications to the field equations then follow. However, there is a third component necessary for a successful level tracking method, mostly overlooked in the past. This third component is a systematic approach to propagate the water levels across the cell boundaries. A detailed discussion on levels crossing cell

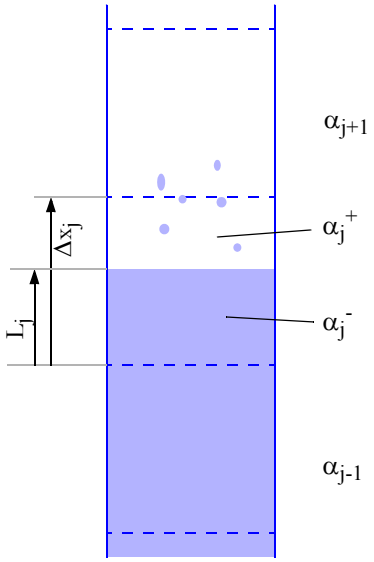

FIGURE 3-3. A computational volume with the stratified liquid-gas interface

boundaries will follow the discussion on modifications to the field equations. These discussions present the new ideas and approaches critical to a robust method of level tracking.

Level Tracking Method

The search for liquid-gas interfaces is conducted using a series of logical decisions that are based on empirical observations. Once it is determined that an interface exists inside a computational volume, its location inside the volume and its velocity are computed along with the separated sub-volumes. A computational volume that consists of a liquid-gas interface is shown in Figure 3-3. The void fraction profile decreasing with increasing height shown in this figure is the simplest case where a stratified interface must satisfy either of the following conditions:

$$(\alpha_j - \alpha_{j\text{-}1} > \delta\alpha) \wedge (\alpha_{j+1} - \alpha_j > \Delta\alpha_{cut}) \wedge (\alpha_{j+1} > \alpha_{lev}) \tag{3-1}$$

$$(\alpha_j - \alpha_{j\text{-}1} > \Delta\alpha_{cut}) \wedge (\alpha_{j+1} - \alpha_j > \delta\alpha) \wedge (\alpha_{j+1} > \alpha_{lev}) \tag{3-2}$$

The recommended values for $\Delta\alpha_{cut}$, $\delta\alpha$ and α_{lev} are 0.2, 0.005, and 0.7, respectively. There are other void fraction profiles (e.g. decreasing with increasing height, reversed void profile above and below obstructions, etc...) for which the liquid-gas interfaces must satisfy different conditions. The level tracking logic and the corresponding conditions that must be satisfied for these void fraction profiles are provided in Appendix C. The void fractions designated for the regions below and above an interface, and the volumes of these regions can then be correlated from the computational volume and its void fraction.

$$\alpha_j^- = \alpha_{j-1} \text{ and } \alpha_j^+ = \alpha_{j+1} \tag{3-3}$$

$$\mathrm{Vol}_j = \mathrm{Vol}_j^- + \mathrm{Vol}_j^+ \tag{3-4}$$

$$\mathrm{Vol}_j\alpha_j = \mathrm{Vol}_j^-\alpha_j^- + \mathrm{Vol}_j^+\alpha_j^+ \tag{3-5}$$

Subvolumes can be evaluated from (3-4) and (3-5).

$$\mathrm{Vol}_j^- = \frac{\alpha_j^+ - \alpha_j}{\alpha_j^+ - \alpha_j^-}\,\mathrm{Vol}_j \tag{3-6}$$

In a computational volume with constant flow area, the location of the interface can be obtained from (3-6) by dividing both sides by the flow area:

$$L_j = \frac{\alpha_j^+ - \alpha_j}{\alpha_j^+ - \alpha_j^-}\,\Delta x_j \tag{3-7}$$

Next, the velocity of the liquid-gas interface is formulated by taking the time derivative of (3-7) as follows:

$$V_{L,j} = \frac{\Delta x_j}{\alpha_j^+ - \alpha_j^-}\left[\frac{d\alpha_j^+}{dt} - \frac{d\alpha_j}{dt}\right] - \frac{L_j}{\alpha_j^+ - \alpha_j^-}\left[\frac{d\alpha_j^+}{dt} - \frac{d\alpha_j^-}{dt}\right] \tag{3-8}$$

$$\begin{aligned} V_{L,j}^n = {} & \frac{\Delta x_j}{(\alpha_j^+)^n - (\alpha_j^-)^n}\left[\frac{(\alpha_j^+)^n - (\alpha_j^+)^{n-1}}{\Delta t} - \frac{\alpha_j^n - \alpha_j^{n-1}}{\Delta t}\right] \\ & - \frac{L_j^n}{(\alpha_j^+)^n - (\alpha_j^-)^n}\left[\frac{(\alpha_j^+)^n - (\alpha_j^+)^{n-1}}{\Delta t} - \frac{(\alpha_j^-)^n - (\alpha_j^-)^{n-1}}{\Delta t}\right] \end{aligned} \tag{3-9}$$

In Equation (3-8), the time derivative of void fractions are first-order approximations. The void fractions and the velocity of the liquid-gas interface in Equation (3-9) are denoted with a superscript indicating the time step number to which these variables belong. At the start of time step *n+1*, the location of the liquid-gas interface (L_j^n) The location of an interface at the end of a time step can be projected from its location and velocity at the beginning of a time step:

$$\tilde{L}_j^{n+1} = L_j^n + \Delta t^{n+1}\ V_{L,j}^n \tag{3-10}$$

When it is determined that a liquid-gas interface exists in a computational volume, an integer variable is set to one to flag its existence. Otherwise, the same variable is set to zero to indicate that no interface is present.

$$\lambda_j^n = \begin{cases} 1 \ , \text{for } \ 0 < L_j^n < \Delta x_j \\ 0 \ , \text{otherwise} \end{cases} \tag{3-11}$$

λ_j^n in Equation (3-11) flags the presence of water level at time step *n*. Another flag is set based on the projected location of the liquid-gas interface at time step *n+1*.

$$\tilde{\lambda}_j^{n+1} = \begin{cases} 1 \text{ , for } 0 < \tilde{L}_j^{n+1} < \Delta x_j \\ 0 \text{ , otherwise} \end{cases} \tag{3-12}$$

In the above equations, a tilde signifies that the value of a variable is an estimate and not its final value at the end of a time step. It should be emphasized that the "expected" location of a liquid-gas interface is not necessarily equal to the "calculated" location at the end of a time step, i.e.

$$\tilde{L}_j^{n+1} \neq L_j^{n+1} \tag{3-13}$$

Modifications To The Field Equations

Once it is determined that a liquid-gas interface is present in a computational cell, a new variable, λ_E, is defined to specify the distance between the liquid-gas interface and the cell boundaries. A second variable, α_E, is defined to specify the void fraction of the two-phase fluid convected across the boundaries between two adjacent volumes.

$$\tilde{\lambda}_{E,j+1/2}^{n+1} = \begin{cases} \tilde{L}_{j+1}^{n+1} & \text{, if } \tilde{\lambda}_{j+1}^{n+1} = 1 \\ \tilde{L}_j^{n+1} - \Delta x_j & \text{, if } \tilde{\lambda}_j^{n+1} = 1 \\ 0 & \text{, otherwise} \end{cases} \tag{3-14}$$

$$\alpha_{E,j\text{-}1/2} = \begin{cases} \alpha_j^- & , \text{if } \tilde{\lambda}^{n+1}_{E,j\text{-}1/2} > 0 \\ \alpha_{j\text{-}1}^+ & , \text{if } \tilde{\lambda}^{n+1}_{E,j\text{-}1/2} < 0 \\ \langle \alpha \rangle_{j\text{-}1/2} & , \text{if } \tilde{\lambda}^{n+1}_{E,j\text{-}1/2} = 0 \end{cases} \tag{3-15}$$

$$\alpha_{E,j+1/2} = \begin{cases} \alpha_{j+1}^- & , \text{if } \tilde{\lambda}^{n+1}_{E,j+1/2} > 0 \\ \alpha_j^+ & , \text{if } \tilde{\lambda}^{n+1}_{E,j+1/2} < 0 \\ \langle \alpha \rangle_{j+1/2} & , \text{if } \tilde{\lambda}^{n+1}_{E,j+1/2} = 0 \end{cases} \tag{3-16}$$

In the above equations, $\langle \alpha \rangle$ is the void fraction at a boundary defined as a weighted average of void fractions computed for the cells adjacent to a boundary.

Mass and Energy Equations

When a liquid-gas interface is present in a computational cell, its presence must be accounted for by the terms that describe the flux of mass and energy across the cell boundaries. The flux terms in (1-21) to (1-26) use an average of properties from adjacent cells as an approximation for the state properties, which are defined and calculated at cell centers by definition, across the cell boundary. Once it is determined that a liquid-gas interface is present adjacent to a cell boundary, averaging of the properties at the boundary must account for the presence of the interface. The following erdefined flux terms account for the presence of an interface by redefining the flow area at the cell boundary:

$$\phi_{g,j+1/2} = \langle \alpha \rho_g \rangle^n_{j+1/2} A^{\alpha}_{g,j+1/2} V^{n+1}_{g,j+1/2} \tag{3-17}$$

$$\phi_{l,j+1/2} = \langle (1-\alpha) \rho_l \rangle^n_{j+1/2} A^{\alpha}_{l,j+1/2} V^{n+1}_{l,j+1/2} \tag{3-18}$$

$$\zeta_{g,j+1/2} = \langle \alpha \rho_g e_g \rangle^n_{j+1/2} A^{\alpha}_{g,j+1/2} V^{n+1}_{g,j+1/2} \tag{3-19}$$

$$\zeta_{l,j+1/2} = \langle (1-\alpha) \rho_l e_l \rangle^n_{j+1/2} A^{\alpha}_{l,j+1/2} V^{n+1}_{l,j+1/2} \tag{3-20}$$

$$\omega_{g,j+1/2} = \langle \alpha \rangle^n_{j+1/2} A^{\alpha}_{g,j+1/2} V^{n+1}_{g,j+1/2} \tag{3-21}$$

$$\omega_{l,j+1/2} = \langle 1-\alpha \rangle^n_{j+1/2} A^{\alpha}_{l,j+1/2} V^{n+1}_{l,j+1/2} \tag{3-22}$$

where the newly defined "phasic" flow areas, i.e. $A^{\alpha}_{g,j+1/2}$ and $A^{\alpha}_{l,j+1/2}$, are:

$$A^{\alpha}_{g,j+1/2} = \begin{cases} A_{j+1/2} \dfrac{\alpha_{E,j+1/2}}{\alpha_j} & \text{, if } (\tilde{\lambda}^{n+1}_{E,j+1/2} < 0) \text{ and } (\tilde{V}^{n+1}_{g,j+1/2} > 0) \\ A_{j+1/2} \dfrac{\alpha_{E,j+1/2}}{\alpha_{j+1}} & \text{, if } (\tilde{\lambda}^{n+1}_{E,j+1/2} > 0) \text{ and } (\tilde{V}^{n+1}_{g,j+1/2} < 0) \\ A_{j+1/2} & \text{, otherwise} \end{cases} \tag{3-23}$$

$$A^{\alpha}_{l,j+1/2} = \begin{cases} A_{j+1/2} \dfrac{1-\alpha_{E,j+1/2}}{1-\alpha_j} & \text{, if } (\tilde{\lambda}^{n+1}_{E,j+1/2} < 0) \text{ and } (\tilde{V}^{n+1}_{l,j+1/2} > 0) \\ A_{j+1/2} \dfrac{1-\alpha_{E,j+1/2}}{1-\alpha_{j+1}} & \text{, if } (\tilde{\lambda}^{n+1}_{E,j+1/2} > 0) \text{ and } (\tilde{V}^{n+1}_{l,j+1/2} < 0) \\ A_{j+1/2} & \text{, otherwise} \end{cases} \tag{3-24}$$

The above equations redefine the flux terms in the mass and energy equations of the basic step, i.e. Equations (1-15) to (1-18), accurately in terms of void fractions above and below a water level. However, these corrections to the flux terms in the basic step equations do not work for the flux terms in the stabilizer step equations, i.e. Equations (1-48) to (1-51), as the flux terms in these equations are formulated in

terms of $\tilde{\alpha}^{n+1}$ from the basic step, not α^n of the previous time step. The following equations further adjust the "phasic" flow areas so that the flux terms in the stabilizer step equations remain consistent with the solution to the basic step equations.

$$A^{\alpha}_{g,j+1/2} \rightarrow \begin{cases} A^{\alpha}_{g,j+1/2} \dfrac{\alpha^n_j}{\tilde{\alpha}^{n+1}_j} & \text{, if } (\tilde{\lambda}^{n+1}_{E,j+1/2} < 0) \text{ and } (V^{n+1}_{g,j+1/2} > 0) \\ A^{\alpha}_{g,j+1/2} \dfrac{\alpha^n_{j+1}}{\tilde{\alpha}^{n+1}_{j+1}} & \text{, if } (\tilde{\lambda}^{n+1}_{E,j+1/2} > 0) \text{ and } (V^{n+1}_{g,j+1/2} < 0) \end{cases} \tag{3-25}$$

$$A^{\alpha}_{l,j+1/2} \rightarrow \begin{cases} A^{\alpha}_{l,j+1/2} \dfrac{(1-\alpha^n_j)}{(1-\tilde{\alpha}^{n+1}_j)} & \text{, if } (\tilde{\lambda}^{n+1}_{E,j+1/2} < 0) \text{ and } (V^{n+1}_{l,j+1/2} > 0) \\ A^{\alpha}_{l,j+1/2} \dfrac{(1-\alpha^n_{j+1})}{(1-\tilde{\alpha}^{n+1}_{j+1})} & \text{, if } (\tilde{\lambda}^{n+1}_{E,j+1/2} > 0) \text{ and } (V^{n+1}_{l,j+1/2} < 0) \end{cases} \tag{3-26}$$

Redefining the macroscopic quantities that are convected across the cell boundaries in terms of the void fractions above and below an interface curtails the otherwise inadvertent flux of quantities based on cell average void fraction. The modifications above are necessary but not sufficient for a successful method of level tracking. Additional considerations must be given to the other terms which make up the fluxes, i.e. the liquid and gas velocities.

Momentum Equations

Equations (1-27) and (1-28) are substituted into (3-17) to (3-22) eliminating the velocities as unknowns from the flux terms. Thus, the flux terms consists of two components before the iterative solution begins: 1) the known portion in terms of the tilde fluid velocities ($\tilde{V}^{n+1}_{j+1/2}$), and 2) the variable portion in terms of the unknown

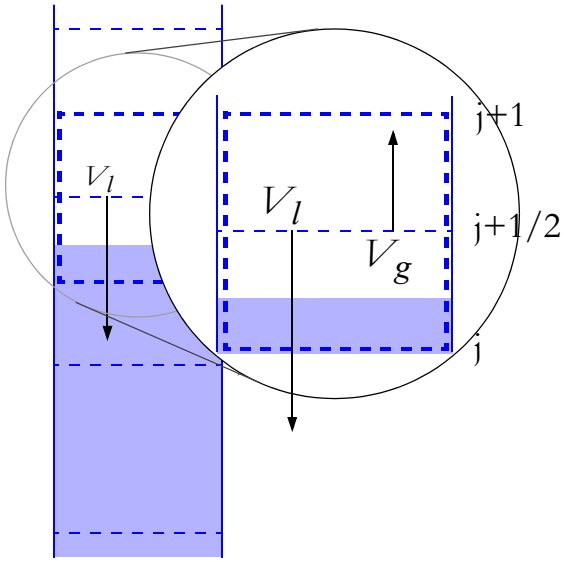

FIGURE 3-4. A staggered control volume with the stratified liquid-gas interface

changes in pressures (δP_j^i). The flux quantities modified by (3-23) and (3-24) multiply both the known and the variable portions of flux terms. It should not be overlooked that the product of the tilde velocities and modified flux quantities will be inconsistent unless the momentum equations, i.e. (1-13) and (1-14), are also adjusted to account for the presence of liquid-gas interfaces.

This subtle detail pertinent to Equations (1-13) and (1-14) deserves further clerification. Equations (1-13) and (1-14) balance the fluid momentum across a staggered control volume for liquid and gas fields, i.e. the control volume drawn with thick dotted lines in Figure 3-4 that stretches from the center of Cell j to the center of Cell j+1. The use of staggered control volumes allows the expression of the net force due to pressure drop across the fluid enclosed by the staggered volume simply as $P_{j\text{-}1} - P_j$ without the need for any further approximation. In the meantime, other variables such as fluid density and void fraction in (1-13) and (1-14) are approximations since these variables are defined at cell centers. From the balance of momentum across a

staggered cell, Equations (1-13) and (1-14) are formulated for the liquid and gas velocities. Later, the product of these velocities and the flux quantities at cell boundaries, depicted by the arrows located at j+½ in Figure 3-4, define the flux of mass and energy across the cell boundary. A solution with the standard upstream donor method defines the flux quantities at cell boundaries as an average of quantities from the adjacent cells. This picture must be revisited when the fluid enclosed by the staggered control volume is no longer uniform and it consists of two regions divided by an interface.

In the presence of a liquid-gas interface, the flux terms at cell boundaries given in (3-17) to (3-22) are modified by the newly defined phasic flow areas, i.e. $A^{\alpha}_{g,j+1/2}$ and $A^{\alpha}_{l,j+1/2}$. For the example shown in Figure 3-4, the phasic flow areas correct the flux quantities so that the velocities multiply the quantities only that belong to the region above the interface, i.e. the white region. On the other hand, Equations (1-13) and (1-14) will continue to be formulated for an average fluid mixture of regions below and above the interface, i.e. the white and shaded regions, unless properly corrected. Corrections to (1-13) and (1-14) must be made so that these equations balance the forces acting on the white region above the interface that prevails at j+1/2 and the velocities from these equations be consistent with the flux quantities that they multiply.

First, the fluid inertia terms in (1-13) and (1-14) are redefined using the void fractions below and above an interface:

$$\langle \alpha\rho_g \rangle^{n}_{j+1/2} = \begin{cases} \alpha_{E,j+1/2} \langle \rho_g \rangle^{n}_{j+1/2} & , \text{if } \tilde{\lambda}^{n+1}_{E,j+1/2} \neq 0 \\ \alpha_{j+1/2} \langle \rho_g \rangle^{n}_{j+1/2} & , \text{if } \tilde{\lambda}^{n+1}_{E,j+1/2} = 0 \end{cases} \tag{3-27}$$

$$\langle (1-\alpha)\rho_l \rangle_{j+1/2}^{n} = \begin{cases} (1-\alpha_{E,j+1/2})\langle \rho_l \rangle_{j+1/2}^{n} & \text{, if } \tilde{\lambda}_{E,j+1/2}^{n+1} \neq 0 \\ (1-\alpha_{j+1/2})\langle \rho_l \rangle_{j+1/2}^{n} & \text{, if } \tilde{\lambda}_{E,j+1/2}^{n+1} = 0 \end{cases} \tag{3-28}$$

Second, the pressure gradient term in (1-13) and (1-14) is redefined as

$$\left.\frac{\partial P}{\partial x}\right|_{j+1/2}^{n} = \frac{P_{j+1}^{n} - P_{j}^{n} + \delta P_{L,j+1/2}}{\Delta x_{j+1/2}} \tag{3-29}$$

where the correction term to account for the presence of a liquid-gas interface is given by the following equation.

$$\delta P_{L,j+1/2} = \begin{cases} (0.5\Delta x_{j+1} - \tilde{L}_{j+1}^{n+1}) \left.\frac{\partial P}{\partial x}\right|_{j\text{-}1/2}^{n} & \text{, if } \tilde{L}_{j+1}^{n+1} < 0.5\Delta x_{j+1} \\ (0.5\Delta x_{j} - \tilde{L}_{j}^{n+1}) \left.\frac{\partial P}{\partial x}\right|_{j\text{-}3/2}^{n} & \text{, if } \tilde{L}_{j}^{n+1} > 0.5\Delta x_{j} \\ 0 & \text{, otherwise} \end{cases} \tag{3-30}$$

While the pressure drop correction given by Equation (3-30) works well for the momentum equations of the basic step, the use of the "expected" location of the liquid-gas interface to determine the pressure drop correction does not work for the stabilizer momentum equations, i.e. (1-39) and (1-40). Although the stabilizer momentum equations are presented as the first step of a time step, these equations constitute the last step that determines the final values of liquid and gas velocities. Therefore, the pressure drop correction for these equations must be based on the "calculated" location of the liquid-gas interface at the end of a time step, i.e. L_j^n.

$$\delta P_{L,j+1/2} = \begin{cases} (0.5\Delta x_{j+1} - L_{j+1}^{n})\left.\dfrac{\partial P}{\partial x}\right|_{j\text{-}1/2}^{n} & \text{, if } L_{j+1}^{n} < 0.5\Delta x_{j+1} \\ (0.5\Delta x_{j} - L_{j}^{n})\left.\dfrac{\partial P}{\partial x}\right|_{j\text{-}3/2}^{n} & \text{, if } L_{j}^{n} > 0.5\Delta x_{j} \\ 0 & \text{, otherwise} \end{cases} \tag{3-31}$$

It should also be noted that (3-30) yields an accurate pressure drop from the interface to the cell boundary not only due to the hydrostatic head of fluid but also due to the fluid acceleration. This detail should not be overlooked and it is important for situations in which an interface accelerates. It should also be emphasized that Equation (3-30) yields to the weight of the fluid below the interface between the interface and the cell boundary in the hydrostatic limit, i.e. when there is no pressure drop due to fluid acceleration $\frac{\partial V}{\partial t} = 0$. Where neither of $\left.\frac{\partial P}{\partial x}\right|_{j\text{-}1/2}^{n}$ or $\left.\frac{\partial P}{\partial x}\right|_{j\text{-}3/2}^{n}$ is available, such as near the boundary of a flow segment, Equation (3-30) assumes that these gradients are equal to the hydrostatic head of the fluid in Cell *j*.

Third, the gradients of liquid and gas velocities across the cell boundary are set to zero based on an assumption that the changes in fluid velocity across the interface will not contribute to the pressure drop across the staggered control volume. For example, the gas bubbles that reach the liquid-gas interface rise at a terminal velocity. The velocity of gas escaping from the interface is generally much smaller than the terminal rise velocity of gas bubbles below the interface. However, this sudden slowdown of gas across the interface, which is due to continuity, should not cause additional pressure changes across the staggered cell. Similarly, the liquid droplets entrained into the region above the interface may have higher velocity than the continuous liquid region below the interface. Any additional pressure drop due to this change of liquid velocity

across the staggered cell is incorrect, too. Therefore, the velocity gradient of a field at any cell boundary is set to zero when a liquid-gas interface is present in the upstream direction of that field. The correction to the gradients of liquid and gas velocities are formulated into Equations (1-13) and (1-14) as follows:

$$\left.\frac{\partial V_l}{\partial x}\right|_{j+1/2}^{n} = 0 \text{ when } \begin{cases} (\tilde{\lambda}_{E,j+1/2}^{n+1} < 0) \text{ and } (V_{l,j+1/2}^{n} > 0) \\ (\tilde{\lambda}_{E,j+1/2}^{n+1} > 0) \text{ and } (V_{l,j+1/2}^{n} < 0) \end{cases} \tag{3-32}$$

$$\left.\frac{\partial V_g}{\partial x}\right|_{j+1/2}^{n} = 0 \text{ when } \begin{cases} (\tilde{\lambda}_{E,j+1/2}^{n+1} < 0) \text{ and } (V_{g,j+1/2}^{n} > 0) \\ (\tilde{\lambda}_{E,j+1/2}^{n+1} > 0) \text{ and } (V_{g,j+1/2}^{n} < 0) \end{cases} \tag{3-33}$$

As the level tracking method and the necessary modifications to the field equations described (3-1) to (3-33) are incorporated, the numerical experiments presented in CHAPTER 2 must be simulated to test the method and the modifications to the field equations. A thorough testing is critical to a successful implementation of the level tracking method. Figure 3-5 shows the cell void fractions along the test pipe of the single-phase fill and drain test. Comparing it to Figure 2-4, the results indicate significant improvements. The rising water levels fills the computational volumes as expected and a sharp front is retained. However, a close up of the cell void fractions in Figure 3-5 shows that small amounts of gas is trapped in the tail of the "ascending" liquid-gas interface. The void fraction in these cells behind the interface approach to zero asymptotically as the trapped gas is convected out continuously in smaller amounts. As the pressure gradient behind the water level is adjusted by the level tracking method, the "trapped" gas accelerates rapidly causing the pressure spikes recorded in Figure 3-6.

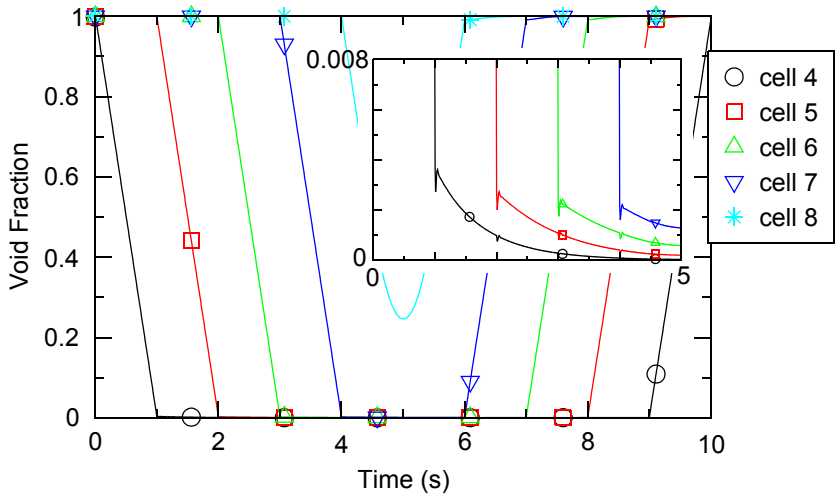

FIGURE 3-5. Void fractions of the single-phase fill and drain test (simulated with the level tracking and no treatment for boundary crossing)

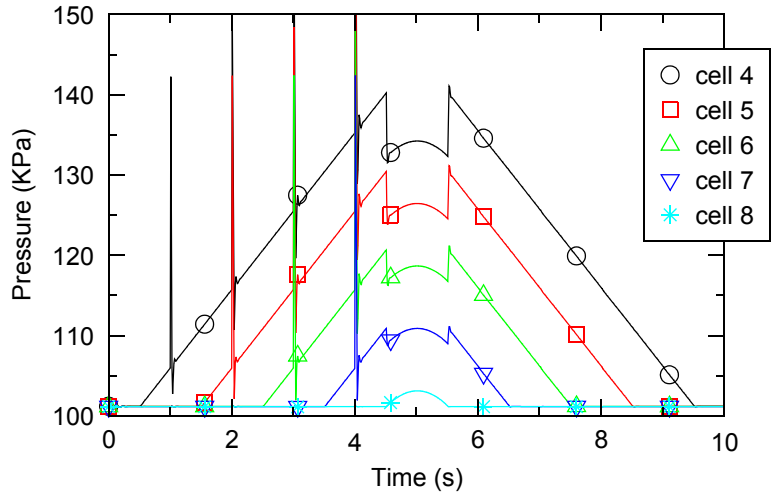

FIGURE 3-6. Pressures of the single-phase fill and drain test (simulated with the level tracking and no treatment for boundary crossing)

The results from the repeat simulation of the two-phase fill and drain test indicate similar troubles. In Figure 3-7, a close up of the void fractions shows that small fragments of liquid is left behind the "descending" water level. The void fraction in these cells approach to one asymptotically as the liquid is convected out in smaller amounts. More trouble is evident in Figure 3-8 that shows the cell pressures. The pressures

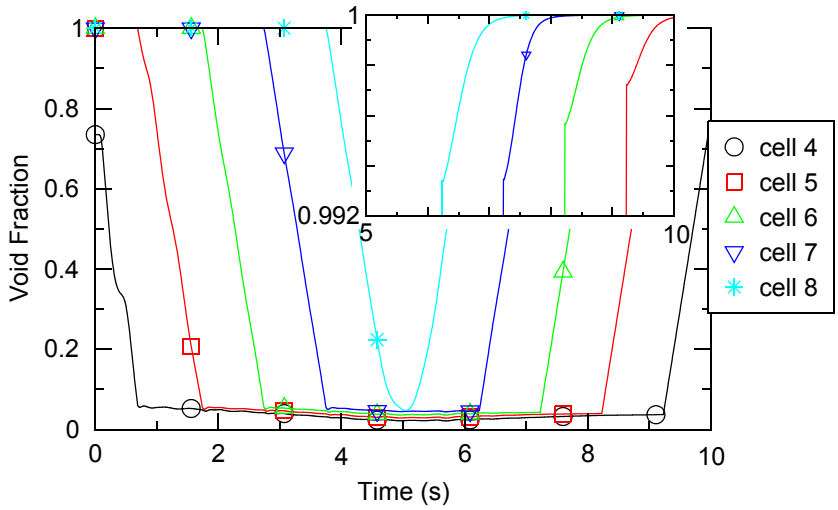

FIGURE 3-7. Void fractions of the two-phase fill and drain test (simulated with the level tracking and no treatment for boundary crossing)

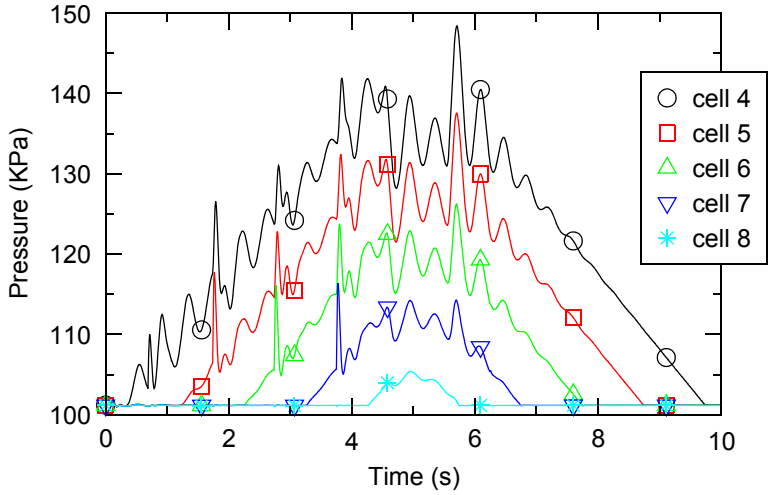

FIGURE 3-8. Pressures of the two-phase fill and drain test (simulated with the level tracking and no treatment for boundary crossing)

indicate pressure waves "traversing" the column of liquid and gas mixture initiated by pressure spikes following the crossing of water level across cell boundaries.

As seen in Figure 3-9 and Figure 3-10, the troubles of simulating these two experiments are sufficient to make the solution fail to simulate the oscillating manometer

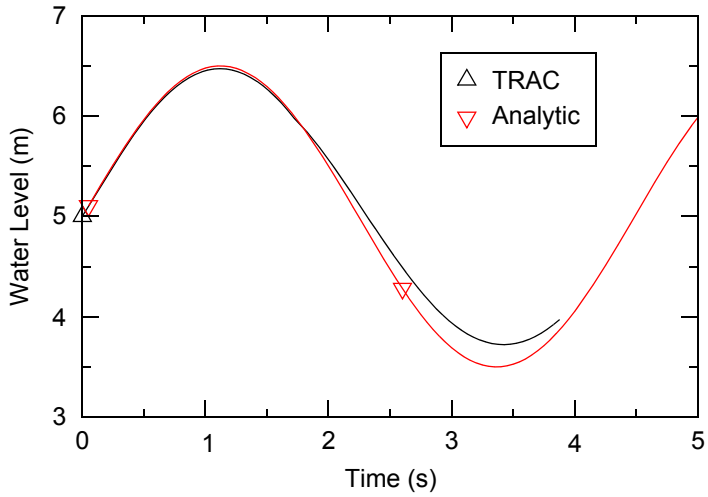

FIGURE 3-9. Water level of the oscillating manometer (simulated with the level tracking and no treatment for boundary crossing)

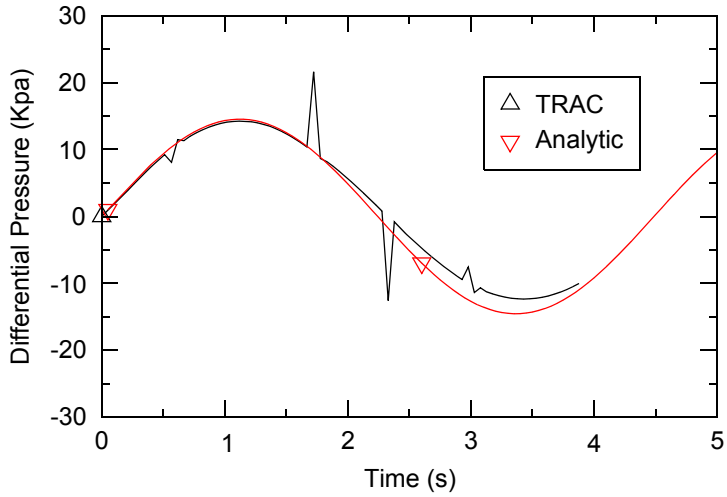

FIGURE 3-10. The net force on the fluid segment below 2.5m elevation of the manometer arms (simulated with the level tracking and no treatment for boundary crossing)

test. The simulation fails into the second cycle of oscillations. The cause of failure is the pressure spikes that occur and apparent from the driving force in Figure 3-10 as the liquid-gas interface moves across the cell boundaries.

These simulations demonstrate their significance to the testing of interface tracking methods as they magnify the troubles hidden in results which otherwise might be

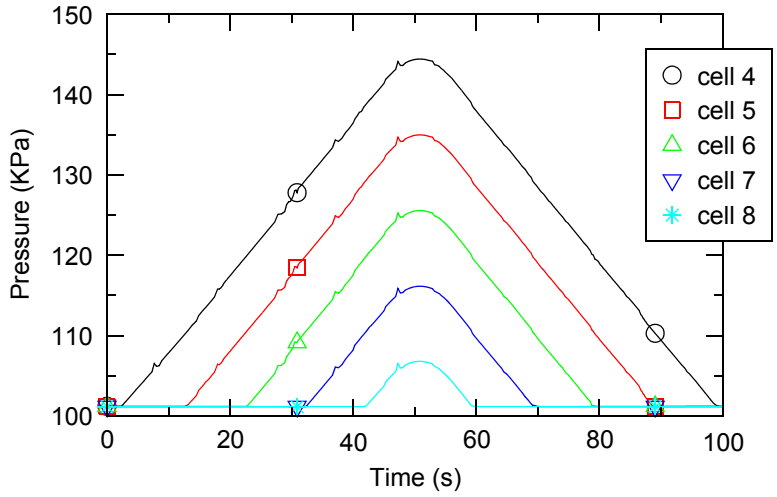

FIGURE 3-11. Pressures of the "prolonged" two-phase fill and drain test (simulated with the level tracking and no treatment for boundary crossing)

regarded as minute details. This oversight has often been the case in the past. For instance, the simulations of the fill and drain test would not reveal these troubles had they been simulating a rising and falling water level ten times slower. Figure 3-11, which contrasts Figure 3-6, demonstrates this point in which the pressures along the test pipe of the two-phase fill and drain test show no signs of trouble but very small spikes that can be regarded acceptable.

As it is evident from these simulations, a special care must be given to a solution method modified by the level tracking method, which is described in Equations (3-1) to (3-33), to counter for situations when liquid-gas interfaces cross over cell boundaries.

Level Crossing Cell Boundaries

The reason why the previous section makes no attempt to improve the solution in situations when levels crossing cell boundaries is to emphasize strongly the importance of special care given to these situations in order to counter for the adverse

imprint of level crossing. This section discusses in detail the special care that must be given to the solution method of TRAC to achieve a robust method of level tracking. Although some discussion detailing the steps to modify the semi-implicit method will be unique for TRAC, most of its substance is applicable to similar methods of solution for the six-equation model.

First, the method should determine when the liquid-gas interface will cross the cell boundary. Equations (3-1) to (3-33) are applied to search and locate liquid-gas interfaces at the end of time steps. Once a liquid-gas interface is located, a critical time step size is projected for an interface to cross the cell boundary in the direction of its propagation based on its current location and velocity.

$$\Delta\tau_j = \begin{cases} \dfrac{\Delta x_j - L_j^n}{V_{L,j}^n} & \text{, if } V_{L,j}^n > 0 \\ \dfrac{L_j^n}{V_{L,j}^n} & \text{, if } V_{L,j}^n < 0 \end{cases} \tag{3-34}$$

This critical time step size is then compared to the next time step size to determine whether the interface will cross the cell boundary at the end of the new time step and a new variable is defined to flag the direction of interface crossing across the cell boundary.

$$X_{L,j+1/2} = \begin{cases} +\Delta\tau_j & \text{, if } (\Delta\tau_j < \Delta t) \wedge (V_{L,j}^n > 0) \\ -\Delta\tau_{j+1} & \text{, if } (\Delta\tau_{j+1} < \Delta t) \wedge (V_{L,j+1}^n < 0) \end{cases} \tag{3-35}$$

The root causes of the troubles reported in the previous section were not well recognized at the time when the level tracking method of TRAC-BWR was developed

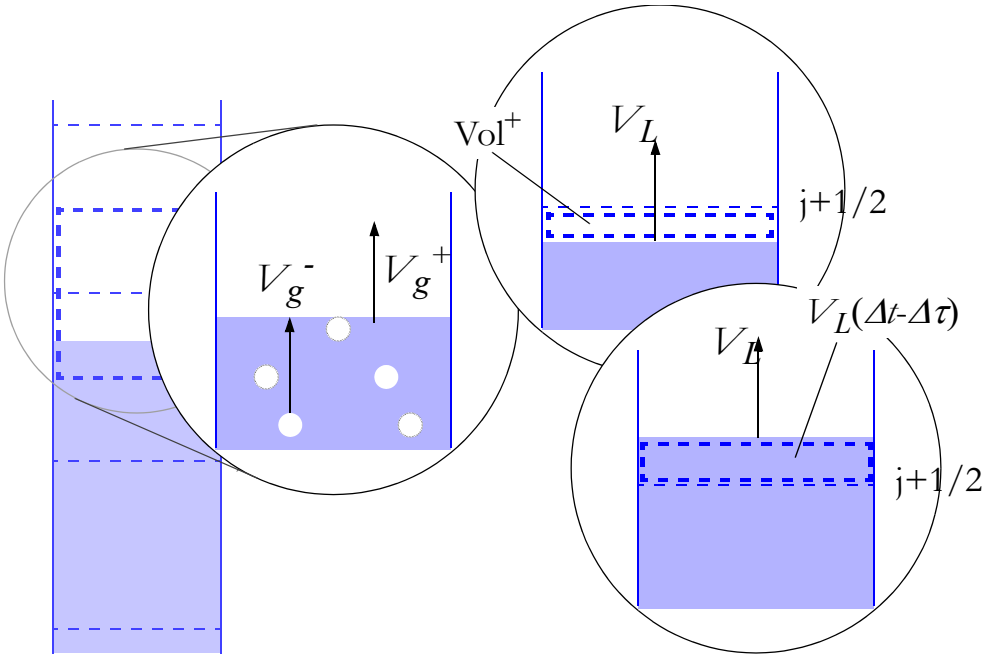

FIGURE 3-12. The stratified liquid-gas interface crossing a cell boundary

and later incorporated into TRAC. Nevertheless, some attempts were made to ease the adverse effects of level crossing cell boundaries. The level tracking method of TRAC-BWR forced an exchange of liquid and gas phases between the two cells adjacent to a boundary at time steps when it is determined that a level will cross the boundary:

$$\alpha_{j+1} \rightarrow \alpha_{j+1} \mp \delta\alpha \text{ and } \alpha_j \rightarrow \alpha_j \pm \frac{\mathrm{Vol}_{j+1}(\rho_{l,j+1} - \rho_{g,j+1})}{\mathrm{Vol}_j(\rho_{l,j} - \rho_{g,j})}\delta\alpha \tag{3-36}$$

The sole purpose of exchanging liquid and gas between the two cells adjacent to a boundary, given by Equations (3-36), was to prevent the interface location from oscillating between the two cells. An oscillation of this kind was thought to be the cause of pressure spikes. Figure 3-1 and Figure 3-2 are the proof of failure of this ad hoc

approach. There is absolutely a need for a better and more systemic approach to deal with the root cause of troubles associated with levels crossing cell boundaries.

Let us first consider a situation where a rising liquid-gas interface is about to cross a cell boundary. Figure 3-12 pictures the interface near a cell boundary before and after it crosses the cell boundary. Three close-ups shown in bubbles are sequenced from back to the front. The close-up in the middle shows the interface before it crosses. The close-up in the foreground shows the interface after it crosses. The root cause of troubles associated with levels crossing cell boundaries is hidden in the switching of the void fraction at cell boundary, i.e. α_E, from α^+ to α^- after it is determined that the interface will be located in the cell above at the end of a time step. α_E can be set to α^- either before or after the time step in which the interface crosses the cell boundary. Both choices can have adverse consequences. If $\alpha_{E,j+1/2}$ is set to α^- before the interface crosses the boundary at j+1/2, the fluid enclosed by Vol^+ will not be convected out of Cell j and be averaged into the fluid of Cell j at the end of time step. If $\alpha_{E,j+1/2}$ is set to α^- after the interface crosses, more fluid of void fraction α^+ by as much as $(V_L \Delta t - \mathrm{Vol}^+)$ will be convected out of Cell j than there is actually enclosed by Vol^+. One way to overcome this trouble is by reducing the time step to reasonably small sizes so that Vol^+ would be very small. However, this option is not always acceptable since reducing the time step size can be too costly and cause other types of numerical instabilities.

Another way is to recognize that the flux terms in Equations (3-17) to (3-22) consist of two parts: 1) the fluid enclosed by Vol^+ before the interface crosses, i.e. the

space enclosed by the dashed lines in the middle close-up, 2) the fluid within the region below interface after the interface crosses, i.e. the space enclosed by the dashed lines in the foreground close-up. So, the flux terms can be reformulated momentarily in terms of these two parts. To illustrate this approach, the gas mass flux term in (3-17) is used as an example below:

$$\phi_{g,j+1/2}\Delta t = (\alpha\rho_g)^{+}\mathrm{Vol}^{+} + (\alpha\rho_g)^{-}A_{j+1/2}V_{g,j+1/2}^{n+1}(\Delta t - \Delta\tau) \tag{3-37}$$

where $(\alpha\rho_g)^{+}$ and $(\alpha\rho_g)^{-}$ are the macroscopic gas densities above and below the interface, respectively. Equation (3-37) is not suitable to be implemented into the solution of two-field equations described by (1-31) to (1-31). First, let us rewrite (3-37) in terms of field velocities above and below the interface, i.e. V_g^{+} and V_g^{-}, as follows:

$$\begin{aligned}\phi_{g,j+1/2}\Delta t &= (\alpha\rho_g)^{+}A_{j+1/2}V_g^{+}\Delta\tau + (\alpha\rho_g)^{-}A_{j+1/2}V_g^{-}(\Delta t - \Delta\tau) \\ &= [(\alpha\rho_g)^{+}V_g^{+} - (\alpha\rho_g)^{-}V_g^{-}]A_{j+1/2}\Delta\tau + (\alpha\rho_g)^{-}A_{j+1/2}V_g^{-}\Delta t\end{aligned} \tag{3-38}$$

where the following assumption is made.

$$V_{g,j+1/2}^{n+1} = V_g^{-} \quad , \text{ when } X_{L,j+1/2} > 0 \tag{3-39}$$

Equation (3-39) implies that the momentum equations at j+1/2 must be set up to solve for the field velocities of the region below the interface. Next, variable $\Delta\tau$ in (3-38) is eliminated in favor of other variables that contribute only to the left hand side of (1-36) by substituting the "jump condition" that relates the phasic velocities to the interface velocity. Starting from the continuity of the gas field across the liquid-gas

interface in a frame of reference moving with the interface velocity, one can derive the following jump condition at the discontinuity.

$$\begin{aligned} \alpha^- V_g'^- &= \alpha^+ V_g'^+ \\ \alpha^-(V_g^- - V_L) &= \alpha^+(V_g^+ - V_L) \\ (\alpha^+ - \alpha^-)V_L &= \alpha^+ V_g^+ - \alpha^- V_g^- \end{aligned} \tag{3-40}$$

$$V_L = \frac{J_g^+ - J_g^-}{\alpha^+ - \alpha^-} \tag{3-41}$$

where the velocity in the frame of reference moving with the interface is given by $V_g' = V_g - V_L$ and the superficial velocity by $J_g = \alpha V_g$. Assuming that the gas density is constant in the vicinity of the interface, (3-40) is rewritten in terms of macroscopic density.

$$(\alpha\rho_g)^+ V_g^+ - (\alpha\rho_g)^- V_g^- = [(\alpha\rho_g)^+ - (\alpha\rho_g)^-]V_L \tag{3-42}$$

Substituting the left hand side of (3-42) into (3-38) to yields,

$$\begin{aligned} \phi_{g,j+1/2}\Delta t &= [(\alpha\rho_g)^+ - (\alpha\rho_g)^-]V_L A_{j+1/2}\Delta\tau + (\alpha\rho_g)^- A_{j+1/2} V_g^- \Delta t \\ &= [(\alpha\rho_g)^+ - (\alpha\rho_g)^-]\mathrm{Vol}^+ + (\alpha\rho_g)^- A_{j+1/2} V_g^- \Delta t \end{aligned} \tag{3-43}$$

The second term of (3-43) describes the total mass of gas that would be convected across j+1/2 if Vol^+ were zero at the time step when the interface is expected to cross the boundary at j+1/2. Since Vol^+ can be zero only when the interface is located precisely at the cell boundary, which is an unlikely event, the first term of (3-43) subtracts the extra mass convected due to this erroneous assumption.

Equation (3-44) is obtained by performing a similar analysis to derive the equivalent of (3-43) for the situation when the liquid-gas interface is crossing the boundary at j+1/2 from Cell j+1 to Cell j.

$$\phi_{g,j+1/2}\Delta t = [(\alpha\rho_g)^- - (\alpha\rho_g)^+]\mathrm{Vol}^- + (\alpha\rho_g)^+ A_{j+1/2} V_g^+ \Delta t \tag{3-44}$$

Equations (3-43) and (3-44) can then be combined into a final form that redefines the total flux of gas mass over time step Δt:

$$\phi_{g,j+1/2}\Delta t = \langle\alpha\rho_g\rangle_{j+1/2}^n A_{g,j+1/2}^{\alpha} V_{g,j+1/2}^{n+1}\Delta t + \frac{\langle\alpha\rho_g\rangle_{j+1/2}^n}{\langle\alpha\rangle_{j+1/2}^n}\delta\mathrm{Vol}_{g,j+1/2} \tag{3-45}$$

where the volume correction for the gas field is defined as follows:

$$\delta\mathrm{Vol}_{g,j+1/2} = \begin{cases} (\alpha_j^+ - \alpha_j^-)\mathrm{Vol}_j^+ & , \text{ when } X_{L,j+1/2} > 0 \\ (\alpha_j^- - \alpha_j^+)\mathrm{Vol}_{j+1}^- & , \text{ when } X_{L,j+1/2} < 0 \end{cases} \tag{3-46}$$

Equation (3-45) can be readily incorporated into the solution. Following the same analysis, the other flux terms are reformulated as follow:

$$\phi_{l,j+1/2}\Delta t = \langle(1-\alpha)\rho_l\rangle_{j+1/2}^n A_{l,j+1/2}^{\alpha} V_{l,j+1/2}^{n+1}\Delta t + \frac{\langle(1-\alpha)\rho_l\rangle_{j+1/2}^n}{\langle 1-\alpha\rangle_{j+1/2}^n}\delta\mathrm{Vol}_{l,j+1/2} \tag{3-47}$$

$$\zeta_{g,j+1/2}\Delta t = \langle \alpha\rho_g e_g \rangle^n_{j+1/2} A^{\alpha}_{g,j+1/2} V^{n+1}_{g,j+1/2}\Delta t + \frac{\langle \alpha\rho_g e_g \rangle^n_{j+1/2}}{\langle \alpha \rangle^n_{j+1/2}} \delta \mathrm{Vol}_{g,j+1/2} \tag{3-48}$$

$$\zeta_{l,j+1/2}\Delta t = \langle (1-\alpha)\rho_l e_l \rangle^n_{j+1/2} A^{\alpha}_{l,j+1/2} V^{n+1}_{l,j+1/2}\Delta t + \frac{\langle (1-\alpha)\rho_l e_l \rangle^n_{j+1/2}}{\langle 1-\alpha \rangle^n_{j+1/2}} \delta \mathrm{Vol}_{l,j+1/2} \tag{3-49}$$

$$\omega_{g,j+1/2}\Delta t = \langle \alpha \rangle^n_{j+1/2} A^{\alpha}_{g,j+1/2} V^{n+1}_{g,j+1/2}\Delta t + \delta \mathrm{Vol}_{g,j+1/2} \tag{3-50}$$

$$\omega_{l,j+1/2}\Delta t = \langle 1-\alpha \rangle^n_{j+1/2} A^{\alpha}_{l,j+1/2} V^{n+1}_{l,j+1/2}\Delta t + \delta \mathrm{Vol}_{l,j+1/2} \tag{3-51}$$

where the volume correction for the liquid field is given by:

$$\delta \mathrm{Vol}_{l,j+1/2} = \begin{cases} (\alpha_j^- - \alpha_j^+)\mathrm{Vol}_j^+ & , \text{ when } X_{L,j+1/2} > 0 \\ (\alpha_j^+ - \alpha_j^-)\mathrm{Vol}_{j+1}^- & , \text{ when } X_{L,j+1/2} < 0 \end{cases} \tag{3-52}$$

In summary, the flux terms in Equations (1-15) to (1-18) are redefined by Equations (3-45), (3-47), (3-48), (3-49), (3-50) and (3-51) along with the volume correction given by Equations (3-45) and (3-46). By applying this correction to the flux terms, the level tracking method eliminates the erroneous fluxes induced by levels crossing cell boundaries. It should be noted that the above corrections apply only to the flux terms in the basic step, i.e. a liquid-gas interface should switch to the other cell at the end of a basic step if it is expected to cross a cell boundary. Therefore, no corrections are needed to the stabilizer step equations. If the void fractions at the end of a basic step do not evolve as expected and the liquid-gas interface remains in the same cell, a

time step back up is forced to restart the time step expecting that the interface will remain in the same cell.

There is one more detail that needs to be addressed for the cases where the void fraction below the interface is absolutely zero, i.e. no bubbles, before the numerical experiments with moving water levels can be simulated again. As indicated in CHAPTER 1, the solution method of TRAC switches to the mean equation set when the void fraction of a computational cell approaches to zero or one. When the liquid-gas interface is about to enter or leave a cell, the solution should determine whether it should switch to the mean equation set and reset the void fraction to zero or one. Otherwise, the iterative solution fails to converge when interfaces cross across cell boundaries prompting a time step size reduction and the backup of a time step. The following equation resets the void fraction into the first iteration of the semi-implicit solution.

$$\alpha_j^{n+i}\Big|_{i=0} = \begin{cases} 0.0 & , \text{ if } \begin{cases} \alpha_j^n + (\omega_{g,j\text{-}1/2}\Delta t - \omega_{g,j+1/2}\Delta t) = 0 \\ X_{L,j+1/2} > 0 \end{cases} \\ 1.0 & , \text{ if } \begin{cases} \alpha_j^n - (\omega_{l,j\text{-}1/2}\Delta t - \omega_{l,j+1/2}\Delta t) = 0 \\ X_{L,j\text{-}1/2} < 0 \end{cases} \end{cases} \tag{3-53}$$

There is no better way to demonstrate the success of the approach outlined in this section, which allows water levels cross cell boundaries without causing any troubles, than simulating the rising/falling water level and the oscillating manometer tests again. Significant improvements stand out immediately when the new results are compared to the results presented in the previous section. Figure 3-13 shows the cell void fractions along the test pipe of the single-phase rising and falling level test. It is evident from this figure that the void fraction of a cell becomes 1.0 as the liquid-gas

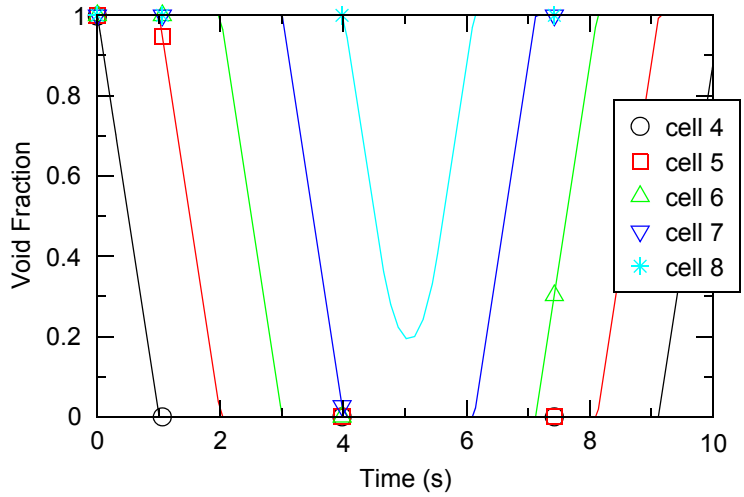

FIGURE 3-13. Void fractions of the single-phase fill and drain test (simulated with the level tracking method)

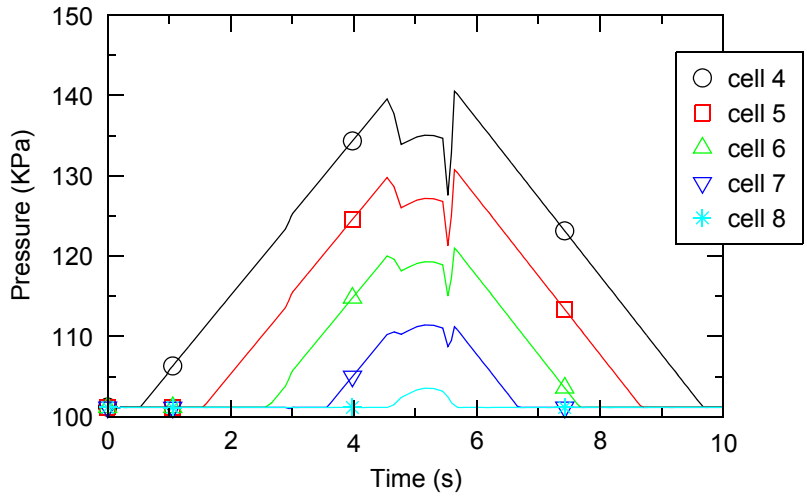

FIGURE 3-14. Pressures of the single-phase fill and drain test (simulated with the level tracking method)

interface descends to the lower adjacent cell. Previously shown in Figure 3-7, the close up of void fractions revealed that a fragment of liquid would be left behind as the interface descended into the lower cell. The spike changes in cell pressures of the same test pipe, previously seen in Figure 3-8, are also gone in Figure 3-14. The two-phase fill and drain test also shows none of the troubles that were reported in the pre-

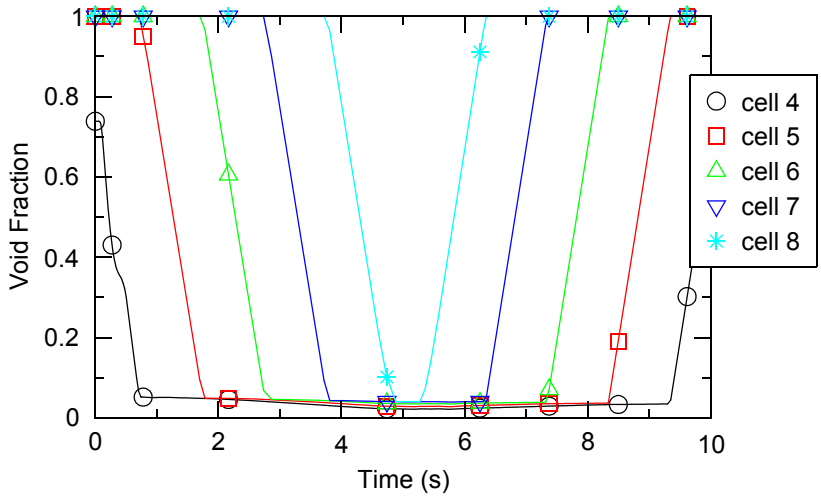

FIGURE 3-15. Void fractions of the two-phase fill and drain test (simulated with the level tracking method)

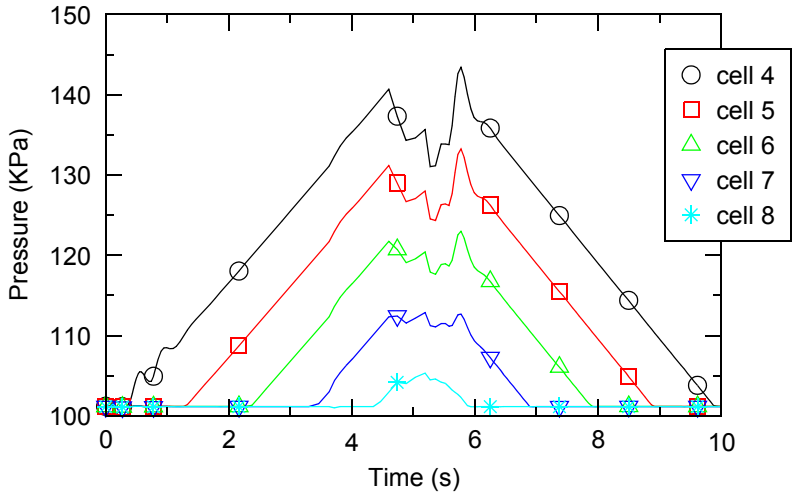

FIGURE 3-16. Pressures of the two-phase fill and drain test (simulated with the level tracking method)

vious section. For example, the troubling cell void fractions from 0 to 5 seconds seen in Figure 3-5 are no longer present in Figure 3-15. Previously, the cell void fractions approached to zero which was well below the expected value of void fraction for the bubbly mixture of liquid and air simulated in this experiment. The cell pressures reported previously for the same test in Figure 3-6 suffered from spike changes and oscillations as the water level crossed the cell boundaries. The cell pressures shown in

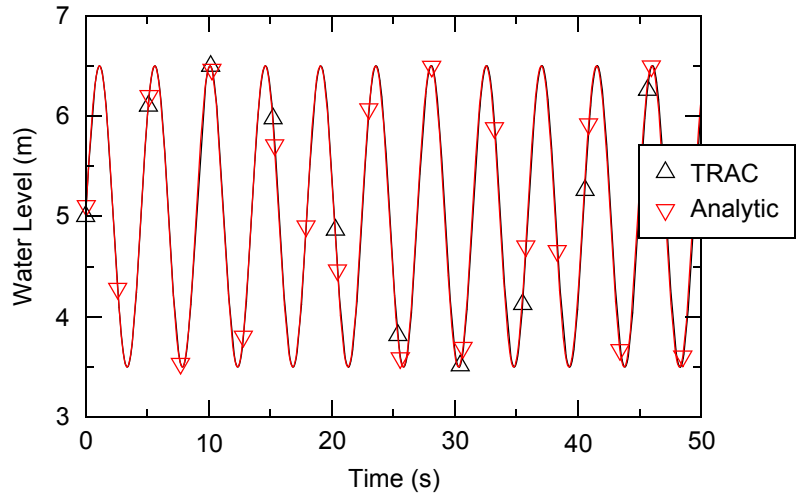

FIGURE 3-17. Water level of the oscillating manometer (simulated with the level tracking method)

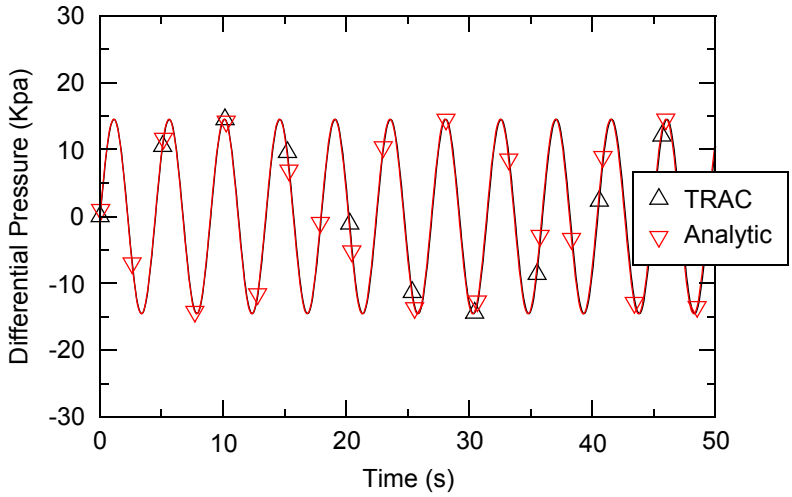

FIGURE 3-18. The net force on the fluid segment below 2.5m elevation of the manometer arms (simulated with the level tracking method)

Figure 3-16 are clean and from these spike changes and oscillations. It should be noted that the sudden drop in cell pressures as the bubbly mixture of liquid and gas reverses direction is due to the fluid acceleration in the opposite direction of gravity.

The next test simulated in this section is the oscillating manometer. As shown in Figure 3-9 and Figure 3-10, the solution method with the level tracking failed to simulate this test prior to the additional considerations made for the liquid-gas interface

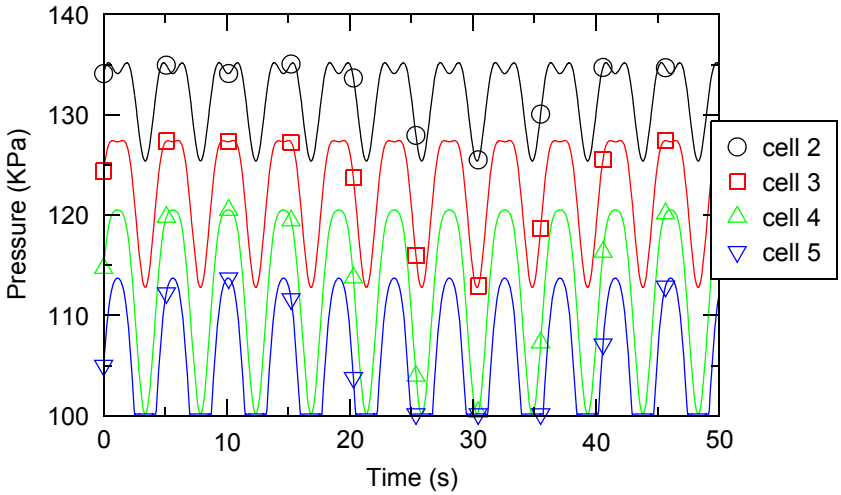

FIGURE 3-19. Pressures along the oscillating manometer arm (simulated with the level tracking method)

crossing the cell boundaries. The leading cause of this failure to simulate the oscillating manometer was the pressure spikes caused by the interface crossing cell boundaries. Figure 3-18 shows none of these pressure spikes. Thus, the water level of the manometer arm oscillates without any sign of decay as expected in Figure 3-17. Further, the simulated cell pressures below the oscillating water level in Figure 3-19 compare almost perfectly to the pressures predicted analytically in Figure 2-17. These results for the oscillating manometer test are as close as a discrete solution can be to the analytical solution for the oscillating manometer, which is a point that demonstrates the success of the approach outlined in this section to propagate interfaces across cell boundaries.

Corrections to The Closure Models

The modifications to the field equations and the extra measures taken to ensure that the water levels cross the cell boundaries without harming the solution are not sufficient alone for a successful level tracking method. Although it was not discussed in the previous sections, a correction was necessary to the definition of the interfacial

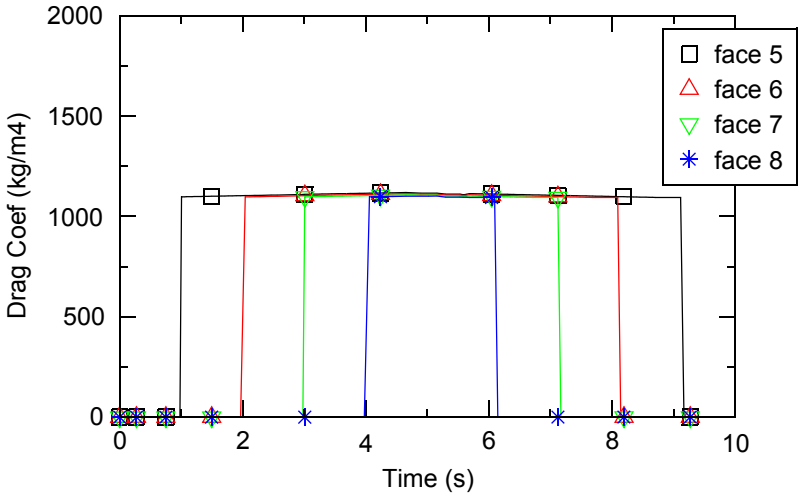

FIGURE 3-20. Interfacial drag coefficients at cell boundaries of the single-phase fill and drain test (simulated with the level tracking method)

drag coefficient in terms of fluid properties at a cell boundary when a liquid-gas interface was present in either cell adjacent to the boundary. This correction to the interfacial drag coefficient is explained here along with another correction to the interfacial heat transfer coefficient that is necessary to simulate the condensation test described in CHAPTER 2.

Interfacial Drag

Let us first consider the interfacial drag coefficient, C_i in (1-12). This coefficient relates the drag force between the separated field to the relative velocity of one field to another. Therefore, it is a strong function of the flow regime The void fraction that is used to determine the flow regime for any given staggered cell (see Figure 3-4) is an average of void fractions from half-cells that make up the staggered cell. As emphasized in discussions on modifications to the momentum equations, the use of an average void fraction for the entire staggered volume is not consistent with the corrections made to the flux terms of conservation equations. The conclusion from these discussions is that the balance of forces acting on the fluid should represent the conditions prevailing at cell boundaries, i.e. the center of staggered cell. In view of this

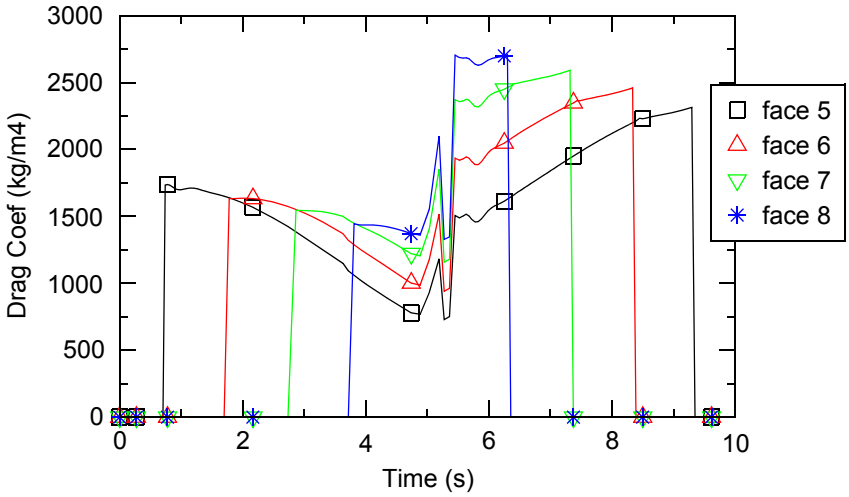

FIGURE 3-21. Interfacial drag coefficients at cell boundaries of the two-phase fill and drain test (simulated with the level tracking method)

conclusion, the interfacial drag coefficient in (1-12) is evaluated in terms of fluid conditions that prevail at the cell boundary when a liquid-gas interface is present in either of cells adjacent to the boundary.

$$C_{i,j+1/2} = \begin{cases} C(\alpha_{E,j+1/2}) & , \quad \text{if } \lambda_{E,j+1/2} \neq 0 \\ C(\langle\alpha\rangle_{j+1/2}) & , \quad \text{if } \lambda_{E,j+1/2} = 0 \end{cases} \tag{3-54}$$

Figure 3-20 shows the interface drag coefficients at cell boundaries (i.e. cell faces) along the test pipe of the single-phase rising and falling test. The sharp change in the drag coefficient is expected as the water level crosses the cell boundaries. It should be noted here that it is a common practice among the methods like semi-implicit to impose limits on the rate at which drag coefficients change. Such limits are set to prevent numerical instabilities due to explicit nature of these coefficients. In the case of an interface crossing the cell boundary, however, no limit should be imposed on the interfacial drag coefficient since a sharp change is expected and the remainder of equations are already preconditioned to account for sharp changes and to remain sta-

ble. Contrary to the other cases, imposing any such limit renders the solution unstable in this case.

The interfacial drag coefficients at cell faces along the test pipe of the two-phase rising and falling test exhibit sharp changes, as expected, as the mixture level crosses the cell boundaries. In addition to the expected sharp changes, the interfacial drag coefficients in Figure 3-21 also show how strongly the drag coefficient depends on the void fraction that prevails at the cell boundary along with the relative motion of fields against each other. In this figure, the decreasing drag coefficient at a cell boundary realizes the slight depression of void fraction in the adjacent cells, already seen in Figure 3-15, as the column of bubbly liquid and gas mixture rises above a cell boundary. This behavior is physically sensible since the void fraction of a bubbly liquid-gas mixture is expected to decrease under an increasing weight of the rising mixture column.

Interfacial Heat and Mass Transfer

The closure model for the interfacial heat transfer (IHT) between the liquid and gas fields must account for the presence of water levels in computational cells. A brief description of the IHT model in TRAC is therefore appropriate here before discussing how the IHT model should be adjusted. The following two equations describe the heat transfer to and from liquid and gas at the phase interface.

$$\begin{aligned} q_g &= q_{ig} + q_{dg} \\ &= \frac{P_s}{P} H_{\mathrm{CHTI}}(T_g - T_{sv}) + \frac{P_a}{P} H_{\mathrm{CHTA}}(T_g - T_l) \end{aligned} \tag{3-55}$$

$$\begin{aligned} q_l &= q_{il} + q_{dl} \\ &= [H_{\mathrm{ALVE}}(T_l - T_{sv}) + H_{\mathrm{ALV}}\langle T_l - T_{sat}\rangle^{\dagger}] + \frac{P_a}{P} H_{\mathrm{CHTA}}(T_l - T_g) \end{aligned} \tag{3-56}$$

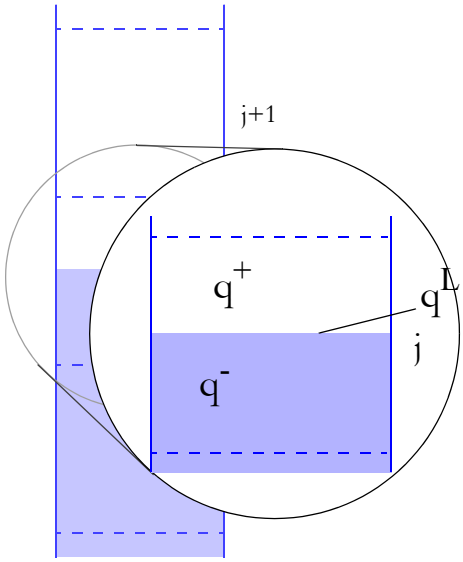

FIGURE 3-22. Interfacial HT terms designated for a computational volume with the stratified liquid-gas interface

where

$$\langle T_l - T_{sat} \rangle^{\dagger} = \begin{cases} 0 & \text{if } T_l \le T_{sat} \\ T_l - T_{sat} & \text{if } T_l > T_{sat} \end{cases}. \tag{3-57}$$

In the above equations, P_s is the steam partial pressure, P_a the non-condensable partial pressure, P the total pressure (i.e. $P_s + P_a$), T_{sv} the saturation temperature at the steam partial pressure, and T_{sat} the saturation temperature at the total pressure. Equation (3-55) assumes that the gas field is a homogeneous mixture of water vapor and non condensable gas in thermodynamic equilibrium. The first term in (3-55) accounts for heat transfer to or from the interface (q_{ig}) and is converted to or released as latent heat through phase change. The second term in (3-55), which has the P_a/P multiplier, is the direct sensible heat exchange between the liquid and the gas fields. Similarly, the first term in (3-56) corresponds to the sensible heat trans-

ferred to or from the interface, which is converted to or released as latent heat. The second term in (3-56) is the direct sensible heat exchange between the liquid and the gas fields. It should be noted that the liquid to interface term has two heat transfer coefficients, H_{ALV} and H_{ALVE}, for condensation and evaporation. Evaporation occurs if $T_{sv} < T_l < T_{sat}$ and flashing occurs if $T_l > T_{sat}$. Equations (3-55) and (3-56) are added to calculate the total rate of heat exchange at the phase interface where the direct sensible heat transfer terms, q_{dg} and q_{dl}, cancel out.

$$Vol\ h_{fg} \cdot \Gamma_i = q_{ig} + q_{il} \tag{3-58}$$

When there is a water level inside a computational cell, the IHT coefficients must be determined for each region above and below the level along with the coefficients that describe the heat transfer at the level as follows:

$$q_g = (q_{ig}^{-} + q_{dg}^{-}) + (q_{ig}^{\mathrm{L}} + q_{dg}^{\mathrm{L}}) + (q_{ig}^{+} + q_{dg}^{+}) \tag{3-59}$$

$$q_l = (q_{il}^{-} + q_{dl}^{-}) + (q_{il}^{\mathrm{L}} + q_{dl}^{\mathrm{L}}) + (q_{il}^{+} + q_{dl}^{+}) \tag{3-60}$$

The heat transfer coefficients for regions above and below the interfaces can be easily determined using the same procedures that apply to an entire computational cells. However, it should be noted that the field temperatures are assumed identical above and below the interface. This is an assumption which may lead to significant errors. Another area of concern is the description heat transfer at the level. In the presence of a strong condensation, the temperature of stratified liquid near the level may be very close to the saturation temperature, and thus, create a resistance to further condensation. As this may sound like a subtle detail, it is a situation which should be considered very carefully and accounted for by the IHT terms "from" and "to" the

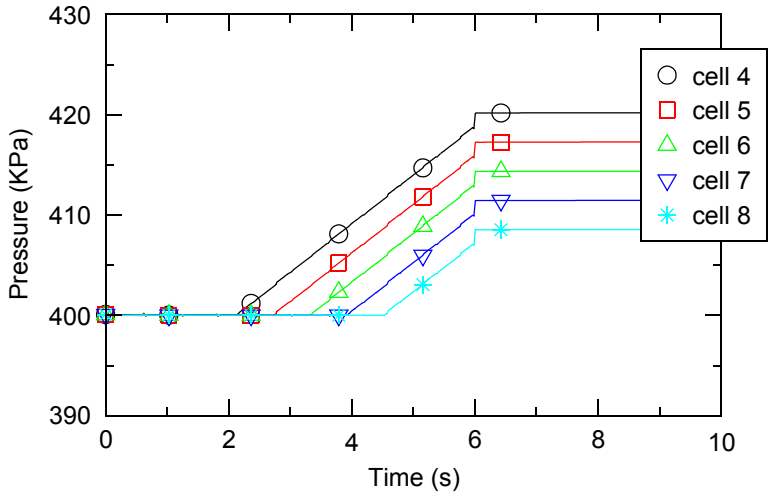

FIGURE 3-23. Pressures along the condensation test pipe (simulated with the level tracking method)

saturation interface at the water level, i.e. q_{ig}^{L} and q_{il}^{L}. For the purpose of this thesis, these two terms will be determined using TRAC's special treatment for the computational volumes that represent the accumulator or pressurizer of a nuclear plant while it is noted that evaluating these two terms accurately requires an investigation of its own.

The results from the repeated condensation test, after the corrections in (3-59) and (3-60) are incorporated into the interfacial heat transfer model, demonstrate significant improvements to the simulation. First, the cell pressures along the test pipe show none of the spikes and other problems that had been recorded previously in Figure 2-26 and Figure 2-27. Previously, this test was simulated without and with the water packing model of TRAC to illustrate the difficulty of simulating this test. A comparison of the required number of time steps as a function of the simulation time from the two simulations in Figure 2-30 had revealed a limited success with the water packing. When the water packing model of TRAC was engaged, the total number of time steps was reduced from 3000s to just below 1000. The adjustments made to the

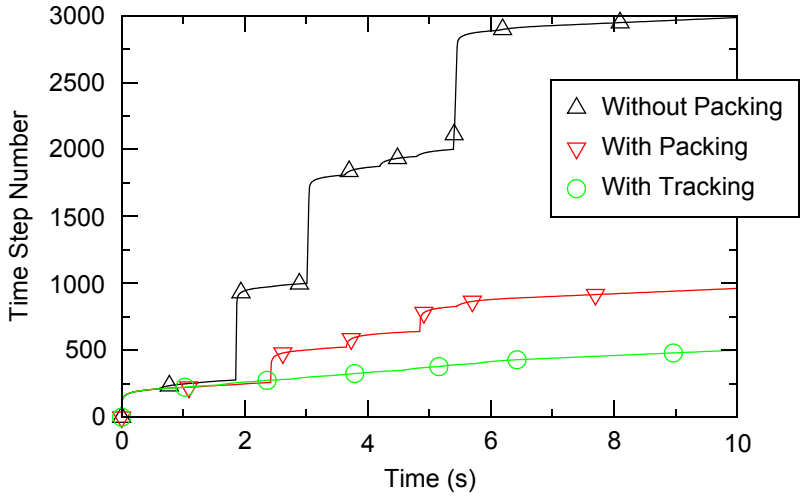

FIGURE 3-24. Comparison of total time step numbers of the condensation test simulations

IHT model reduces the total number of time steps to 500. Figure 3-24 compares the number of time steps required to simulate the condensation test with the standard solution, with the solution aided by the water packing model, and with the solution improved by the level tracking method. It is clear from Figure 3-24 that no additional time steps are needed as the moving front crosses the cell boundaries when the level tracking method is engaged. The time step number as function of simulation time from the water packing exercise is compared to the repeated simulation following the changes to IHT in Figure 3-24 where the total number of time steps is reduced to 500. Figure 3-24 shows that the solution spends no extra time steps as the moving water level fills up the cells with liquid water. This improvement is expected since the water packing model is a remedy for troubles after a cell is already "packed" while the level tracking method predicts the "packing" before it happens and adjusts the initial conditions of a time step to avoid the "packing."

As discussed in CHAPTER 2, the superheated steam is withdrawn into the test pipe at the top to replenish the steam being condensed at it meets the subcooled water at the interface. Previously, large rates of steam flow were recorded in Figure

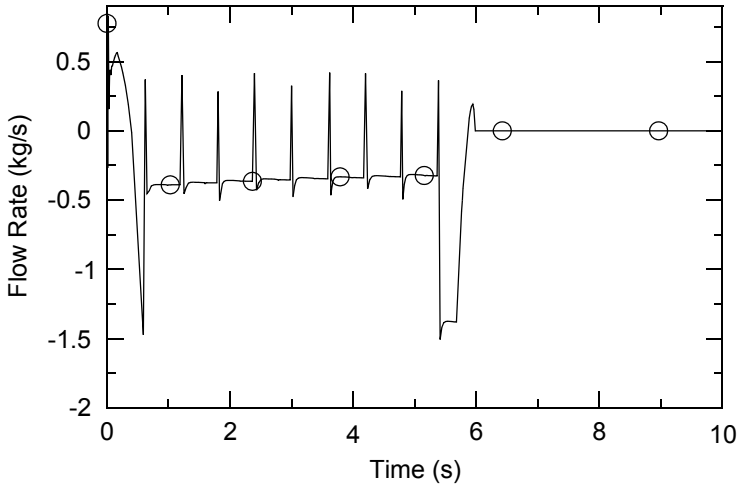

FIGURE 3-25. Steam flow at the top of the condensation test pipe (simulated with the level tracking method)

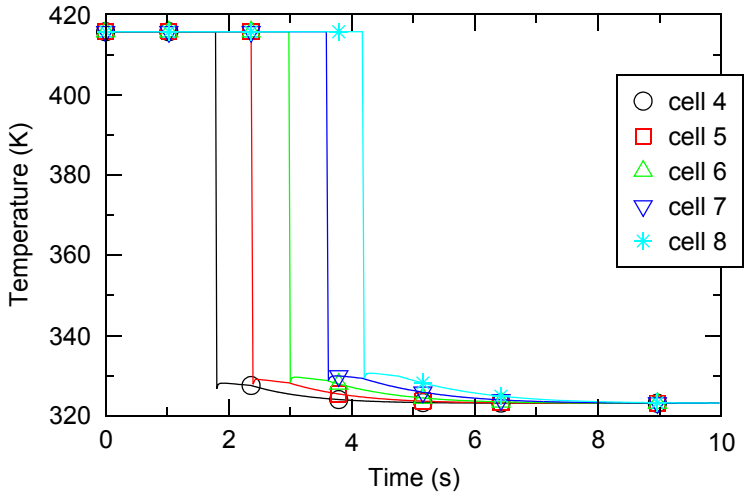

FIGURE 3-26. Liquid temperatures along the condensation test pipe (simulated with the level tracking method)

2-29 because of erroneous condensation taking place inside the test pipe. Figure 3-25 shows that the steam flow rate is much smaller and orderly when the solution is improved by the level tracking method. However, an irregular change in condensation is observed as the water level traverses the "inlet" and "exit" computational volumes of the test pipe. This inaccurate behavior is due to an inconsistent treatment of the

end cells of one-dimensional flow segments defined within TRAC, and not due to the level tracking method.

One of difficulties stated for this exercise was the added complexity due to the build-up of a saturated layer of liquid at the tail of the moving water level. As this layer builds up, it should continuously decrease the rate at which the steam condenses at the surface. While there is no assurance yet for the accuracy of TRAC's ability to predict the condensation at the interface, a slight and gradual decrease in the condensation is observed as the water level traverses the "interior" cells of the test pipe. This is a result of gradual increase in liquid temperatures near the interface (see Figure 3-26), that reflects the build up of a warmer liquid layer. While a comparison of the liquid temperatures in Figure 3-26 to the temperatures previously recorded in Figure 2-28 leaves no doubt about the improvements to TRAC realized by the level tracking method, it is extremely important to assess TRAC's ability to predict the interfacial heat transfer rate at the surface of liquid-gas interfaces by simulating an experiment with available data. The desired capability for TRAC is to predict the "correct" rate of condensation and the build-up of warmer liquid layer only due to the IHT at the surface of the water level.

References

3-1. Charboneau, B.L., "Overview of TRAC-BF1/MOD1 Assessment Studies," NUREG/CR-4428 (1985), 22-26

3-2. B. Aktas and J. Uhle, "USNRC Code Consolidation and Development Effort," Proceedings of the OECD-CSNI Workshop on Advanced Thermal-Hydraulic and Neutronic Codes: Current and Future Applications, Barcelona, Spain, (2000)

CHAPTER 4

Tracking Water Levels in Three-Dimensional Flows

The numerical experiments in CHAPTER 2 clearly demonstrate the need for a robust method in TRAC to handle the moving water levels when the flow is simulated using three-dimensional field equations. The troubles of TRAC's solution method certainly applies to most solution methods of the same class seen in other TH codes. There is a viable cure for these troubles. Modifications to TRAC's one-dimensional field equations described in CHAPTER 3 demonstrate that a robust method for tracking water levels is attainable. The results also prove that there is a strong correlation between the successful simulations of the numerical experiments presented in CHAPTER 3, and the consistency within the modifications made to the field equations to achieve this success. This correlation reemphasizes the already known fact that half measures do not produce satisfactory results when the field equations are modified to augment the solution methods of TH codes. As proven by the results presented in CHAPTER 3, this argument certainly holds true for the changes made to the field equations whose purpose is to account for the divided nature of computational volumes that consist of water levels. Considering the full implications of extending the modifications to the field equations becomes even more critical to attain a robust method that works for the three-dimensional field equations of TRAC.

The picture of a computational volume that consists of two sub-volumes, each with its own distinct flow topology, separated by an interface, suits well the use of one-dimensional field equations to simulate vertical two-phase flows. When the liquid-gas interface is confined into a computational volume, no assumption needs to be made with respect to its surface topology or the evolution of its shape. Approximating the state of fluid inside the regions above and below the interface is sufficient to redefine the fluid motion across cell boundaries. Redefining the fluid motion hence stops the inadvertent flux of quantities across a cell boundary from the sub-volume on the opposite side of a divided cell, i.e. the region below an interface for the upper cell boundary and the region above an interface for the lower cell boundary. However, it becomes necessary to assume a shape for the interface as the evolving conditions inside a computational volume set the interface on a path to cross across a cell boundary. Assuming that the liquid-gas interface is simply a flat surface reduces the interface into a moving point of discontinuity along the one-dimensional axis of flow and allows the tracking method to propagate it instantly across a cell boundary. The presentation in CHAPTER 3 proves that this approach works well for TRAC's one-dimensional field equations. However, it is critical to develop a rigorous understanding of how this approach works so well before it can be extended for vertical flows simulated using three-dimensional field equations.

Redefining the gas fraction of a fluid (i.e. void fraction) convected across the boundaries of a vertical cell that consists of a water level is a direct and efficient way to stop the inadvertent flux of quantities, i.e. Equations (3-15) and (3-16). However, these newly defined void fractions across cell boundaries must be propagated to every applicable term in the field equations in order to maintain the consistency within the field equations. While it is relatively straightforward to maintain this consistency in TRAC's one-dimensional field equations, repeating the same success with its three-dimensional field equations is a more daunting task. Figure 4-1 compares the picture

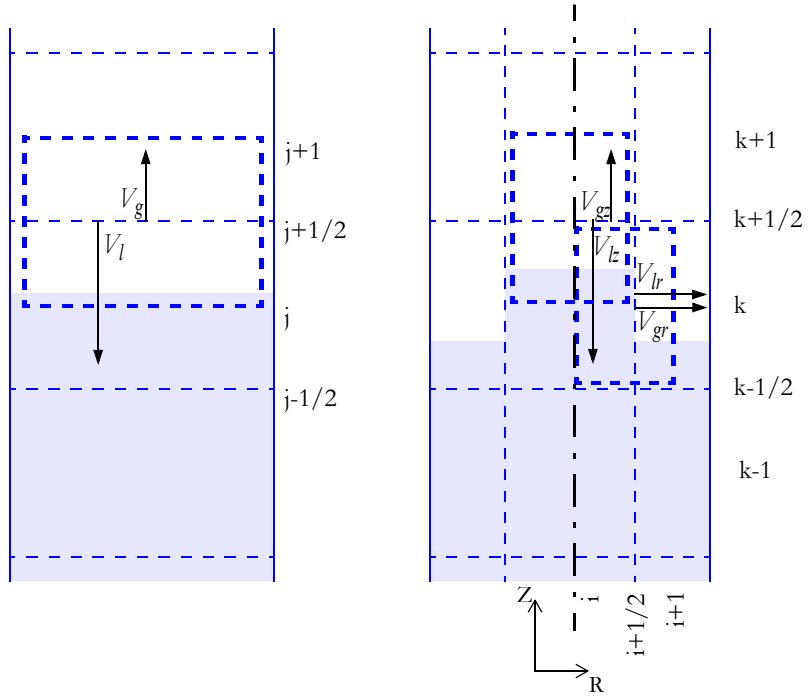

FIGURE 4-1. 1D and 3D computational volumes with the liquid-gas interface

of two vertical flow models. The model on the left is a section of the one-dimensional fill and drain test pipe while the one on the right is a section of the two-dimensional fill and drain test pipe. Assuming a flat shape for the liquid-gas interface suits well the one-dimensional model since the fluid motion is modified only at Junctions j-1/2 and j+1/2. However, the flat shape assumption requires that additional details be worked out before it can be implemented in the three-dimensional model. For instance, one must ensure that the modifications to stop the inadvertent flux of quantities in the Z-direction do not have unintended consequences on the fluid motion in the lateral directions (i.e. in the R-Θ plane). Therefore, a set of rules must be developed which can form the basis for modifications to the field equations in the R- and Θ-directions. These rules should help the fluid motion in the R-Θ plane to recognize the discontinuous nature of the fluid in the Z-direction. Thus, the field equations in the R- and Θ-directions can remain consistent while the field equations in all three directions are

modified to account for the presence of a liquid-gas interface with an "assumed" flat shape.

A road map to a robust level tracking method for TRAC's three-dimensional field equations begins with implementing the modifications of the one-dimensional field equations, already described in CHAPTER 3, into the Z-direction component of the three-dimensional field equations. Thus, the modifications to the one-dimensional field equations will form the basis for modifications to the three-dimensional field equations. Equations (3-1) to (3-12) will continue to be used to determine the conditions that favor the presence of a liquid-gas interface in a three-dimensional volume. Next, the field equations in the R- and Θ-directions will be modified to account for the discontinuous nature of the fluid in the Z-direction.

Modifications to the Z-Direction Field Equations

Once the level tracking method (Equations (3-1) to (3-12)) determines that a stratified liquid-gas interface is present in a three-dimensional computational volume, a new variable, λ_{zE}, is defined to specify the distance between the liquid-gas interface (with an assumed flat shape) and the cell boundaries in the Z-direction. A second variable, α_{zE}, is defined to specify the void fraction of the two-phase fluid to be convected across the axial boundaries.

$$\tilde{\lambda}^{n+1}_{zE\ i,j,k+1/2} = \begin{cases} \tilde{L}^{n+1}_{i,j,k+1} & \text{, if } \tilde{\lambda}^{n+1}_{i,j,k+1} = 1 \\ \tilde{L}^{n+1}_{i,j,k} - \Delta z_k & \text{, if } \tilde{\lambda}^{n+1}_{i,j,k} = 1 \\ 0 & \text{, otherwise} \end{cases} \tag{4-1}$$

where $\tilde{\lambda}^{n+1}_{i,j,k}$ is set to one to flag the existence of a water level in cell i,j,k or to zero when there is no level water level. It should be noted that this variable is based on the projected location of the liquid-gas interface at time step *n+1*.

$$\alpha_{zE\ i,j,k\text{-}1/2} = \begin{cases} \alpha^{-}_{i,j,k} & , \text{if } \tilde{\lambda}^{n+1}_{zE\ i,j,k\text{-}1/2} > 0 \\ \alpha^{+}_{i,j,k\text{-}1} & , \text{if } \tilde{\lambda}^{n+1}_{zE\ i,j,k\text{-}1/2} < 0 \\ \langle\alpha\rangle_{i,j,k\text{-}1/2} & , \text{if } \tilde{\lambda}^{n+1}_{zE\ i,j,k\text{-}1/2} = 0 \end{cases} \tag{4-2}$$

$$\alpha_{zE\ i,j,k+1/2} = \begin{cases} \alpha^{-}_{i,j,k+1} & , \text{if } \tilde{\lambda}^{n+1}_{zE\ i,j,k+1/2} > 0 \\ \alpha^{+}_{i,j,k} & , \text{if } \tilde{\lambda}^{n+1}_{zE\ i,j,k+1/2} < 0 \\ \langle\alpha\rangle_{i,j,k+1/2} & , \text{if } \tilde{\lambda}^{n+1}_{zE\ i,j,k+1/2} = 0 \end{cases} \tag{4-3}$$

In the above equations, $\langle\alpha\rangle$ is the void fraction at a boundary defined as an average of void fractions computed for the cells adjacent to a boundary.

The Z-Direction Components of Mass and Energy Equations

Averaging of the properties at the axial faces, i.e. Faces 5 and 6, are modified by redefining the flow areas of these cell faces in Equation (1-75) as follows.

$$\begin{aligned} \phi_{gm} &= \langle\alpha\rho_g\rangle^n_m A^{\alpha}_{gm} V^{n+1}_{gm} \\ \phi_{lm} &= \langle(1-\alpha)\rho_l\rangle^n_m A^{\alpha}_{lm} V^{n+1}_{lm} \\ \zeta_{gm} &= \langle\alpha\rho_g e_g\rangle^n_m A^{\alpha}_{gm} V^{n+1}_{gm} \\ \zeta_{lm} &= \langle(1-\alpha)\rho_l e_l\rangle^n_m A^{\alpha}_{lm} V^{n+1}_{lm} \\ \omega_{gm} &= \langle\alpha\rangle^n_m A^{\alpha}_{gm} V^{n+1}_{gm} \\ \omega_{lm} &= \langle 1-\alpha\rangle^n_m A^{\alpha}_{lm} V^{n+1}_{lm} \end{aligned} \tag{4-4}$$

where m =5,6 and the new definition of flow area in the gas and liquid terms accounts for the presence of an interface in either of axial cells adjacent to Faces 5 and 6.

For m =1,2,3,4, the flux terms are defined by Equation (1-75) until the flux terms of these faces are modified.

$$A_{g5}^{\alpha} = \begin{cases} A_5 \dfrac{\alpha_{zE\ i,j,k\text{-}1/2}}{\alpha_{i,j,k\text{-}1}} & \text{, if } (\tilde{\lambda}_{zE\ i,j,k\text{-}1/2}^{n+1} < 0) \text{ and } (V_{g5} > 0) \\ A_5 \dfrac{\alpha_{zE\ i,j,k\text{-}1/2}}{\alpha_{i,j,k}} & \text{, if } (\tilde{\lambda}_{zE\ i,j,k\text{-}1/2}^{n+1} > 0) \text{ and } (V_{g5} < 0) \\ A_5 & \text{, otherwise} \end{cases} \tag{4-5}$$

$$A_{l5}^{\alpha} = \begin{cases} A_5 \dfrac{1-\alpha_{zE\ i,j,k\text{-}1/2}}{1-\alpha_{i,j,k\text{-}1}} & \text{, if } (\tilde{\lambda}_{zE\ i,j,k\text{-}1/2}^{n+1} < 0) \text{ and } (V_{l5} > 0) \\ A_5 \dfrac{1-\alpha_{zE\ i,j,k\text{-}1/2}}{1-\alpha_{i,j,k}} & \text{, if } (\tilde{\lambda}_{zE\ i,j,k\text{-}1/2}^{n+1} > 0) \text{ and } (V_{l5} < 0) \\ A_5 & \text{, otherwise} \end{cases} \tag{4-6}$$

$$A_{g6}^{\alpha} = \begin{cases} A_6 \dfrac{\alpha_{zE\ i,j,k+1/2}}{\alpha_{i,j,k}} & \text{, if } (\tilde{\lambda}_{zE\ i,j,k+1/2}^{n+1} < 0) \text{ and } (V_{g6} > 0) \\ A_6 \dfrac{\alpha_{zE\ i,j,k+1/2}}{\alpha_{i,j,k+1}} & \text{, if } (\tilde{\lambda}_{zE\ i,j,k+1/2}^{n+1} > 0) \text{ and } (V_{g6} < 0) \\ A_6 & \text{, otherwise} \end{cases} \tag{4-7}$$

$$A_{l6}^{\alpha} = \begin{cases} A_6 \dfrac{1-\alpha_{zE\ i,j,k+1/2}}{1-\alpha_{i,j,k}} & \text{, if } (\tilde{\lambda}_{zE\ i,j,k+1/2}^{n+1} < 0) \text{ and } (V_{l6} > 0) \\ A_6 \dfrac{1-\alpha_{zE\ i,j,k+1/2}}{1-\alpha_{i,j,k+1}} & \text{, if } (\tilde{\lambda}_{zE\ i,j,k+1/2}^{n+1} > 0) \text{ and } (V_{l6} < 0) \\ A_6 & \text{, otherwise} \end{cases} \tag{4-8}$$

The above equations redefine the Z-direction component flux terms in the mass and energy equations of the basic step. However, these corrections to the flux terms in the basic step equations do not work for the flux terms in the stabilizer step equations as the flux terms in these equations are formulated in terms of $\tilde{\alpha}^{n+1}$ from the basic step, not α^{n} of the previous time step. Similar to Equations (3-25) and (3-26) of the one-dimensional field equations, the following equations are used to adjust the "phasic" flow areas at Faces 5 and 6 so that the flux terms of these faces in the stabilizer step equations remain consistent with the solution to the basic step equations.

$$A_{g5}^{\alpha} \rightarrow \begin{cases} A_{g5}^{\alpha} \dfrac{\alpha_{i,j,k-1}^{n}}{\tilde{\alpha}_{i,j,k-1}^{n+1}} & \text{, if } (\tilde{\lambda}_{zE\ i,j,k-1/2}^{n+1} < 0) \text{ and } (V_{g5} > 0) \\ A_{g5}^{\alpha} \dfrac{\alpha_{i,j,k}^{n}}{\tilde{\alpha}_{i,j,k}^{n+1}} & \text{, if } (\tilde{\lambda}_{zE\ i,j,k-1/2}^{n+1} > 0) \text{ and } (V_{g5} < 0) \end{cases} \tag{4-9}$$

$$A_{l5}^{\alpha} \rightarrow \begin{cases} A_{l5}^{\alpha} \dfrac{(1-\alpha_{i,j,k-1}^{n})}{(1-\tilde{\alpha}_{i,j,k-1}^{n+1})} & \text{, if } (\tilde{\lambda}_{zE\ i,j,k-1/2}^{n+1} < 0) \text{ and } (V_{l5} > 0) \\ A_{l5}^{\alpha} \dfrac{(1-\alpha_{i,j,k}^{n})}{(1-\tilde{\alpha}_{i,j,k}^{n+1})} & \text{, if } (\tilde{\lambda}_{zE\ i,j,k-1/2}^{n+1} > 0) \text{ and } (V_{l5} < 0) \end{cases} \tag{4-10}$$

$$A_{g6}^{\alpha} \rightarrow \begin{cases} A_{g6}^{\alpha} \dfrac{\alpha_{i,j,k}^{n}}{\tilde{\alpha}_{i,j,k}^{n+1}} & \text{, if } (\tilde{\lambda}_{zE\ i,j,k+1/2}^{n+1} < 0) \text{ and } (V_{g6} > 0) \\ A_{g6}^{\alpha} \dfrac{\alpha_{i,j,k+1}^{n}}{\tilde{\alpha}_{i,j,k+1}^{n+1}} & \text{, if } (\tilde{\lambda}_{zE\ i,j,k+1/2}^{n+1} > 0) \text{ and } (V_{g6} < 0) \end{cases} \tag{4-11}$$

$$A_{l6}^{\alpha} \rightarrow \begin{cases} A_{l6}^{\alpha} \dfrac{(1-\alpha_{i,j,k}^{n})}{(1-\alpha_{i,j,k}^{\tilde{}\,n+1})} & \text{, if } (\tilde{\lambda}_{zE\ i,j,k+1/2}^{n+1} < 0) \text{ and } (V_{l6} > 0) \\ A_{l6}^{\alpha} \dfrac{(1-\alpha_{i,j,k+1}^{n})}{(1-\alpha_{i,j,k+1}^{\tilde{}\,n+1})} & \text{, if } (\tilde{\lambda}_{zE\ i,j,k+1/2}^{n+1} > 0) \text{ and } (V_{l6} < 0) \end{cases} \tag{4-12}$$

Redefining the macroscopic quantities that are convected across Faces 5 and 6 of three-dimensional cells curtails the otherwise inadvertent flux of quantities in the Z-direction of the flow. As they were for the one-dimensional field equations, the modifications above are necessary but not sufficient for a successful method of level tracking. Liquid and gas velocities in Equation (4-4) must also be adjusted to agree with the prevailing fluid conditions at Faces 5 and 6.

Just as it was important to counter the situation when a liquid-gas interface crossed over a cell boundary, the same special care must be given to the Z-direction component of the field equations in order to achieve a robust method of level tracking.

First, a critical time step size must be projected for an interface to cross the cell boundary in the direction of its propagation based on its current location and velocity.

$$\Delta\tau_{i,j,k} = \begin{cases} \dfrac{\Delta z_k - L_{i,j,k}^{n}}{V_{L,i,j,k}^{n}} & \text{, if } V_{L,i,j,k}^{n} > 0 \\ \dfrac{L_{i,j,k}^{n}}{V_{L,i,j,k}^{n}} & \text{, if } V_{L,i,j,k}^{n} < 0 \end{cases} \tag{4-13}$$

This critical time step size should then be compared to the next time step size to determine whether the interface will cross the cell boundary within the new time step

and a new variable is defined to flag the direction in which the interface is about to cross a cell boundary.

$$X_{L6} = \begin{cases} +\Delta\tau_{i,j,k} & , \text{if } (\Delta\tau_{i,j,k} < \Delta t) \wedge (V^n_{L,i,j,k} > 0) \\ -\Delta\tau_{i,j,k+1} & , \text{if } (\Delta\tau_{i,j,k+1} < \Delta t) \wedge (V^n_{L,i,j,k+1} < 0) \end{cases} \tag{4-14}$$

The following equations, which are analogous to Equations (3-34) to (3-44), are applied to redefine the flux terms of Face 6 in a time step when a liquid-gas interface is expected to cross this cell boundary.

$$\phi_{g6}\Delta t = \langle \alpha\rho_g \rangle^n_6 A^\alpha_{g6} V^{n+1}_{g6} \Delta t + \frac{\langle \alpha\rho_g \rangle^n_6}{\langle \alpha \rangle_6} \delta\mathrm{Vol}_{g6} \tag{4-15}$$

$$\phi_{l6}\Delta t = \langle (1-\alpha)\rho_l \rangle^n_6 A^\alpha_{l6} V^{n+1}_{l6} \Delta t + \frac{\langle (1-\alpha)\rho_l \rangle^n_6}{\langle 1-\alpha \rangle^n_6} \delta\mathrm{Vol}_{l6} \tag{4-16}$$

$$\zeta_{g6}\Delta t = \langle \alpha\rho_g e_g \rangle^n_6 A^\alpha_{g6} V^{n+1}_{g6} \Delta t + \frac{\langle \alpha\rho_g e_g \rangle^n_6}{\langle \alpha \rangle^n_6} \delta\mathrm{Vol}_{g6} \tag{4-17}$$

$$\zeta_{l6}\Delta t = \langle (1-\alpha)\rho_l e_l \rangle^n_6 A^\alpha_{l,6} V^{n+1}_{l6} \Delta t + \frac{\langle (1-\alpha)\rho_l e_l \rangle^n_6}{\langle 1-\alpha \rangle^n_6} \delta\mathrm{Vol}_{l6} \tag{4-18}$$

$$\omega_{g6}\Delta t = \langle \alpha \rangle^n_6 A^\alpha_{g6} V^{n+1}_{g6} \Delta t + \delta\mathrm{Vol}_{g6} \tag{4-19}$$

$$\omega_{l6}\Delta t = \langle 1-\alpha \rangle^n_{j6} A^\alpha_{l6} V^{n+1}_{l6} \Delta t + \delta\mathrm{Vol}_{l6} \tag{4-20}$$

where the volume correction for the liquid and gas fields are given by:

$$\delta \mathrm{Vol}_{g6} = \begin{cases} (\alpha^{+}_{i,j,k} - \alpha^{-}_{i,j,k})\mathrm{Vol}^{+}_{j} & \text{, when } X_{L6} > 0 \\ (\alpha^{-}_{i,j,k+1} - \alpha^{+}_{i,j,k+1})\mathrm{Vol}^{-}_{i,j,k+1} & \text{, when } X_{L6} < 0 \end{cases} \tag{4-21}$$

$$\delta \mathrm{Vol}_{l6} = \begin{cases} (\alpha^{-}_{i,j,k} - \alpha^{+}_{i,j,k})\mathrm{Vol}^{+}_{i,j,k} & \text{, when } X_{L6} > 0 \\ (\alpha^{+}_{i,j,k+1} - \alpha^{-}_{i,j,k+1})\mathrm{Vol}^{-}_{i,j,k+1} & \text{, when } X_{L6} < 0 \end{cases} \tag{4-22}$$

As argued for the one-dimensional flows in CHAPTER 3, these corrections are applied only in the basic step and the back up of a time step is enforced if the void fractions of a basic step do not evolve as expected letting the interface remain in the same cell. The initial guess for the void fraction of a cell must also be reset in the basic step when an interface leaves or enters it.

$$\alpha^{n+\mathrm{i}}_{i,j,k}\Big|_{i=0} = \begin{cases} 0.0 & \text{, if } \left(\alpha^{n}_{j} + \sum \omega_g \Delta t\right) \text{ and } (X_{L6} > 0) \\ 1.0 & \text{, if } \left(\alpha^{n}_{j} - \sum \omega_l \Delta t = 0\right) \text{ and } (X_{L5} < 0) \end{cases} \tag{4-23}$$

The Z-Direction Momentum Equations

The same argument made for modifications to the momentum equations of the one-dimensional field equations is valid here for modifications to the Z-direction momentum equations. Corrections to Equation (1-66) and its counterpart for the liquid phase are needed to predict the change in fluid motion inside the region (either above or below an interface) that prevails across an axial cell face.

First, the fluid inertia terms are redefined using the void fractions below and above an interface.

$$\langle \alpha\rho_g \rangle_6^n = \begin{cases} \alpha_{zE\ i,j,k+1/2} \langle \rho_g \rangle_6^n & , \text{if } \tilde{\lambda}_{zE\ i,j,k+1/2}^{n+1} \neq 0 \\ \langle \alpha \rangle_6 \langle \rho_g \rangle_6^n & , \text{if } \tilde{\lambda}_{zE\ i,j,k+1/2}^{n+1} = 0 \end{cases} \tag{4-24}$$

$$\langle (1-\alpha)\rho_l \rangle_6^n = \begin{cases} (1-\alpha_{zE\ i,j,k+1/2}) \langle \rho_l \rangle_6^n & , \text{if } \tilde{\lambda}_{zE\ i,j,k+1/2}^{n+1} \neq 0 \\ (1-\langle \alpha \rangle_6) \langle \rho_l \rangle_6^n & , \text{if } \tilde{\lambda}_{zE\ i,j,k+1/2}^{n+1} = 0 \end{cases} \tag{4-25}$$

Second, the pressure gradient term in (1-65) and its counterpart for the liquid field is redefined as

$$\left.\frac{\partial P}{\partial z}\right|_{i,j,k+1/2}^{n} = \frac{P_{i,j,\mathrm{k+1}}^{n} - P_{i,j,k}^{n} + \delta P_{L6}}{\Delta z_6} \tag{4-26}$$

where the correction term is given by the following equation.

$$\delta P_{L6} = \begin{cases} (0.5\Delta z_{k+1} - \tilde{L}_{i,j,k+1}^{n+1}) \left.\frac{\partial P}{\partial z}\right|_{i,j,k\text{-}1/2}^{n} & , \text{if } \tilde{L}_{i,j,k+1}^{n+1} < 0.5\Delta z_{k+1} \\ (0.5\Delta z_k - \tilde{L}_{i,j,k}^{n+1}) \left.\frac{\partial P}{\partial z}\right|_{i,j,k\text{-}3/2}^{n} & , \text{if } \tilde{L}_{i,j,k}^{n+1} > 0.5\Delta z_k \\ 0.0 & , \text{otherwise} \end{cases} \tag{4-27}$$

As argued for the one-dimensional stabilizer momentum equations, the pressure drop correction given in the above equation can not be applied to the Z-direction stabilizer momentum equations. The pressure drop correction for the Z-direction stabilizer momentum equations must be based on the "calculated" location of the liquid-gas interface at the end of a time step, i.e. $L_{i,j,k}^{n}$, using an equation analogous to Equation (3-31).

$$\delta P_{L6} = \begin{cases} (0.5\Delta z_{k+1} - L^n_{i,j,k+1}) \left.\dfrac{\partial P}{\partial z}\right|^n_{i,j,k\text{-}1/2} & \text{, if } L^n_{i,j,k+1} < 0.5\Delta z_{k+1} \\ (0.5\Delta z_k - L^n_{i,j,k}) \left.\dfrac{\partial P}{\partial z}\right|^n_{i,j,k\text{-}3/2} & \text{, if } L^n_{i,j,k} > 0.5\Delta z_k \\ 0.0 & \text{, otherwise} \end{cases} \tag{4-28}$$

Third, the gradients of liquid and gas velocities across Faces 5 and 6 are set to zero based on an assumption that the changes in fluid velocity across the liquid-gas interface will not contribute to the pressure drop across these faces. The arguments made for Equations (3-29) and (3-30) are valid for the Z-direction momentum equations and the corrections to the axial momentum flux terms are given by the following equations.

$$\left.\frac{\partial V_{lz}}{\partial z}\right|^n_{i,j,k+1/2} = 0 \text{ when } \begin{cases} (\tilde{\lambda}^{n+1}_{zE\ i,j,k+1/2} < 0) \text{ and } (V^n_{l6} > 0) \\ (\tilde{\lambda}^{n+1}_{zE\ i,j,k+1/2} > 0) \text{ and } (V^n_{l6} < 0) \end{cases} \tag{4-29}$$

$$\left.\frac{\partial V_{gz}}{\partial z}\right|^n_{i,j,k+1/2} = 0 \text{ when } \begin{cases} (\tilde{\lambda}^{n+1}_{zE\ i,j,k+1/2} < 0) \text{ and } (V^n_{g6} > 0) \\ (\tilde{\lambda}^{n+1}_{zE\ i,j,k+1/2} > 0) \text{ and } (V^n_{g6} < 0) \end{cases} \tag{4-30}$$

Lastly, the wall and the interfacial drag force terms in the Z-direction momentum equations must be evaluated in terms of the variables that describe the prevailing flow region (i.e. either the sub-region above or below a liquid-gas interface), i.e. for cell faces m =5,6

$$f_m = \begin{cases} F(\alpha_{zE\ i,j,k+1/2}) & \text{, if } \lambda_{zE\ i,j,k+1/2} \neq 0 \\ F(\langle\alpha\rangle_6) & \text{, if } \lambda_{zE\ i,j,k+1/2} = 0 \end{cases} \tag{4-31}$$

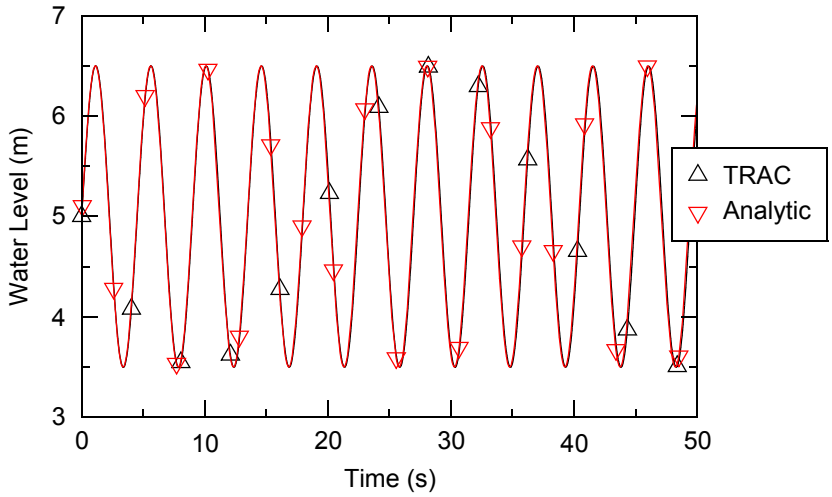

FIGURE 4-2. Collapsed levels of the oscillating 2D manometer test (simulated with the level tracking method)

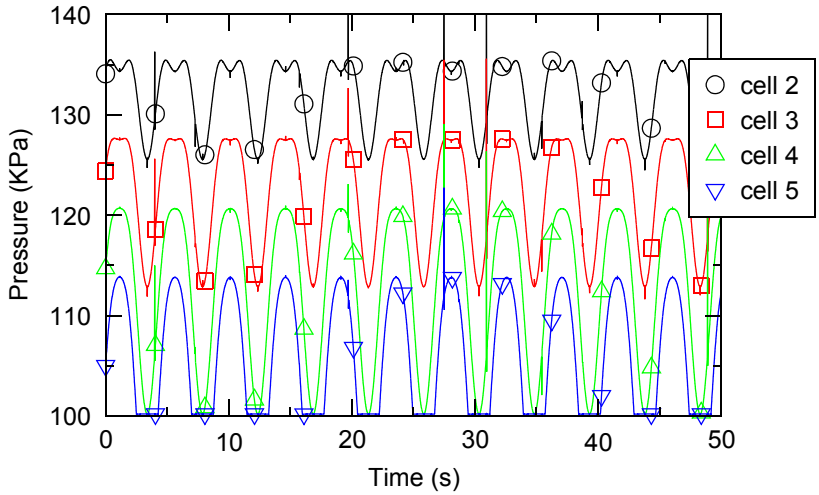

FIGURE 4-3. Pressures along the arm of the 2D oscillating manometer

The modifications to the field equations in the Z-direction were tested by simulating the oscillating manometer formed by two concentric cylinders shown in Figure 2-21. While this version of the manometer is a two-dimensional model, it exercises only the Z-direction components of the three-dimensional field equations since there is no fluid flow in the R-direction. Therefore, it is an ideal test to exercise the modifications to the Z-direction component of the field equations described above.

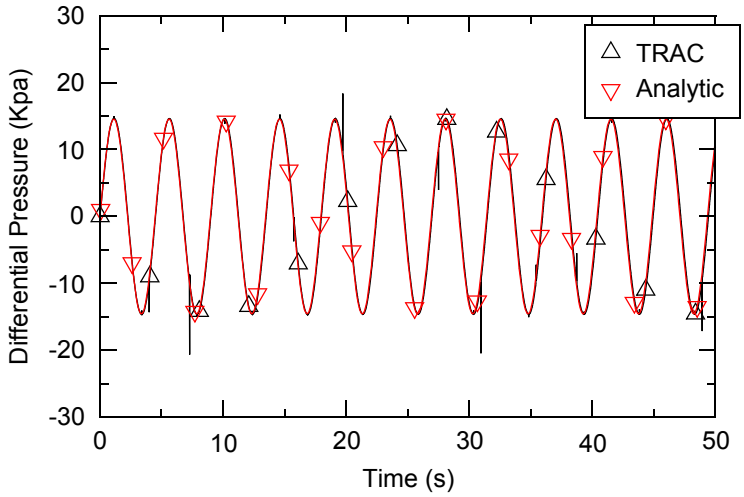

FIGURE 4-4. The net force acting on the fluid segment below 2.5m elevation of the 2D oscillating manometer

Figure 4-2 compares the oscillating water level simulated by TRAC to the level predicted by Equation (2-6). Similarly, in Figure 4-3 and Figure 4-4, the pressures inside the outer ring of the 2D manometer and the net force acting on the segment of the fluid that occupies the space below 2.5m elevation of both arms simulated by TRAC are compared to the closed form predictions of Equations (2-10) and (2-11). All of these comparisons demonstrate the improvement made to TRAC by simply incorporating the level tracking method into its Z-direction component of the three-dimensional field equations.

Modifications to the R- and Θ-Direction Components of the 3D Field Equations

The next step for a robust method that works for truly three-dimensional flows is to factor the "assumed" discontinuous nature of the fluid in the Z-direction into the fluid motion defined in the R- and Θ-direction components of the field equations. There are many ways to accomplish this goal. Some of them can be very complex

approaches, e.g. the use of complex algorithms to determine a surface shape based on the distribution of fluid in adjacent computational volumes. However, the purposes of more complex approaches and the simplest of all, i.e. the flat shape surface, are to achieve the same goal in the end. That is to stop the inadvertent flux of quantities in the vertical direction. Those with long experience in developing models for TH codes have learned that the successful solutions to the problems of TH codes always come in as evolutionary ideas and incremental steps.[4-1] Therefore, a flat shape for the liquid-gas interface will be assumed here to develop the modifications for the R- and Θ-direction components of the field equations.

The R- and Θ-Direction Components of Mass and Energy Equations

While assuming a flat shape for the interface reduces it into a moving point of discontinuity in the Z-direction, it is still a flat surface in the (R-Θ) plane. The fluid motion in the lateral directions must be redefined based on the location of this flat surface with respect to the centers of computational volumes as the lateral motion of the fluid is defined on a grid that links these volume centers across the (R-Θ) plane. Simply, the fluid from the region above an interface should be convected out in the lateral directions if the center of a volume is above the interface, or the fluid from the region below an interface should be convected out if the center is below the interface. Similar to the void fraction defined at the cell boundaries in the Z-direction, i.e. α_{zE}, two new void fractions, α_r and α_θ, are introduced to define the void fraction of the fluid convected out of a three-dimensional volume in the lateral directions. Unlike α_{zE}, these two void fractions are not defined at the cell boundary and they are subscripted with even integers.

$$\alpha_{r\ i,j,k} = \begin{cases} \alpha^{-}_{i,j,k} & \text{, if } \tilde{\lambda}^{n+1}_{zE\ i,j,k\text{-}1/2} > 0.5\Delta z_k \\ \alpha^{+}_{i,j,k\text{-}1} & \text{, if } \tilde{\lambda}^{n+1}_{zE\ i,j,k\text{-}1/2} < 0.5\Delta z_k \\ \alpha_{i,j,k} & \text{, if } \tilde{\lambda}^{n+1}_{zE\ i,j,k\text{-}1/2} = 0 \end{cases} \tag{4-32}$$

$$\alpha_{\theta\ i,j,k} = \begin{cases} \alpha^{-}_{i,j,k} & \text{, if } \tilde{\lambda}^{n+1}_{zE\ i,j,k\text{-}1/2} > 0.5\Delta z_k \\ \alpha^{+}_{i,j,k\text{-}1} & \text{, if } \tilde{\lambda}^{n+1}_{zE\ i,j,k\text{-}1/2} < 0.5\Delta z_k \\ \alpha_{i,j,k} & \text{, if } \tilde{\lambda}^{n+1}_{zE\ i,j,k\text{-}1/2} = 0 \end{cases} \tag{4-33}$$

Next, the above void fractions are used to define the "phasic" flow areas in Equation (4-4) for Faces 1 to 4.

$$A^{\alpha}_{g1} = \begin{cases} A_1 \dfrac{\alpha_{r\ i\text{-}1,j,k}}{\alpha_{i\text{-}1,j,k}} & \text{, if } (\tilde{\lambda}^{n+1}_{zE\ i\text{-}1,j,k\text{-}1/2} > 0) \text{ and } (\tilde{V}^{n+1}_{g1} > 0) \\ A_1 \dfrac{\alpha_{r\ i,j,k}}{\alpha_{i,j,k}} & \text{, if } (\tilde{\lambda}^{n+1}_{zE\ i,j,k\text{-}1/2} > 0) \text{ and } (\tilde{V}^{n+1}_{g1} < 0) \\ A_1 & \text{, otherwise} \end{cases} \tag{4-34}$$

$$A^{\alpha}_{g2} = \begin{cases} A_2 \dfrac{\alpha_{r\ i,j,k}}{\alpha_{i,j,k}} & \text{, if } (\tilde{\lambda}^{n+1}_{zE\ i,j,k\text{-}1/2} > 0) \text{ and } (\tilde{V}^{n+1}_{g2} > 0) \\ A_2 \dfrac{\alpha_{r\ i+1,j,k}}{\alpha_{i+1,j,k}} & \text{, if } (\tilde{\lambda}^{n+1}_{zE\ i+1,j,k\text{-}1/2} > 0) \text{ and } (\tilde{V}^{n+1}_{g2} < 0) \\ A_2 & \text{, otherwise} \end{cases} \tag{4-35}$$

$$A_{g3}^{\alpha} = \begin{cases} A_3 \dfrac{\alpha_{\theta\ i,j\text{-}1,k}}{\alpha_{i,j\text{-}1,k}} & \text{, if } (\tilde{\lambda}_{zE\ i,j\text{-}1,k\text{-}1/2}^{n+1} > 0) \text{ and } (\tilde{V}_{g3}^{n+1} > 0) \\ A_3 \dfrac{\alpha_{\theta\ i,j,k}}{\alpha_{i,j,k}} & \text{, if } (\tilde{\lambda}_{zE\ i,j,k\text{-}1/2}^{n+1} > 0) \text{ and } (\tilde{V}_{g3}^{n+1} < 0) \\ A_3 & \text{, otherwise} \end{cases} \tag{4-36}$$

$$A_{g4}^{\alpha} = \begin{cases} A_4 \dfrac{\alpha_{\theta\ i,j,k}}{\alpha_{i,j,k}} & \text{, if } (\tilde{\lambda}_{zE\ i,j,k\text{-}1/2}^{n+1} > 0) \text{ and } (\tilde{V}_{g4}^{n+1} > 0) \\ A_4 \dfrac{\alpha_{\theta\ i,j+1,k}}{\alpha_{i,j+1,k}} & \text{, if } (\tilde{\lambda}_{zE\ i,j+1,k\text{-}1/2}^{n+1} > 0) \text{ and } (\tilde{V}_{g4}^{n+1} < 0) \\ A_4 & \text{, otherwise} \end{cases} \tag{4-37}$$

Analogous equations hold for the liquid flow areas. These equations redefine the flux terms in the mass and energy equations of the basic step. As before with the Z-direction component of the field equations, these corrections to the flux terms do not work for the flux terms in the stabilizer step equations as the flux terms in these equations are formulated in terms of $\tilde{\alpha}^{n+1}$ from the basic step, not α^{n} of the previous time step. Therefore, the "phasic" flow areas for Faces 1 to 4 must be readjusted to maintain the consistency of the stabilizer step equations with the corrections to the basic step equations.

$$A_{g2}^{\alpha} \rightarrow \begin{cases} A_{g2}^{\alpha} \dfrac{\alpha_{i,j,k}^{n}}{\tilde{\alpha}_{i,j,k}^{n+1}} & \text{, if } (\tilde{\lambda}_{zE\ i,j,k\text{-}1/2}^{n+1} > 0) \text{ and } (\tilde{V}_{g2}^{n+1} > 0) \\ A_{g2}^{\alpha} \dfrac{\alpha_{i+1,j,k}^{n}}{\tilde{\alpha}_{i+1,j,k}^{n+1}} & \text{, if } (\tilde{\lambda}_{zE\ i+1,j,k\text{-}1/2}^{n+1} > 0) \text{ and } (\tilde{V}_{g2}^{n+1} < 0) \end{cases} \tag{4-38}$$

$$A_{l2}^{\alpha} \rightarrow \begin{cases} A_{l2}^{\alpha} \dfrac{(1-\alpha_{i,j,k}^{n})}{(1-\tilde{\alpha}_{i,j,k}^{n+1})} & \text{, if } (\tilde{\lambda}_{zE\ i,j,k\text{-}1/2}^{n+1} > 0) \text{ and } (\tilde{V}_{l2}^{n+1} > 0) \\ A_{l2}^{\alpha} \dfrac{(1-\alpha_{i+1,j,k}^{n})}{(1-\tilde{\alpha}_{i+1,j,k}^{n+1})} & \text{, if } (\tilde{\lambda}_{zE\ i+1,j,k\text{-}1/2}^{n+1} > 0) \text{ and } (\tilde{V}_{l2}^{n+1} < 0) \end{cases} \tag{4-39}$$

$$A_{g4}^{\alpha} \rightarrow \begin{cases} A_{g4}^{\alpha} \dfrac{\alpha_{i,j,k}^{n}}{\tilde{\alpha}_{i,j,k}^{n+1}} & \text{, if } (\tilde{\lambda}_{zE\ i,j,k\text{-}1/2}^{n+1} > 0) \text{ and } (\tilde{V}_{g4}^{n+1} > 0) \\ A_{g4}^{\alpha} \dfrac{\alpha_{i,j+1,k}^{n}}{\tilde{\alpha}_{i,j+1,k}^{n+1}} & \text{, if } (\tilde{\lambda}_{zE\ i,j+1,k\text{-}1/2}^{n+1} > 0) \text{ and } (\tilde{V}_{g4}^{n+1} < 0) \end{cases} \tag{4-40}$$

$$A_{l4}^{\alpha} \rightarrow \begin{cases} A_{l4}^{\alpha} \dfrac{(1-\alpha_{i,j,k}^{n})}{(1-\tilde{\alpha}_{i,j,k}^{n+1})} & \text{, if } (\tilde{\lambda}_{zE\ i,j,k\text{-}1/2}^{n+1} > 0) \text{ and } (\tilde{V}_{l4}^{n+1} > 0) \\ A_{l4}^{\alpha} \dfrac{(1-\alpha_{i,j+1,k}^{n})}{(1-\tilde{\alpha}_{i,j+1,k}^{n+1})} & \text{, if } (\tilde{\lambda}_{zE\ i,j,k\text{-}1/2}^{n+1} > 0) \text{ and } (\tilde{V}_{l4}^{n+1} > 0) \end{cases} \tag{4-41}$$

After implemented, the above redefinition of the macroscopic quantities that are convected across Faces 1 to 4 curtails the inadvertent flux of quantities in the lateral directions from above and below a liquid-gas interface. However, these modifications further require that the liquid and gas velocities in Equation (4-4) for Faces 1 to 4 must be adjusted to agree with the prevailing fluid conditions as well.

The R- and Θ-Direction Momentum Equations

Just as the Z-direction momentum equations are modified to predict the fluid motion inside the sub-region (i.e. above or below an interface) that prevails at a cell face, the R- and Θ-direction momentum equations must be modified to predict the changes in fluid motion across the grid that links the cell centers in the (R-Θ) plane.

Otherwise, the liquid and gas velocities in Equation (4-4) will be inconsistent with the adjusted quantities (i.e. the quantities multiplied by the phasic flow areas) that they multiply. First, the fluid inertia terms are redefined using the void fractions below and above an interface. While the below equations describe the changes to the momentum equation of Face 2, analogous equations are applied to the momentum equations of Faces 1, 3, and 4.

(4-42)

$$\langle \alpha\rho_g \rangle_2^n = \begin{cases} \alpha_{r\ i,j,k} \langle \rho_g \rangle_2^n & \text{, if } (\tilde{\lambda}_{zE\ i,j,k\text{-}1/2}^{n+1} > 0) \text{ and } (\tilde{\lambda}_{zE\ i+1,j,k\text{-}1/2}^{n+1} = 0) \\ \alpha_{r\ i+1,j,k} \langle \rho_g \rangle_2^n & \text{, if } (\tilde{\lambda}_{zE\ i,j,k\text{-}1/2}^{n+1} = 0) \text{ and } (\tilde{\lambda}_{zE\ i+1,j,k\text{-}1/2}^{n+1} > 0) \\ \text{Min}(\alpha_{r\ i,j,k}, \alpha_{r\ i+1,j,k}) \langle \rho_g \rangle_2^n & \text{, if } (\tilde{\lambda}_{zE\ i,j,k\text{-}1/2}^{n+1} > 0) \text{ and } (\tilde{\lambda}_{zE\ i+1,j,k\text{-}1/2}^{n+1} > 0) \\ \alpha_{j+1/2} \langle \rho_g \rangle_2^n & \text{, if } (\tilde{\lambda}_{zE\ i,j,k\text{-}1/2}^{n+1} = 0) \text{ and } (\tilde{\lambda}_{zE\ i+1,j,k\text{-}1/2}^{n+1} = 0) \end{cases}$$

(4-43)

$$\langle (1-\alpha)\rho_l \rangle_2^n = \begin{cases} (1-\alpha_{r\ i,j,k}) \langle \rho_l \rangle_2^n & \text{, if } (\tilde{\lambda}_{zE\ i,j,k\text{-}1/2}^{n+1} > 0) \text{ and } (\tilde{\lambda}_{zE\ i+1,j,k\text{-}1/2}^{n+1} = 0) \\ (1-\alpha_{r\ i+1,j,k}) \langle \rho_l \rangle_2^n & \text{, if } (\tilde{\lambda}_{zE\ i,j,k\text{-}1/2}^{n+1} = 0) \text{ and } (\tilde{\lambda}_{zE\ i+1,j,k\text{-}1/2}^{n+1} > 0) \\ (1-\text{Min}[\alpha_{r\ i,j,k}, \alpha_{r\ i+1,j,k}]) \langle \rho_l \rangle_2^n & \text{, if } (\tilde{\lambda}_{zE\ i,j,k\text{-}1/2}^{n+1} > 0) \text{ and } (\tilde{\lambda}_{zE\ i+1,j,k\text{-}1/2}^{n+1} > 0) \\ (1-\alpha_{j+1/2}) \langle \rho_l \rangle_2^n & \text{, if } (\tilde{\lambda}_{zE\ i,j,k\text{-}1/2}^{n+1} = 0) \text{ and } (\tilde{\lambda}_{zE\ i+1,j,k\text{-}1/2}^{n+1} = 0) \end{cases}$$

Second, the pressure gradient term in (1-65) and its counterpart for the liquid field is redefined by Equation (4-44). While only the equation for Face 2 is given below to avoid repetition, analogous equations are applied to correct the pressure gradient terms in the momentum equations of Face 1, 3, and 4.

$$\left.\frac{\partial P}{\partial z}\right|_{i+1/2,j,k}^{n} = \frac{P_{i+1,j,k}^{n} - P_{i,j,k}^{n} + \delta P_{L2\ i+1/2,j,k}}{\Delta r_2} \tag{4-44}$$

where the correction term is given by the following equation

(4-45)

$$\delta P_{L2\ i+1/2,j,k} = \begin{cases} \delta P_{L6\ i,j,k} & \text{, if } (\tilde{L}^{n+1}_{i,j,k} > 0.5\Delta z_k) \text{ and } (\tilde{L}^{n+1}_{i+1,j,k} = 0) \\ -\delta P_{L6\ i+1,j,k} & \text{, if } (\tilde{L}^{n+1}_{i,j,k} = 0) \text{ and } (\tilde{L}^{n+1}_{i+1,j,k} > 0.5\Delta z_k) \\ \delta P_{L6\ i,j,k} - \delta P_{L6\ i+1,j,k} & \text{, if } (\tilde{L}^{n+1}_{i,j,k} > 0.5\Delta z_k) \text{ and } (\tilde{L}^{n+1}_{i+1,j,k} > 0.5\Delta z_k) \\ 0.0 & \text{, otherwise} \end{cases}$$

As discussed previously, the pressure drop correction given in the above equation does not work well for the R- and Θ-direction stabilizer equations. The pressure drop correction for the stabilizer momentum equations of these directions must be based on the "calculated" location of the liquid-gas interface at the end of a time step, i.e. $L^{n}_{i,j,k}$.

And finally, the wall and the interfacial drag force terms in the R- and Θ-direction momentum equations are modified so that they are evaluated in terms of the variables that describe the prevailing flow region (i.e. either the sub-region above or below a liquid-gas interface) at the center of computational volumes. This correction is consistent with the "redefined" fluid motion in the lateral directions based on the location of the flat liquid-gas interface with respect to the centers of computational volumes as the lateral fluid motion is defined on a grid that links the volume centers across the (R-Θ) plane. For faces m=1,2,3, and 4, the following function redefines the drag terms in the R- and Θ-direction momentum equations.

$$f_m = \begin{cases} F(\alpha^{-}_{i,j,k}) & \text{, if } \lambda_{zE\ i,j,k\text{-}1/2} > 0.5\Delta z_k \\ F(\alpha^{+}_{i,j,k\text{-}1}) & \text{, if } \lambda_{zE\ i,j,k\text{-}1/2} < 0.5\Delta z_k \\ F(\alpha_{i,j,k}) & \text{, if } \lambda_{zE\ i,j,k\text{-}1/2} = 0 \end{cases} \qquad (4\text{-}46)$$

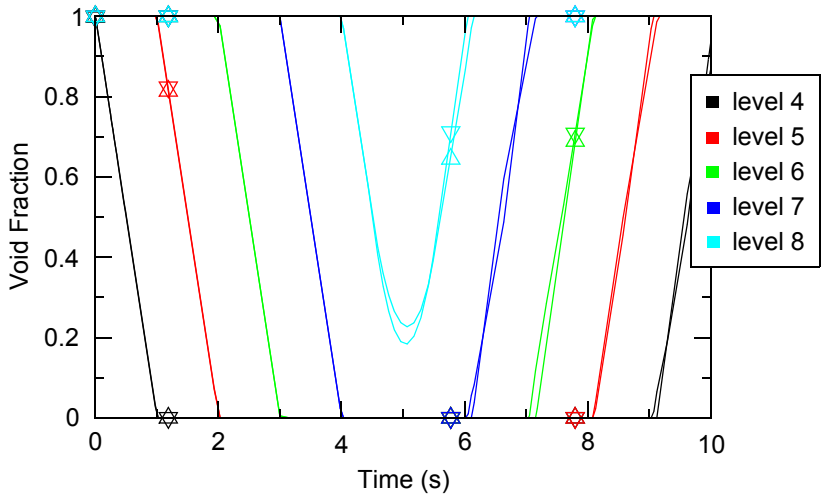

FIGURE 4-5. Void fractions of the 2D single-phase fill and drain test (simulated with the level tracking method)

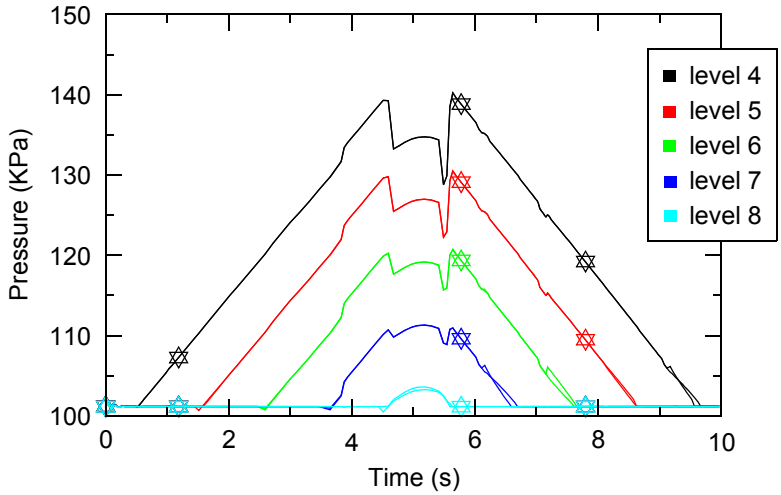

FIGURE 4-6. Pressures of the 2D single-phase fill and drain test (simulated with the level tracking method)

The success of the above modifications to the R- and Θ-direction components of the field equations will be measured by simulating the two- and three-dimensional versions of the fill and drain test described in CHAPTER 2. Each version of the test is repeated with the single-phase liquid and two-phase air-water mixture. The initial results obtained by simulating these tests with the standard solution method of TRAC revealed serious deficiencies of the standard approaches to solving the six-equation

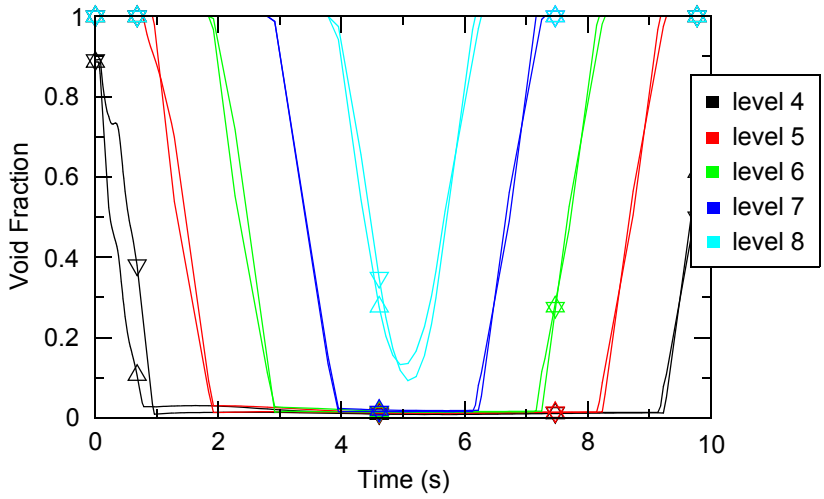

FIGURE 4-7. Void fractions of the 2D two-phase fill and drain test (simulated with the level tracking method)

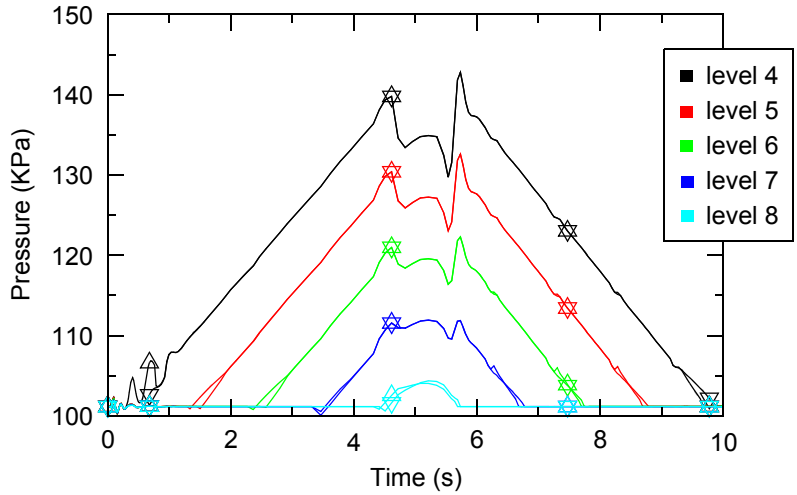

FIGURE 4-8. Pressures of the 2D two-phase fill and drain test (simulated with the level tracking method)

model. A comparison of the void fractions in Figure 4-5 to the ones in Figure 2-8 demonstrates the effectiveness of the level tracking in simulating the two-dimensional single-phase fill and drain test. Disparity between the void fractions of Cells 1 and 2 (see Figure 2-7) at every VESSEL component level are no longer seen in Figure 4-5. Previously in Figure 2-8, the void fractions indicated that the liquid trail behind the descending water level was spread over Levels 4 to 7 during the drain phase of the

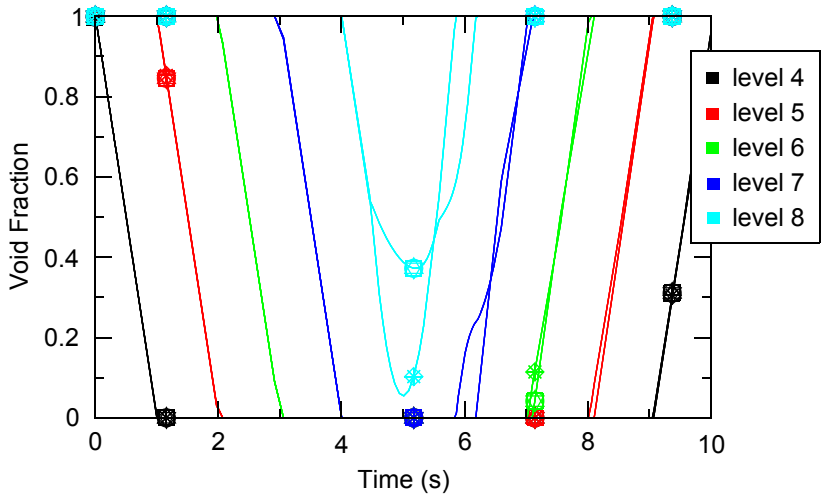

FIGURE 4-9. Void fractions of the 3D single-phase fill and drain test (simulated with the level tracking method)

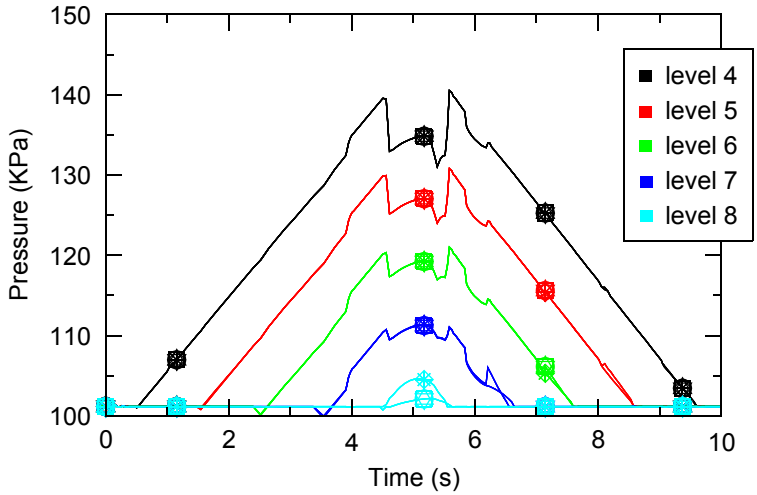

FIGURE 4-10. Pressures of the 3D single-phase fill and drain test (simulated with the level tracking method)

test, i.e. 7 seconds into the transient. While some disparity between Cells 1 and 2 of every level is expected since the fluid is injected into Cell 1 of Level 1 to make the test more challenging to simulate, the results shown in Figure 2-8 are not expected at all. Coupled with the problems in predicting void fractions were the pressure spikes and oscillations shown in Figure 2-9. Figure 4-6 shows none of these problems. A similar improvement is seen in Figure 4-7 and Figure 4-8 for the two-phase fill and drain test.

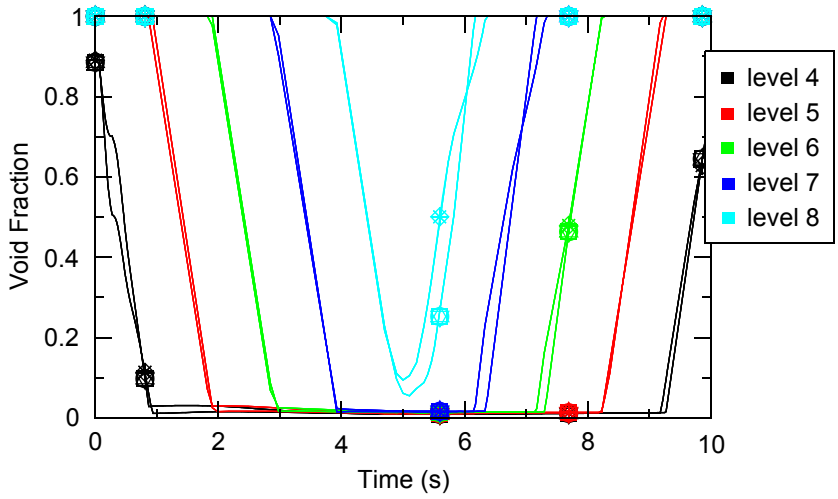

FIGURE 4-11. Void fractions of the 3D two-phase fill and drain test (simulated with the level tracking method)

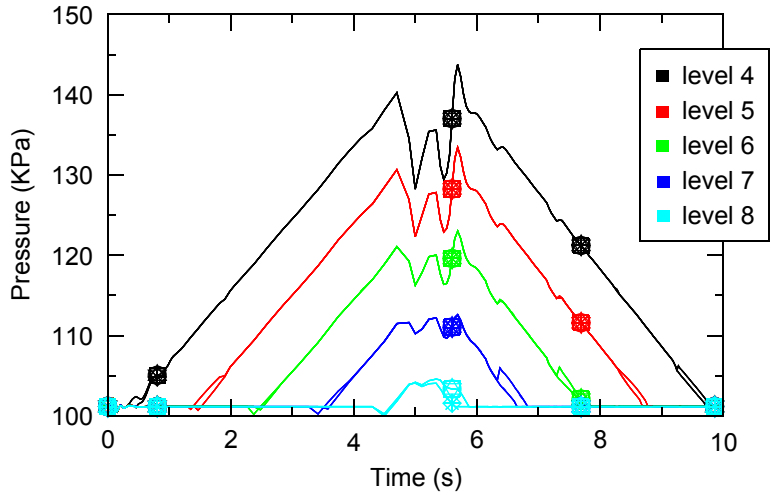

FIGURE 4-12. Pressures of the 3D two-phase fill and drain test (simulated with the level tracking method)

Both void fractions and pressures of this test exhibit none of the problems previously recorded in Figure 2-10 and Figure 2-11 respectively.

Next step in testing the modifications to the R- and Θ-direction components of the field equations was to simulate the three-dimensional fill and drain test (see Figure 2-7). Again, Figure 4-9 and Figure 4-10 demonstrate the effectiveness of the level tracking in handling the discontinuous nature of the fluid in the Z-direction due to

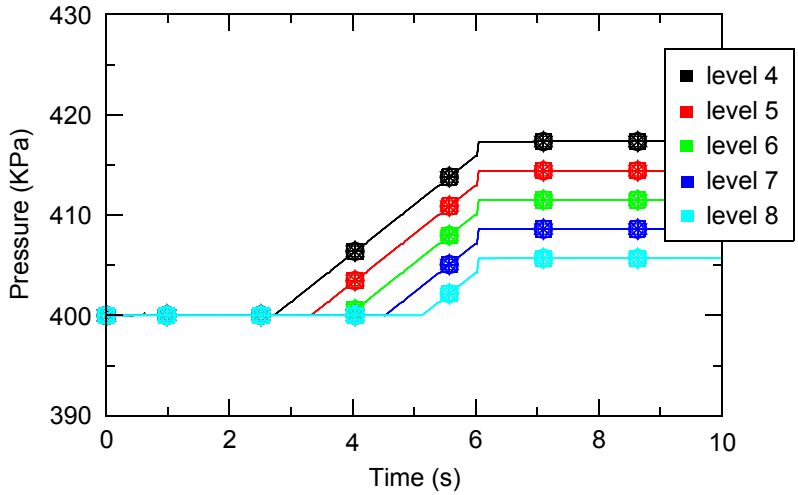

FIGURE 4-13. Pressures along the 3D condensation test pipe (simulated with the level tracking method)

the moving water level during the fill and drain phases of the test. Both figures are significant improvement over Figure 2-12 and Figure 2-13 respectively. The most noticeable improvement is seen in the void fractions of the two-phase version of the three-dimensional fill and drain test. A comparison of the void fractions in Figure 4-11 to the almost "chaotic" void fractions in Figure 2-14 is a real measure for the success of the modifications to the three-dimensional field equations described in this chapter.

Interfacial Heat and Mass Transfer

The interfacial heat and mass transfer terms of the three-dimensional computational volumes must also be modified in the same way which the terms of the one-dimensional computational volumes were described by Equations (3-59) and (3-60). The three-dimensional condensation test (see Figure 2-25) is the benchmark for measuring the success of these modifications.

The simulated pressures along the three-dimensional pipe that consists of 80 computational volumes (as opposed to the 10 volumes of the one-dimensional test

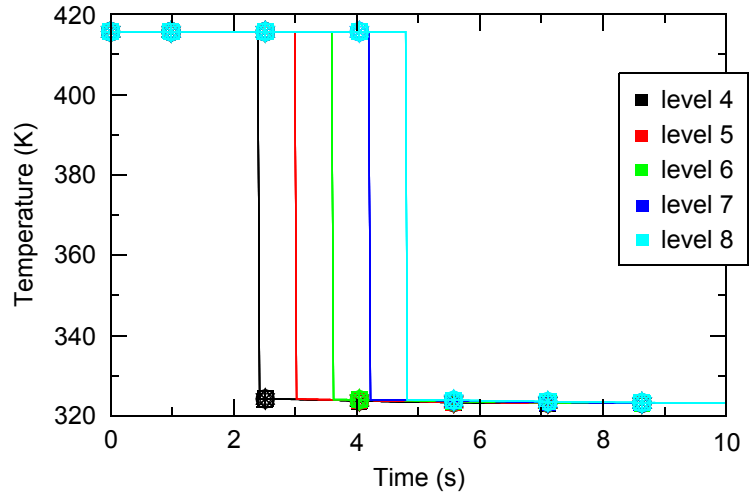

FIGURE 4-14. Liquid temperatures along the 3D condensation test pipe (simulated with the level tracking method)

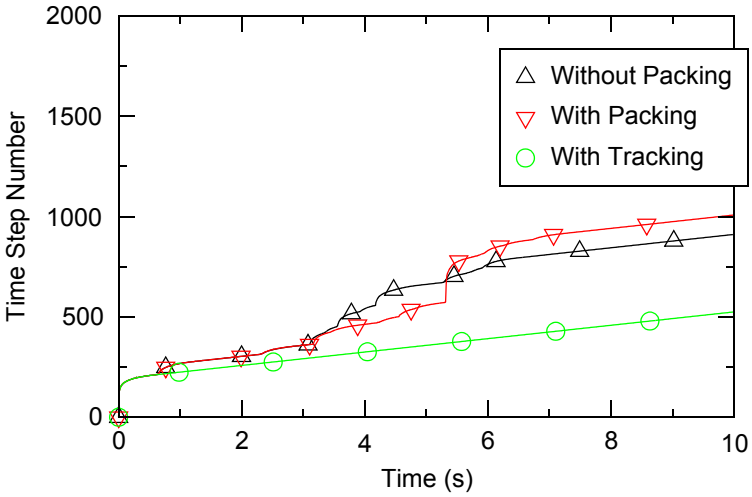

FIGURE 4-15. Comparison of total time step numbers of the 3D condensation test simulations

pipe) exhibit the expected linear increase in Figure 4-13 as the cold water fills the test pipe. Previously in Figure 2-31, the pressures exhibited large spikes and oscillations. Even a special treatment for the "packed" cells[4-2] could not eliminate these pressure spikes (see Figure 2-32). Clearly, the simulated pressures in Figure 4-13 constitute a significant improvement over the ones in both Figure 2-31 and Figure 2-32.

The temperatures of 40 cells, i.e. 8 cells per level, are plotted in Figure 4-14. The temperatures at each level switch instantaneously from the temperature of the superheated gas above the liquid-gas interface to the temperature of the subcooled liquid below the interface. Unlike the temperatures recorded previously in Figure 2-33 for the simulation with the standard method of solution, the temperatures in Figure 4-14 exhibit no signs of trouble as the liquid-gas interface fills up the cells at any given level.

Another evidence for the trouble-free simulation of the three-dimensional condensation test is the total number of time steps required to complete the simulation. As shown in Figure 4-15, it takes little over 500 time steps for TRAC to finish the simulation, i.e. a time step size of 0.05 seconds on the average which is the recommended time step size for this benchmark test.[4-3]

References

4-1. Mahaffy, J. H., personal communication.

4-2. Mahaffy, J.H. and Liles, D.R., "Numerically Induced Pressure Excursions in Two-Phase Flow Calculations," Proceedings of the Second International Topical Meeting on Nuclear Reactor Thermal-Hydraulics, Santa Barbara CA (1983)

4-3. Ransom, V., "Numerical Benchmark Test No. 2.3: Expulsion of Steam by Subcooled Water," **6**, Hemisphere Publishing, New York (1992) 611-621

CHAPTER 5

Summary and Conclusions

The purpose of this study was to develop a cure for thermal-hydraulic codes which suffer severely from their inability to handle moving water levels. First, a set of "thought" experiments was proposed. These tests were then simulated with a well-known solution method for the six-equation model, i.e. the Semi-Implicit and SETS methods (of the TRAC code). The results of these simulations revealed the shortcomings of TRAC's standard solution method in computing fluid volumes that consisted of water levels. Some results were bordering on an almost "chaotic" behavior (see Figure 2-14). Even after engaging a special model designed to alleviate the symptoms induced by moving water levels, the troubles in these benchmark simulations continued, i.e. the water packing option in TRAC (see Figure 2-27). The TRAC simulations of the numerical experiments were instrumental in unveiling the root cause of the symptoms, which was the solution method's inability to recognize the divided nature of a computational volume when "stratified" liquid-gas interfaces were present.

Modifying the field equations to recognize the regions above and below a liquid-gas interface in a "divided" computational volume was recognized as the strategy to develop a cure for this deficiency. This strategy required that the location of a liquid-gas interface, the volumes of regions above and below it, and the

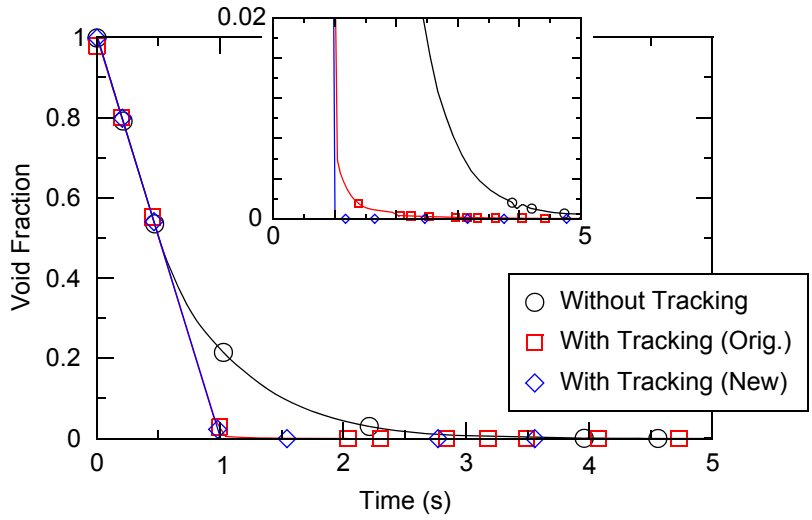

FIGURE 5-1. A comparison of void fractions in Cell 4 during the "fill" phase of the single-phase fill and drain test from various simulations

void fractions inside these regions be known at all times. Since the idea of tracking water levels was not new, the level tracking method of TRAC-BWR was incorporated into TRAC.† The crux of the cure was to modify the field equations systematically based on the whereabouts of a water level.

The field equations were modified in several steps. For instance, the modifications to the one-dimensional field equations of TRAC excluded the measures critical for precision handling of the event in which a water level crosses the boundary of a computational volume. Repeating the simulations with the incomplete modifications to the field equations demonstrated the need for extreme care whenever the field equations had to be modified. While the intent was not a complete coverage of the past attempts to implement a level tracking method in TRAC, simulations of some numerical experiments were also performed and presented here in an effort to put the spot light on the mistakes of these past attempts. Figure 5-1 and Figure 5-2 compares the

†. The reactor safety code referred to as TRAC here is the US NRC Consolidated Thermal-hydraulics Code (a.k.a. TRAC-M), and the code referred to as TRAC-BWR is TRAC-BF1/MOD1 of US NRC.

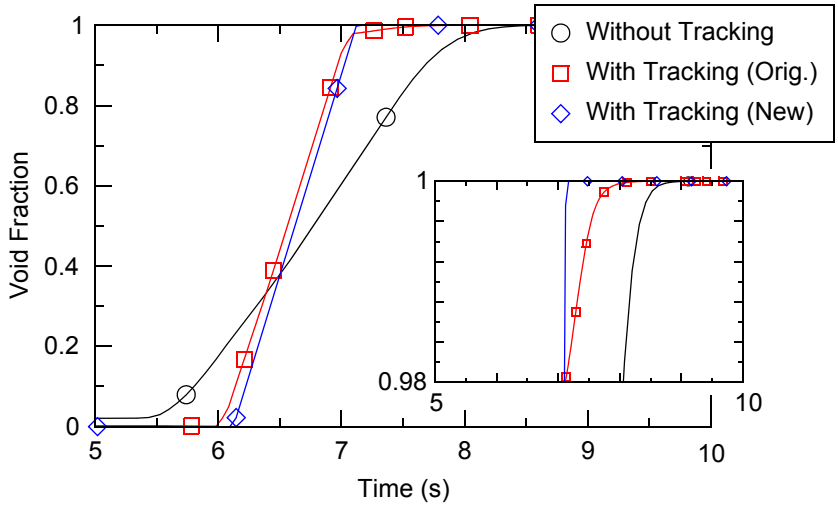

FIGURE 5-2. A comparison of void fractions in Cell 7 during the "drain" phase of the single-phase fill and drain test from various simulations

void fraction for Cells 4 and 7 of the fill and drain test pipe (see Figure 2-2) during the fill and drain phases simulated with the standard method of TRAC, the original level tracking in TRAC, and the new tracking method developed here. The accompanying pressures of these cells can be seen in Figure 3-1. The close ups in Figure 5-1 and Figure 5-2 revealed small amounts of gas trapped behind the ascending water level and the fragments of liquid trailing the descending level. Coupled with the modifications made to the pressure field by the original tracking method, these small errors manifested themselves as sudden changes in cell pressures. This observation enforces the already known fact that half measures do not produce satisfactory results when the field equations are modified to augment the solution methods of thermal-hydraulic codes, and that one must consider the full implications of any change to the field equations. The method developed in this study owes its success to the attention it paid in details which is evident in the close ups of void fractions in Figure 5-1 and Figure 5-2.

The modifications to the three-dimensional field equations were implemented in steps as well. First, the Z-direction component of the field equations was modified

based on the changes made to the one-dimensional field equations. These modifications were tested immediately by simulating the two-dimensional version of the oscillating manometer test (see Figure 2-21). Next, the "assumed" discontinuous nature of the fluid in the Z-direction was incorporated into the R- and Θ-direction components of the field equations. The results from the simulations repeated with the new method demonstrated significant improvements in TRAC's ability to handle moving water levels. These improvements can be judged best by comparing the "improved" void fractions in Figure 4-11 to the almost "chaotic" void fractions in Figure 2-14 of the two-phase fill and drain test conducted with an 8x10 noding of the test pipe (see Figure 2-7).

It is recommended that TRAC's ability to predict the interfacial heat transfer rate at the surfaces of liquid-gas interfaces be assessed by simulating experiments with available data. The desired capability for TRAC is to predict the "correct" rate of condensation and the build-up of warmer liquid layer at the surface of the water level in Figure 3-26.

The method presented here has been implemented in the US NRC Consolidated Thermal-hydraulic Code (a.k.a. TRAC-M).[5-1] Some features of the method were also incorporated in RELAP5 which is the other thermal-hydraulic code of the US NRC. The measures to counter the water levels crossing cell boundaries were not available to the public and not implemented in RELAP5. Currently, an effort is underway to implement these features of the method in RELAP5.[5-2] The Semi-Implicit methods of TRAC and RELAP5 are very common applications of the six-equation model. Therefore, the method developed in this study can be applied readily to the other thermal-hydraulic codes solving similar variations of the six-equation model such as ATHELET,[5-3] CATHARE,[5-4] and COBRA-TF.[5-5]

Anyone attempting to implement this method must pay a close attention to the "time step" synchronization of the variables involved in implementing it, e.g. when a water level crosses boundaries between computational volumes or the centers of computational volumes. While it was not possible to include these "programming" details here, a careful programming to capture these details is utterly important for a successful implementation.

References

5-1. Aktas, B. "A Level Tracking Method for TRAC-M," Infomration Systems Laboratories, Inc., ISL-NSAD-NRC-01-005 (December 2001).

5-2. Mortensen, G., personal communication.

5-3. ATHLETE reference

5-4. Bestion, D., et al., " Methodology, Status and Plans for Development and Assessment of CATHARE code," OECD/CSNI Workshop on Trans. Thermalhydr. and Neutr. Code Req., Annapolis, USA, Nov., (1996).

5-5. Thurgood, M.J, George, M.J., "COBRA/TRAC – A Thermal-Hydraulic Code for Transient Analysis of Nuclear Reactor Vessels and Primary Coolant System," NUREG/CR-3046, **Vol. 1-4**, (March 1983).

APPENDIX A

Implementation of the Semi-Implicit Method in TRAC-M

In the following pages, a Mathematica session derives the one-dimensional field equations of the Semi-Implicit method as they are implemented in TRAC-M. The variable names used here match the Fortran variables in TRAC. For those who are not familiar with the Fortran source code of TRAC, the equations provided in the following pages can bridge the gap between the Semi-Implicit method presented in CHAPTER 1 and its implementation in Subroutine TF1DS of TRAC.

Mathematica is a software developed by Wolfram Research, Inc
(see http://www.wolfram.com for further information).

Various substitutions and linearized fluid quantities

In[266]:=
```
taylorExp = h_[x_^(n+1), y_^(n+1), z_^(n+1)] ->
   h[x^n, y^n, z^n] + ∂x h[x^n, y^n, z^n]/(n x^(n-1)) δ[x] + ∂y h[x^n, y^n, z^n]/(n y^(n-1)) δ[y] + ∂z h[x^n, y^n, z^n]/(n z^(n-1)) δ[z] ;
cancel2nd = {δ[x_] δ[y_] -> 0, δ[x_] δ[x_] -> 0, δ[x_] δ[x_] δ[y_] -> 0,
   δ[x_] δ[y_] δ[y_] -> 0, δ[x_] δ[x_] δ[x_] -> 0} ;
subKdelta = {δ[T_g,_j_] -> δT_g,j, δ[α_j_] -> δα_j, δ[p_j_] -> δp_j};
deldp = {δ[p_(j_+1)] - δ[p_j_] -> δ[p_(j+1) - p_j], δ[p_j_] - δ[p_(j_-1)] -> -δ[p_(j-1) - p_j] } ;
linearQuantities = {
⟨α ρ_g⟩_(j_)^(n+1) ->
   ⟨α ρ_g⟩_j^i + ρ_g[p_j^i, T_g,j^i] δ[α_j] + α_j^i ∂_(p_j) ρ_g[p_j^i, T_g,j^i]/(i p_j^(i-1)) δ[p_j] + α_j^i ∂_(T_g,j) ρ_g[p_j^i, T_g,j^i]/(i T_g,j^(i-1)) δ[T_g,j] ,
⟨(1 - α) ρ_1⟩_(j_)^(n+1) -> ⟨(1 - α) ρ_1⟩_j^i - ρ_1[p_j^i, T_1,j^i] δ[α_j] +
   (1 - α_j^i) ∂_(p_j) ρ_1[p_j^i, T_1,j^i]/(i p_j^(i-1)) δ[p_j] + (1 - α_j^i) ∂_(T_1,j) ρ_1[p_j^i, T_1,j^i]/(i T_1,j^(i-1)) δ[T_1,j] ,
⟨α ρ_g e_g⟩_(j_)^(n+1) -> ⟨α ρ_g e_g⟩_j^i + ρ_g[p_j^i, T_g,j^i] e_g[p_j^i, T_g,j^i] δ[α_j] +
   α_j^i e_g[p_j^i, T_g,j^i] ∂_(p_j) ρ_g[p_j^i, T_g,j^i]/(i p_j^(i-1)) δ[p_j] + α_j^i ρ_g[p_j^i, T_g,j^i] ∂_(p_j) e_g[p_j^i, T_g,j^i]/(i p_j^(i-1)) δ[p_j] +
   α_j^i e_g[p_j^i, T_g,j^i] ∂_(T_g,j) ρ_g[p_j^i, T_g,j^i]/(i T_g,j^(i-1)) δ[T_g,j] + α_j^i ρ_g[p_j^i, T_g,j^i] ∂_(T_g,j) e_g[p_j^i, T_g,j^i]/(i T_g,j^(i-1)) δ[T_g,j] ,
⟨(1 - α) ρ_1 e_1⟩_(j_)^(n+1) -> ⟨(1 - α) ρ_1 e_1⟩_j^i - ρ_1[p_j^i, T_1,j^i] e_1[p_j^i, T_1,j^i] δ[α_j] +
   (1 - α_j^i) e_1[p_j^i, T_1,j^i] ∂_(p_j) ρ_1[p_j^i, T_1,j^i]/(i p_j^(i-1)) δ[p_j] +
```

$$(1 - \alpha_j^{\,i})\ \rho_1[p_j^{\,i},\ T_{1,j}^{\,i}]\ \frac{\partial_{p_j}\ e_1[p_j^{\,i},\ T_{1,j}^{\,i}]}{i\ p_j^{\,i-1}}\ \delta[p_j] + (1 - \alpha_j^{\,i})\ e_1[p_j^{\,i},\ T_{1,j}^{\,i}]$$

$$\frac{\partial_{T_{1,j}}\ \rho_1[p_j^{\,i},\ T_{1,j}^{\,i}]}{i\ T_{1,j}^{\,i-1}}\ \delta[T_{1,j}] + (1 - \alpha_j^{\,i})\ \rho_1[p_j^{\,i},\ T_{1,j}^{\,i}]\ \frac{\partial_{T_{1,j}}\ e_1[p_j^{\,i},\ T_{1,j}^{\,i}]}{i\ T_{1,j}^{\,i-1}}\ \delta[T_{1,j}]$$

};

newTime = { $\alpha_{j\_}^{\,n+1}$ -> $\alpha_j^{\,i} + \delta[\alpha_j]$, $p_{j\_}^{\,n+1}$ -> $p_j^{\,i} + \delta[p_j]$ };

xvset = { $\langle \alpha\,\rho\rangle_{g,j\_}$ -> $\gamma\,\langle \alpha\,\rho_g\rangle_j^{\,n+1} + (1-\gamma)\,\langle \alpha\,\rho_g\rangle_j^{\,n}$,

$\langle (1-\alpha)\,\rho\rangle_{1,j\_}$ -> $\gamma\,\langle (1-\alpha)\,\rho_1\rangle_j^{\,n+1} + (1-\gamma)\,\langle (1-\alpha)\,\rho_1\rangle_j^{\,n}$,

$\langle \alpha\,\rho\,e\rangle_{g,j\_}$ -> $\gamma\,\langle \alpha\,\rho_g\,e_g\rangle_j^{\,n+1} + (1-\gamma)\,\langle \alpha\,\rho_g\,e_g\rangle_j^{\,n}$,

$\langle (1-\alpha)\,\rho\,e\rangle_{1,j\_}$ -> $\gamma\,\langle (1-\alpha)\ \rho_1\,e_1\rangle_j^{\,n+1} + (1-\gamma)\,\langle (1-\alpha)\,\rho_1\,e_1\rangle_j^{\,n}$,

$\langle \alpha\rangle_{j\_}$ -> $\alpha_j^{\,n}$,

$\langle 1-\alpha\rangle_{j\_}$ -> $\langle 1-\alpha_j^{\,n}\rangle$ };

Cell-edge flux quantities: mass, energy and volume

In[2]:=

$$\phi_{g,j+1/2} = \left(w_{g,j+1/2}\,\langle\alpha\,\rho\rangle_{g,j} + (1 - w_{g,j+1/2})\,\langle\alpha\,\rho_g\rangle_{j+1}{}^{n}\right) A_{j+1/2}\; V_{g,j+1/2}[p_j{}^{n+1},\; p_{j+1}{}^{n+1}];$$

$$\phi_{g,j-1/2} = \left(w_{g,j-1/2}\,\langle\alpha\,\rho_g\rangle_{j-1}{}^{n} + (1 - w_{g,j-1/2})\,\langle\alpha\,\rho\rangle_{g,j}\right) A_{j-1/2}\; V_{g,j-1/2}[p_{j-1}{}^{n+1},\; p_j{}^{n+1}];$$

$$\phi_{l,j+1/2} = \left(w_{l,j+1/2}\,\langle(1-\alpha)\,\rho\rangle_{l,j} + (1 - w_{l,j+1/2})\,\langle(1-\alpha)\,\rho_l\rangle_{j+1}{}^{n}\right) A_{j+1/2}\; V_{l,j+1/2}[p_j{}^{n+1},\; p_{j+1}{}^{n+1}];$$

$$\phi_{l,j-1/2} = \left(w_{l,j-1/2}\,\langle(1-\alpha)\,\rho_l\rangle_{j-1}{}^{n} + (1 - w_{l,j-1/2})\,\langle(1-\alpha)\,\rho\rangle_{l,j}\right) A_{j-1/2}\; V_{l,j-1/2}[p_{j-1}{}^{n+1},\; p_j{}^{n+1}];$$

$$\xi_{g,j+1/2} = \left(w_{g,j+1/2}\,\langle\alpha\,\rho\,e\rangle_{g,j} + (1 - w_{g,j+1/2})\,\langle\alpha\,\rho_g\,e_g\rangle_{j+1}{}^{n}\right) A_{j+1/2}\; V_{g,j+1/2}[p_j{}^{n+1},\; p_{j+1}{}^{n+1}];$$

$$\xi_{g,j-1/2} = \left(w_{g,j-1/2}\,\langle\alpha\,\rho_g\,e_g\rangle_{j-1}{}^{n} + (1 - w_{g,j-1/2})\,\langle\alpha\,\rho\,e\rangle_{g,j}\right) A_{j-1/2}\; V_{g,j-1/2}[p_{j-1}{}^{n+1},\; p_j{}^{n+1}];$$

$$\xi_{l,j+1/2} = \left(w_{l,j+1/2}\,\langle(1-\alpha)\,\rho\,e\rangle_{l,j} + (1 - w_{l,j+1/2})\,\langle(1-\alpha)\,\rho_l\,e_l\rangle_{j+1}{}^{n}\right) A_{j+1/2}\; V_{l,j+1/2}[p_j{}^{n+1},\; p_{j+1}{}^{n+1}];$$

$$\xi_{l,j-1/2} = \left(w_{l,j-1/2}\,\langle(1-\alpha)\,\rho_l\,e_l\rangle_{j-1}{}^{n} + (1 - w_{l,j-1/2})\,\langle(1-\alpha)\,\rho\,e\rangle_{l,j}\right) A_{j-1/2}\; V_{l,j-1/2}[p_{j-1}{}^{n+1},\; p_j{}^{n+1}];$$

$$\omega_{g,j+1/2} = \left(w_{g,j+1/2}\,\langle\alpha\rangle_j + (1 - w_{g,j+1/2})\,\alpha_{j+1}{}^{n}\right) A_{j+1/2}\; V_{g,j+1/2}[p_j{}^{n+1},\; p_{j+1}{}^{n+1}];$$

$$\omega_{g,j-1/2} = \left(w_{g,j-1/2}\,\alpha_{j-1}{}^{n} + (1 - w_{g,j-1/2})\,\langle\alpha\rangle_j\right) A_{j-1/2}\; V_{g,j-1/2}[p_{j-1}{}^{n+1},\; p_j{}^{n+1}];$$

$$\omega_{l,j+1/2} = \left(w_{l,j+1/2}\,\langle 1-\alpha\rangle_j + (1 - w_{l,j+1/2})\,\langle 1-\alpha_{j+1}{}^{n}\rangle\right) A_{j+1/2}\; V_{l,j+1/2}[p_j{}^{n+1},\; p_{j+1}{}^{n+1}];$$

$$\omega_{l,j-1/2} = \left(w_{l,j-1/2}\,\langle 1-\alpha_{j-1}{}^{n}\rangle + (1 - w_{l,j-1/2})\,\langle 1-\alpha\rangle_j\right) A_{j-1/2}\; V_{l,j-1/2}[p_{j-1}{}^{n+1},\; p_j{}^{n+1}];$$

TRAC variable substitutions

In[3]:=
```
tracDp = { Δt V^(0,1)_(x_, j-1/2) (p^n_(j-1), p^n_j) -> dvdp_(x, j-1/2), Δt V^(0,1)_(x_, j+1/2) (p^n_j, p^n_(j+1)) -> dvdp_(x, j+1/2) };
tracDonor1 = { A_(j_) w_(g, j_) -> faWvM_j ,
  A_(j_) (1 - w_(g, j_)) -> faWvP_j ,  A_(j_) w_(1, j_) -> faWlM_j , A_(j_) (1 - w_(1, j_)) -> faWlP_j };
tracDonor2 = { faWvM_(j_+1/2) ⟨α ρ_g⟩_(j_)^n + faWvP_(j_+1/2) ⟨α ρ_g⟩_(j_+1)^n -> faArv_(j+1/2) ,
                faWvM_(j_-1/2) ⟨α ρ_g⟩_(j_-1)^n + faWvP_(j_-1/2) ⟨α ρ_g⟩_(j_)^n -> faArv_(j-1/2) ,
                faWlM_(j_+1/2) ⟨(1 - α) ρ_1⟩_(j_)^n + faWlP_(j_+1/2) ⟨(1 - α) ρ_1⟩_(j_+1)^n -> faArl_(j+1/2) ,
                faWlM_(j_-1/2) ⟨(1 - α) ρ_1⟩_(j_-1)^n + faWlP_(j_-1/2) ⟨(1 - α) ρ_1⟩_(j_)^n -> faArl_(j-1/2) ,
                faWvM_(j_+1/2) ⟨α e_g ρ_g⟩_(j_)^n + faWvP_(j_+1/2) ⟨α e_g ρ_g⟩_(j_+1)^n -> faArev_(j+1/2) ,
                faWvM_(j_-1/2) ⟨α e_g ρ_g⟩_(j_-1)^n + faWvP_(j_-1/2) ⟨α e_g ρ_g⟩_(j_)^n -> faArev_(j-1/2) ,
                faWlM_(j_+1/2) ⟨(1 - α) e_1 ρ_1⟩_(j_)^n + faWlP_(j_+1/2) ⟨(1 - α) e_1 ρ_1⟩_(j_+1)^n -> faArel_(j+1/2) ,
                faWlM_(j_-1/2) ⟨(1 - α) e_1 ρ_1⟩_(j_-1)^n + faWlP_(j_-1/2) ⟨(1 - α) e_1 ρ_1⟩_(j_)^n -> faArel_(j-1/2) ,
              faWvM_(j_+1/2) α_(j_)^n + faWvP_(j_+1/2) α_(j_+1)^n -> faVapFrac_(j+1/2) ,
                faWvM_(j_-1/2) α_(j_-1)^n + faWvP_(j_-1/2) α_(j_)^n -> faVapFrac_(j-1/2) ,
                  faWlM_(j_+1/2) ⟨1 - α_(j_)^n⟩ + faWlP_(j_+1/2) ⟨1 - α_(j_+1)^n⟩ -> faLiqFrac_(j+1/2) ,
                  faWlM_(j_-1/2) ⟨1 - α_(j_-1)^n⟩ + faWlP_(j_-1/2) ⟨1 - α_(j_)^n⟩ -> faLiqFrac_(j-1/2) };
```

In[4]:=
```
φ̂g,j+1/2 = Collect[Distribute[φg,j+1/2 /. xvset] /. tracDonor1, γ] ;
φ̂g,j-1/2 = Collect[Distribute[φg,j-1/2 /. xvset] /. tracDonor1, γ] ;
φ̂1,j+1/2 = Collect[Distribute[φ1,j+1/2 /. xvset] /. tracDonor1, γ] ;
φ̂1,j-1/2 = Collect[Distribute[φ1,j-1/2 /. xvset] /. tracDonor1, γ] ;
ξ̂g,j+1/2 = Collect[Distribute[ξg,j+1/2 /. xvset] /. tracDonor1, γ] ;
ξ̂g,j-1/2 = Collect[Distribute[ξg,j-1/2 /. xvset] /. tracDonor1, γ] ;
ξ̂1,j+1/2 = Collect[Distribute[ξ1,j+1/2 /. xvset] /. tracDonor1, γ] ;
ξ̂1,j-1/2 = Collect[Distribute[ξ1,j-1/2 /. xvset] /. tracDonor1, γ] ;
ω̂g,j+1/2 = Collect[Distribute[ωg,j+1/2 /. xvset] /. tracDonor1, γ] ;
ω̂g,j-1/2 = Collect[Distribute[ωg,j-1/2 /. xvset] /. tracDonor1, γ] ;
ω̂1,j+1/2 = Collect[Distribute[ω1,j+1/2 /. xvset] /. tracDonor1, γ] ;
ω̂1,j-1/2 = Collect[Distribute[ω1,j-1/2 /. xvset] /. tracDonor1, γ] ;
```

In[5]:=
```
φg,j+1/2 = Collect[ φ̂g,j+1/2, V_[p_^(n+1), p_^(n+1)] ] /. tracDonor2 ;
φg,j-1/2 = Collect[ φ̂g,j-1/2, V_[p_^(n+1), p_^(n+1)] ] /. tracDonor2 ;
φ1,j+1/2 = Collect[ φ̂1,j+1/2, V_[p_^(n+1), p_^(n+1)] ] /. tracDonor2 ;
φ1,j-1/2 = Collect[ φ̂1,j-1/2, V_[p_^(n+1), p_^(n+1)] ] /. tracDonor2 ;
ξg,j+1/2 = Collect[ ξ̂g,j+1/2, V_[p_^(n+1), p_^(n+1)] ] /. tracDonor2 ;
ξg,j-1/2 = Collect[ ξ̂g,j-1/2, V_[p_^(n+1), p_^(n+1)] ] /. tracDonor2 ;
ξ1,j+1/2 = Collect[ ξ̂1,j+1/2, V_[p_^(n+1), p_^(n+1)] ] /. tracDonor2 ;
ξ1,j-1/2 = Collect[ ξ̂1,j-1/2, V_[p_^(n+1), p_^(n+1)] ] /. tracDonor2 ;
ωg,j+1/2 = Collect[ ω̂g,j+1/2, V_[p_^(n+1), p_^(n+1)] ] /. tracDonor2 ;
ωg,j-1/2 = Collect[ ω̂g,j-1/2, V_[p_^(n+1), p_^(n+1)] ] /. tracDonor2 ;
ω1,j+1/2 = Collect[ ω̂1,j+1/2, V_[p_^(n+1), p_^(n+1)] ] /. tracDonor2 ;
ω1,j-1/2 = Collect[ ω̂1,j-1/2, V_[p_^(n+1), p_^(n+1)] ] /. tracDonor2 ;
```

Liquid/gas mass and energy equations

In[6]:=
$$GM0 = \left(\langle \alpha \rho_g \rangle_j^{n+1} - \langle \alpha \rho_g \rangle_j^{n}\right) vol_j + (\phi_{g,j+1/2} - \phi_{g,j-1/2})\,\Delta t\ ;$$

$$LM0 = (\langle (1-\alpha)\,\rho_l \rangle_j^{n+1} - \langle (1-\alpha)\,\rho_l \rangle_j^{n})\, vol_j + (\phi_{l,j+1/2} - \phi_{l,j-1/2})\,\Delta t\ ;$$

$$GE0 = \left(\langle \alpha \rho_g e_g \rangle_j^{n+1} - \langle \alpha \rho_g e_g \rangle_j^{n}\right) vol_j + (\xi_{g,j+1/2} - \xi_{g,j-1/2})\,\Delta t + \left((\alpha_j^{n+1} - \alpha_j^{n})\, vol_j + (\omega_{g,j+1/2} - \omega_{g,j-1/2})\,\Delta t\right) p_j^{n+1}\ ;$$

$$LE0 = (\langle (1-\alpha)\,\rho_l e_l \rangle_j^{n+1} - \langle (1-\alpha)\,\rho_l e_l \rangle_j^{n})\, vol_j + (\xi_{l,j+1/2} - \xi_{l,j-1/2})\,\Delta t + \left((\alpha_j^{n} - \alpha_j^{n+1})\, vol_j + (\omega_{l,j+1/2} - \omega_{l,j-1/2})\,\Delta t\right) p_j^{n+1};$$

Mixture mass and energy equations

In[7]:=
$$MM0 = GM0 + LM0;\quad ME0 = GE0 + LE0;$$

Liquid and gas velocities as functions of new time pressures

In[8]:=
$$V_{g,j+1/2}[p_j^{n+1}, p_{j+1}^{n+1}] = V_{g,j+1/2}[p_j^{n}, p_{j+1}^{n}] + \frac{\partial_{p_{j+1}} V_{g,j+1/2}[p_j^{n}, p_{j+1}^{n}]}{n\, p_{j+1}^{n-1}} (\delta[p_{j+1}] - \delta[p_j])\ ;$$

$$V_{l,j+1/2}[p_j^{n+1}, p_{j+1}^{n+1}] = V_{l,j+1/2}[p_j^{n}, p_{j+1}^{n}] + \frac{\partial_{p_{j+1}} V_{l,j+1/2}[p_j^{n}, p_{j+1}^{n}]}{n\, p_{j+1}^{n-1}} (\delta[p_{j+1}] - \delta[p_j])\ ;$$

$$V_{g,j-1/2}[p_{j-1}^{n+1}, p_j^{n+1}] = V_{g,j-1/2}[p_{j-1}^{n}, p_j^{n}] + \frac{\partial_{p_j} V_{g,j-1/2}[p_{j-1}^{n}, p_j^{n}]}{n\, p_j^{n-1}} (\delta[p_j] - \delta[p_{j-1}])\ ;$$

$$V_{l,j-1/2}[p_{j-1}^{n+1}, p_j^{n+1}] = V_{l,j-1/2}[p_{j-1}^{n}, p_j^{n}] + \frac{\partial_{p_j} V_{l,j-1/2}[p_{j-1}^{n}, p_j^{n}]}{n\, p_j^{n-1}} (\delta[p_j] - \delta[p_{j-1}])\ ;$$

TRAC variable substitutions

In[216]:=

```
tracFlux1 = {
        faWvM_{j+1/2} V_{g,j+1/2}[p_j^n, p_{j+1}^n] - faWvP_{j-1/2} V_{g,j-1/2}[p_{j-1}^n, p_j^n] -> - faWvInVvSum ,
        faWvP_{j-1/2} V_{g,j-1/2}[p_{j-1}^n, p_j^n] - faWvM_{j+1/2} V_{g,j+1/2}[p_j^n, p_{j+1}^n] -> faWvInVvSum ,
        faWlM_{j+1/2} V_{l,j+1/2}[p_j^n, p_{j+1}^n] - faWlP_{j-1/2} V_{l,j-1/2}[p_{j-1}^n, p_j^n] -> - faWlInVlSum ,
        faWlP_{j-1/2} V_{l,j-1/2}[p_{j-1}^n, p_j^n] - faWlM_{j+1/2} V_{l,j+1/2}[p_j^n, p_{j+1}^n] -> faWlInVlSum ,
        faArv_{j+1/2} V_{g,j+1/2}[p_j^n, p_{j+1}^n] - faArv_{j-1/2} V_{g,j-1/2}[p_{j-1}^n, p_j^n] -> -fluxSum[1] ,
        faArl_{j+1/2} V_{l,j+1/2}[p_j^n, p_{j+1}^n] - faArl_{j-1/2} V_{l,j-1/2}[p_{j-1}^n, p_j^n] -> -fluxSum[2] ,
        faArev_{j+1/2} V_{g,j+1/2}[p_j^n, p_{j+1}^n] - faArev_{j-1/2} V_{g,j-1/2}[p_{j-1}^n, p_j^n] -> -fluxSum[3] ,
        faArel_{j+1/2} V_{l,j+1/2}[p_j^n, p_{j+1}^n] - faArel_{j-1/2} V_{l,j-1/2}[p_{j-1}^n, p_j^n] -> -fluxSum[4] ,
      faVapFrac_{j+1/2} V_{g,j+1/2}[p_j^n, p_{j+1}^n] - faVapFrac_{j-1/2} V_{g,j-1/2}[p_{j-1}^n, p_j^n] -> -vapVolFluxSum ,
      faLiqFrac_{j+1/2} V_{l,j+1/2}[p_j^n, p_{j+1}^n] - faLiqFrac_{j-1/2} V_{l,j-1/2}[p_{j-1}^n, p_j^n] -> -liqVolFluxSum
};
tracFlux2 = {
        vol_j - faWvInVvSum γ Δt -> xvolv ,
        faWvInVvSum γ Δt - vol_j -> -xvolv ,
        vol_j - faWlInVlSum γ Δt -> xvoll ,
        faWlInVlSum γ Δt - vol_j -> -xvoll
};
tracFlux3 = {
      xvolv ρ_g^(1,0)(p_j^i, T_{g,j}^i) α_j^i -> darvp ,
        xvolv ρ_g[p_j^i, T_{g,j}^i] -> darva ,
        xvolv ρ_g^(0,1)(p_j^i, T_{g,j}^i) α_j^i -> darvt ,
        xvoll (α_j^i - 1) ρ_l^(1,0)(p_j^i, T_{l,j}^i) -> -darlp ,
      xvoll (1 - α_j^i) ρ_l^(1,0)(p_j^i, T_{l,j}^i) -> darlp ,
      xvoll ρ_l[p_j^i, T_{l,j}^i] -> -darla ,
      xvoll (α_j^i - 1) ρ_l^(0,1)(p_j^i, T_{l,j}^i) -> -darlt ,
   darla (α_j^i - 1) -> - xvoll ⟨(1 - α) ρ_l⟩_j^i
};
```

In[221]:=
```
GM1 = Collect[ Expand[ GM0 /. deldp /. linearQuantities ] /. cancel2nd,
     { δ[_] , ϒ , 1 } , Simplify ] /. tracFlux1 /. tracFlux2 /. tracDp;
GM2 = Collect[ FullSimplify[ GM1[[{1, 2, 3, 4, 7, 8, 9}]] ] /. tracFlux2 , δ[_] ] +
   FullSimplify[ GM1[[{5, 6}]] ] /. tracFlux3;


LM1 = Collect[ Expand[ LM0 /. deldp /. linearQuantities ] /. cancel2nd,
     { δ[_] , ϒ , 1 } , Simplify ] /. tracFlux1 /. tracFlux2 /. tracDp;
LM2 = Collect[ FullSimplify[ LM1[[{1, 2, 3, 4, 7, 8, 9}]] ] /. tracFlux2 , δ[_] ] +
   FullSimplify[ LM1[[{5, 6}]] ] /. tracFlux3;


MM2 = Collect[ GM2 + LM2, δ[_], FullSimplify] ;


GE1 = Collect[ Expand [GE0 /. deldp /. linearQuantities /. newTime ] /. cancel2nd ,
    { δ[_] , pj-, ϒ } , Simplify ] /. tracFlux1 /. tracFlux2 ;
GE2 = Collect[ FullSimplify[ GE1[[{1, 2, 3, 4, 5}]] ] +
      Expand[ Simplify[ GE1[[{6, 7}]] ] /. tracFlux2 ]
+ GE1[[10, 1]] Expand[ Collect[ Map[ Distribute, GE1[[10, 2]] , 2 ] ,
          {αj, ρ_[pj^i, T_,j^i] e_^(1,0)(pj^i, T_,j^i) , e_[pj^i, T_,j^i] ρ_^(1,0)(pj^i, T_,j^i) } ] /.
         tracFlux2 ] + FullSimplify[ GE1[[{ 8, 9}]] ]
/. tracFlux2 /. tracFlux3 /. tracDp , δ[_] , Simplify] ;


LE1 = Collect[ Expand[ LE0 /. deldp /. linearQuantities /. newTime] /. cancel2nd ,
    { δ[_] , pj-, ϒ } , Simplify ] /. tracFlux1 /. tracFlux2 ;
LE2 = FullSimplify[ LE1[[{1, 2, 3, 4, 5}]] ] + LE1[[10, 1]]
        Collect[ Simplify[ Collect[ Expand[ Collect[ LE1[[10, 2]] , Δt ] /. tracFlux1 ] ,
```

```
      {αj, ρ_[pj^i, T_,j^i] e_^(1,0)(pj^i, T_,j^i) , e_[pj^i, T_,j^i] ρ_^(1,0)(pj^i, T_,j^i) } ] /.
     tracFlux2 /. tracFlux3 ] , xvoll e_[p_^i, T_,j^i] ρ_^(1,0)(pj^i, T_,j^i) ] +
   Collect[ Expand[ Simplify[ LE1[[{6, 7}]] ] /. tracFlux2 ] ,
    { δ[_] , ρ_^(0,1)(pj^i, T_,j^i) } , Simplify] + FullSimplify[ LE1[[{ 8, 9}]] ] /.
  tracFlux2 /. tracDp /. tracFlux2 /. tracFlux3 /. tracFlux3 ;

ME2 = Collect[ GE2 + LE2, δ[_], FullSimplify] ;

In[320]:= GasMass =
    Drop[GM2, 3] == - Collect[Take[ GM2, 3], xvolv ] /. GM2[[2, 2]] -> αj^i ρg[pj^i, Tg,j^i] ;
  LiquidMass = Drop[LM2, 3] == -Collect[ Take[ LM2, 3] , xvoll ] /.
     LM2[[2, 2]] -> (1 - αj^i) ρl[pj^i, Tl,j^i] ;
  GasEnergy = Drop[GE2, 4] == -Collect[ Take[ GE2, 4] , xvolv] /.
     GE2[[3, 2]] -> αj^i ρg[pj^i, Tg,j^i] eg[pj^i, Tg,j^i] ;
  MixtureEnergy = Drop[ME2, 5] == -Collect[ Take[ ME2, 5] , {xvolv, xvoll} , Simplify] /.
     { ME2[[5, 2, 1]] -> (1 - αj^i) ρl[pj^i, Tl,j^i] el[pj^i, Tl,j^i] , ME2[[10, 2, 2, 3]] ->
       (1 - αj^i) ρl[pj^i, Tl,j^i] el[pj^i, Tl,j^i] , GE2[[3, 2]] -> (1 - αj^i) ρl[pj^i, Tl,j^i] el[pj^i, Tl,j^i] } ;

Two fluid matrix equations as implemented into TRAC

In[303]:= GasMass

Out[303]= darvp δ(pj) + darva δ(αj) + darvt δ(Tg,j) +
    dvdp_(g,j+1/2) δ(pj+1 - pj) (faArv_(j+1/2) + γ faWvM_(j+1/2) (αj^i ρg[pj^i, Tg,j^i] - (⟨α ρg⟩)j^n)) +
    dvdp_(g,j-1/2) δ(pj-1 - pj) (faArv_(j-1/2) + γ faWvP_(j-1/2) (αj^i ρg[pj^i, Tg,j^i] - (⟨α ρg⟩)j^n)) ==
   Δt fluxSum(1) - xvolv (αj^i ρg[pj^i, Tg,j^i] - (⟨α ρg⟩)j^n)
```

In[304]:= **LiquidMass**

Out[304]=
$$\begin{aligned}&\mathbf{darlp}\,\delta(p_j) + \mathbf{darla}\,\delta(\alpha_j) + \mathbf{darlt}\,\delta(T_{1,j}) + \\ &\quad \mathbf{dvdp}_{1,j+\frac{1}{2}}\,\delta(p_{j+1}-p_j)\left(\mathbf{faArl}_{j+\frac{1}{2}} + \gamma\,\mathbf{faWlM}_{j+\frac{1}{2}}\,((1-\alpha_j^i)\,\rho_1[p_j^i,\,T_{1,j}^i] - (\langle -(\alpha-1)\,\rho_1\rangle)_j^n)\right) + \\ &\quad \mathbf{dvdp}_{1,j-\frac{1}{2}}\,\delta(p_{j-1}-p_j)\left(\mathbf{faArl}_{j-\frac{1}{2}} + \gamma\,\mathbf{faWlP}_{j-\frac{1}{2}}\,((1-\alpha_j^i)\,\rho_1[p_j^i,\,T_{1,j}^i] - (\langle -(\alpha-1)\,\rho_1\rangle)_j^n)\right) == \\ &\Delta t\,\mathbf{fluxSum}(2) - \mathbf{xvoll}\,((1-\alpha_j^i)\,\rho_1[p_j^i,\,T_{1,j}^i] - (\langle -(\alpha-1)\,\rho_1\rangle)_j^n)\end{aligned}$$

In[305]:= **GasEnergy**

Out[305]=
$$\begin{aligned}&\delta(\alpha_j)\,(\mathbf{vol}_j\,p_j^i + \mathbf{darva}\,e_g[p_j^i,\,T_{g,j}^i]) + \mathbf{dvdp}_{g,j+\frac{1}{2}}\,\delta(p_{j+1}-p_j) \\ &\quad \left(\mathbf{faVapFrac}_{j+\frac{1}{2}}\,p_j^i + \mathbf{faArev}_{j+\frac{1}{2}} + \gamma\,\mathbf{faWvM}_{j+\frac{1}{2}}\left(\alpha_j^i\,e_g[p_j^i,\,T_{g,j}^i]\,\rho_g[p_j^i,\,T_{g,j}^i] - (\langle\alpha\,e_g\,\rho_g\rangle)_j^n\right)\right) + \\ &\quad \mathbf{dvdp}_{g,j-\frac{1}{2}}\,\delta(p_{j-1}-p_j) \\ &\quad \left(\mathbf{faVapFrac}_{j-\frac{1}{2}}\,p_j^i + \mathbf{faArev}_{j-\frac{1}{2}} + \gamma\,\mathbf{faWvP}_{j-\frac{1}{2}}\left(\alpha_j^i\,e_g[p_j^i,\,T_{g,j}^i]\,\rho_g[p_j^i,\,T_{g,j}^i] - (\langle\alpha\,e_g\,\rho_g\rangle)_j^n\right)\right) + \\ &\quad \delta(T_{g,j})\,(\mathbf{darva}\,e_g^{(0,1)}(p_j^i,\,T_{g,j}^i)\,\alpha_j^i + \mathbf{darvt}\,e_g[p_j^i,\,T_{g,j}^i]) + \\ &\quad \delta(p_j)\,(\mathbf{darva}\,e_g^{(1,0)}(p_j^i,\,T_{g,j}^i)\,\alpha_j^i - \mathbf{vapVolFluxSum}\,\Delta t + \mathbf{vol}_j\,(\alpha_j^i - \alpha_j^n) + \mathbf{darvp}\,e_g[p_j^i,\,T_{g,j}^i]) == \\ &(\mathbf{vapVolFluxSum}\,\Delta t + \mathbf{vol}_j\,(\alpha_j^n - \alpha_j^i))\,p_j^i + \Delta t\,\mathbf{fluxSum}(3) - \\ &\quad \mathbf{xvolv}\left(\alpha_j^i\,e_g[p_j^i,\,T_{g,j}^i]\,\rho_g[p_j^i,\,T_{g,j}^i] - (\langle\alpha\,e_g\,\rho_g\rangle)_j^n\right)\end{aligned}$$

In[321]:=
```
MixtureEnergy
```

Out[321]=
$$\delta(\alpha_j)\ (\text{darva}\ e_g[p_j^i,\ T_{g,j}^i] + \text{darla}\ e_1[p_j^i,\ T_{1,j}^i]) +$$
$$\delta(p_{j+1} - p_j)\ \left(\text{dvdp}_{g,j+\frac{1}{2}}\ \left(\text{faVapFrac}_{j+\frac{1}{2}}\ p_j^i + \text{faArev}_{j+\frac{1}{2}} + \right.\right.$$
$$\left.\gamma\ \text{faWvM}_{j+\frac{1}{2}}\ \left((1-\alpha_j^i)\ e_1[p_j^i,\ T_{1,j}^i]\ \rho_1[p_j^i,\ T_{1,j}^i] - (\langle\alpha\ e_g\ \rho_g\rangle)_j^n\right)\right) + \text{dvdp}_{1,j+\frac{1}{2}}\ \left(\text{faLiqFrac}_{j+\frac{1}{2}}\ p_j^i + \right.$$
$$\left.\left.\text{faArel}_{j+\frac{1}{2}} + \gamma\ \text{faWlM}_{j+\frac{1}{2}}\ ((1-\alpha_j^i)\ e_1[p_j^i,\ T_{1,j}^i]\ \rho_1[p_j^i,\ T_{1,j}^i] - (\langle-(\alpha-1)\ e_1\ \rho_1\rangle)_j^n)\right)\right) +$$
$$\delta(p_{j-1} - p_j)\ \left(\text{dvdp}_{g,j-\frac{1}{2}}\ \left(\text{faVapFrac}_{j-\frac{1}{2}}\ p_j^i + \text{faArev}_{j-\frac{1}{2}} + \gamma\ \text{faWvP}_{j-\frac{1}{2}}\right.\right.$$
$$\left.\left((1-\alpha_j^i)\ e_1[p_j^i,\ T_{1,j}^i]\ \rho_1[p_j^i,\ T_{1,j}^i] - (\langle\alpha\ e_g\ \rho_g\rangle)_j^n\right)\right) + \text{dvdp}_{1,j-\frac{1}{2}}\ \left(\text{faLiqFrac}_{j-\frac{1}{2}}\ p_j^i + \right.$$
$$\left.\left.\text{faArel}_{j-\frac{1}{2}} + \gamma\ \text{faWlP}_{j-\frac{1}{2}}\ ((1-\alpha_j^i)\ e_1[p_j^i,\ T_{1,j}^i]\ \rho_1[p_j^i,\ T_{1,j}^i] - (\langle-(\alpha-1)\ e_1\ \rho_1\rangle)_j^n)\right)\right) +$$
$$\delta(T_{g,j})\ (\text{darva}\ e_g^{(0,1)}(p_j^i,\ T_{g,j}^i)\ \alpha_j^i + \text{darvt}\ e_g[p_j^i,\ T_{g,j}^i]) +$$
$$\delta(T_{1,j})$$
$$\left(\text{darlt}\ e_1[p_j^i,\ T_{1,j}^i] - \text{xvoll}\ (1-\alpha_j^i)\ e_1[p_j^i,\ T_{1,j}^i]\ \rho_1[p_j^i,\ T_{1,j}^i]\ e_1^{(0,1)}(p_j^i,\ T_{1,j}^i)\right) +$$
$$\delta(p_j)\ \left(\text{darva}\ e_g^{(1,0)}(p_j^i,\ T_{g,j}^i)\ \alpha_j^i - (\text{liqVolFluxSum} + \text{vapVolFluxSum})\ \Delta\text{t} + \text{darvp}\ e_g[p_j^i,\ T_{g,j}^i] + \right.$$
$$\left.\text{darlp}\ e_1[p_j^i,\ T_{1,j}^i] - \text{xvoll}\ (1-\alpha_j^i)\ e_1[p_j^i,\ T_{1,j}^i]\ \rho_1[p_j^i,\ T_{1,j}^i]\ e_1^{(1,0)}(p_j^i,\ T_{1,j}^i)\right) ==$$
$$(\text{liqVolFluxSum} + \text{vapVolFluxSum})\ \Delta\text{t}\ p_j^i + \Delta\text{t}\ (\text{fluxSum}(3) + \text{fluxSum}(4)) -$$
$$\text{xvolv}\ \left((1-\alpha_j^i)\ e_1[p_j^i,\ T_{1,j}^i]\ \rho_1[p_j^i,\ T_{1,j}^i] - (\langle\alpha\ e_g\ \rho_g\rangle)_j^n\right) -$$
$$\text{xvoll}\ ((1-\alpha_j^i)\ e_1[p_j^i,\ T_{1,j}^i]\ \rho_1[p_j^i,\ T_{1,j}^i] - (\langle-(\alpha-1)\ e_1\ \rho_1\rangle)_j^n)$$

In[16]:=
```
<< LinearAlgebra`MatrixManipulation`;
```

In[15]:=
```
tflds = LinearEquationsToMatrices[
  {GasMass, LiquidMass, GasEnergy, MixtureEnergy}, {δ[p_j] , δ[α_j] , δ[T_g,j] , δ[T_1,j] } ] ;
```

APPENDIX B

A Program for Solving an Oscillating Manometer

The following Fortran program computes the position of the water level and the pressures inside the manometer arms based on Equations (2-6) to (2-11):

```
      PROGRAM mano

      REAL*8 Ps,L,V0,T,time,dt,rho
      REAL*8 :: pi
      REAL*8, PARAMETER :: g = 9.8066 ! m/s2
      REAL*8, DIMENSION(6) :: dx,pL,pR,dP

      H(time,T,V0) = 0.5*V0*T/pi*SIN(2.0*pi*time/T) ! meter

      pi = 4.0*ATAN(1.0)

      OPEN (UNIT=20,FILE='manoP.dat')
      OPEN (UNIT=21,FILE='manoDP.dat')
      OPEN (UNIT=22,FILE='manoL.dat')

      dt = 0.05 ! graphics timestep size in secs
      Ps = 1.0010e+05 ! surface pressure in pascal
      L = 10.0 ! length of the oscillating water slug in meters
      V0 = 2.1 ! initial velocity of the water slug in m/s
      rho = 988.8 ! density of the liquid water in kg/m3

      dx=(/0.5,1.5,2.5,3.5,4.5,5.5/) ! elevations of cell centers
      p=Ps

      T = 2.0*pi*SQRT(0.5*L/g) ! period of the oscillating manometer

      time = 0.0
      DO WHILE(.TRUE.)
       time = time+dt
!
!  compute pressures
!
       DO i=1,6
        IF (dx(i).LT.L/2.0+H(time,T,V0)) THEN
!                       left manometer arm
```

```
      pL(i) = Ps+(L/2.0+H(time,T,V0)-dx(i))            &
   &   *(1.0-2.0*H(time,T,V0)/L)*rho*g
     ELSE
      pL(i) = Ps ! water level is below this elev
     ENDIF
     IF (dx(i).LT.L/2.0-H(time,T,V0)) THEN
!                     right manometer arm
      pR(i) = Ps+(L/2.0-H(time,T,V0)-dx(i))            &
   &   *(1.0+2.0*H(time,T,V0)/L)*rho*g
     ELSE
      pR(i) = Ps ! water level is below this elev
     ENDIF
     dP(i) = pL(i)-pR(i)  ! the net force acting on the fluid
    ENDDO
!
    IF (time.GT.50.0) EXIT
    WRITE (20,99) time, (pL(i),i=1,6)
    WRITE (21,99) time, (dP(i),i=1,6)
    WRITE (22,99) time, 5.0+H(time,T,V0)
  99  FORMAT(1x,1p,7e12.4)
   ENDDO

   STOP
   END PROGRAM mano
```

APPENDIX C

Level Tracking Logic For Reversed and Normal Void Fraction Profiles

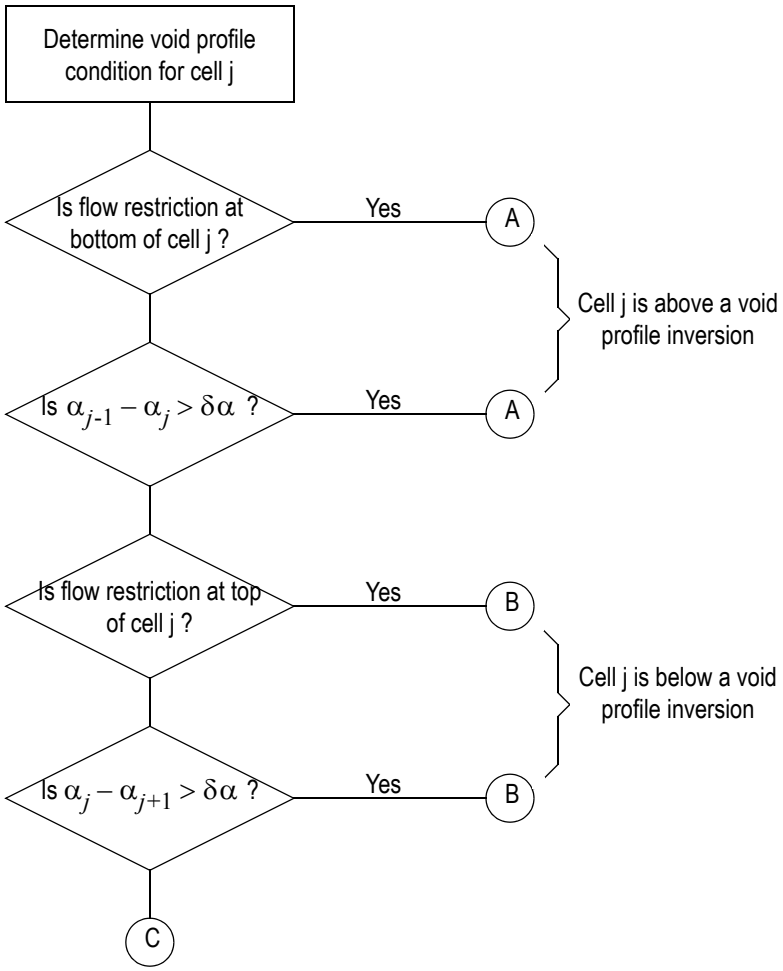

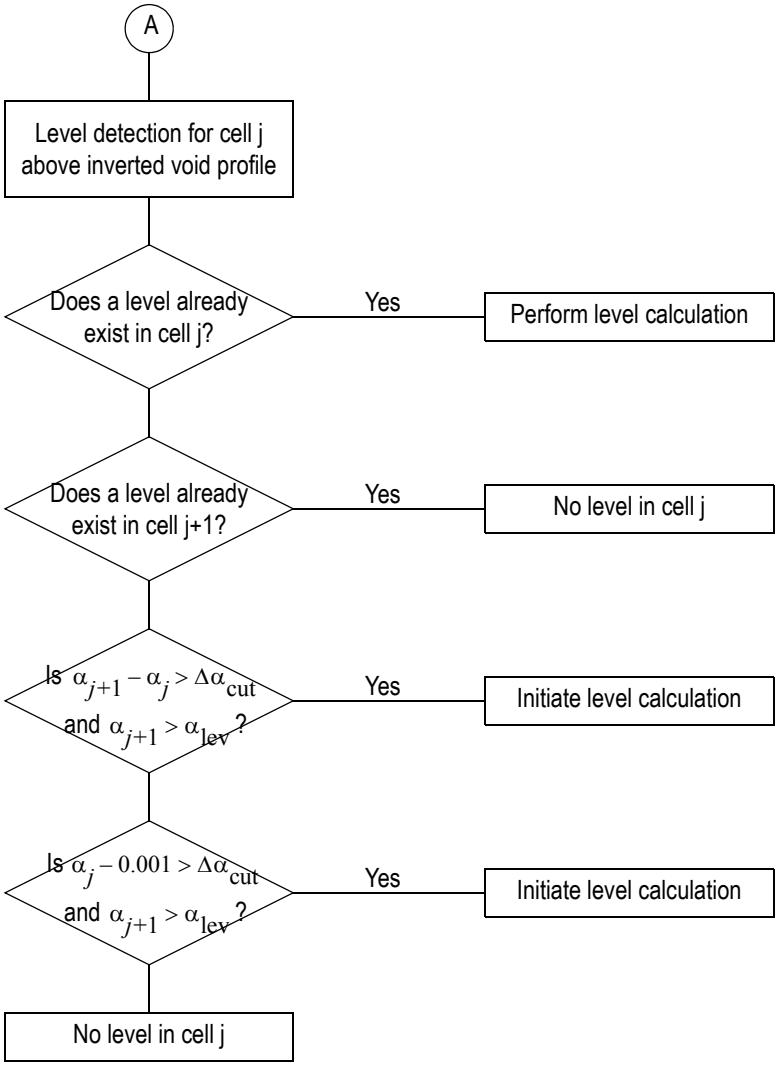
A
Level detection for cell j above inverted void profile
Does a level already exist in cell j?
Yes
Perform level calculation
Does a level already exist in cell j+1?
Yes
No level in cell j
Is $\alpha_{j+1} - \alpha_j > \Delta\alpha_{cut}$ and $\alpha_{j+1} > \alpha_{lev}$?
Yes
Initiate level calculation
Is $\alpha_j - 0.001 > \Delta\alpha_{cut}$ and $\alpha_{j+1} > \alpha_{lev}$?
Yes
Initiate level calculation
No level in cell j

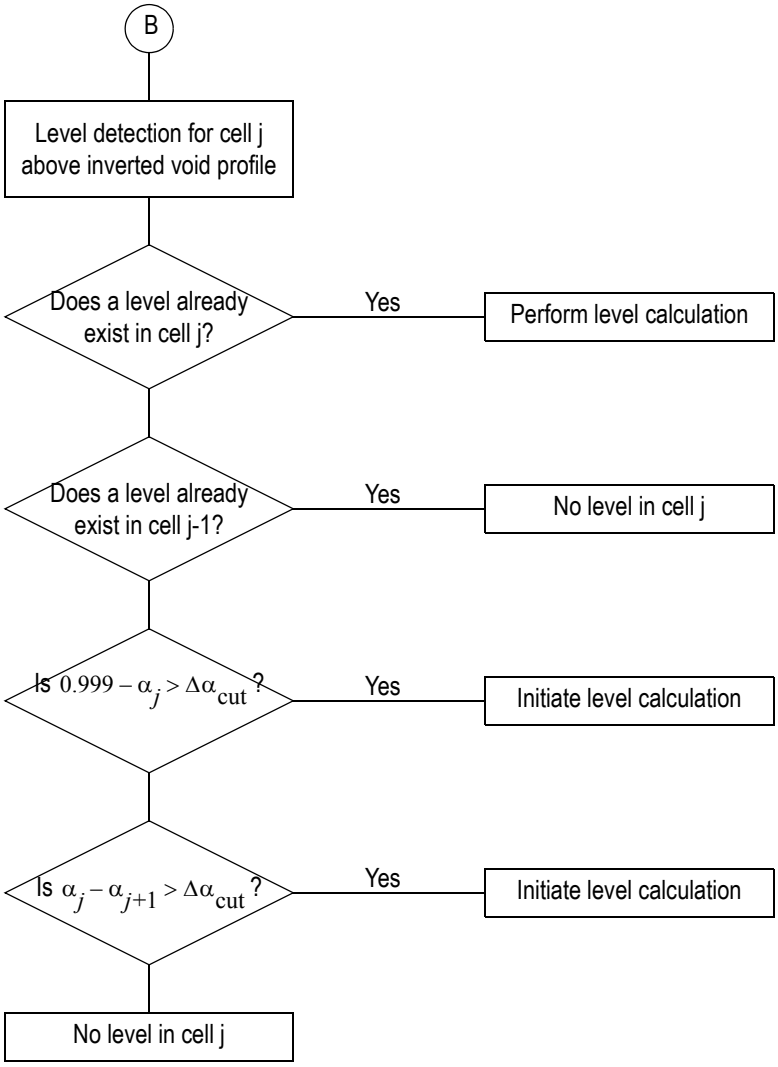
B
Level detection for cell j above inverted void profile
Does a level already exist in cell j?
Yes
Perform level calculation
Does a level already exist in cell j-1?
Yes
No level in cell j
Is $0.999 - \alpha_j > \Delta\alpha_{cut}$?
Yes
Initiate level calculation
Is $\alpha_j - \alpha_{j+1} > \Delta\alpha_{cut}$?
Yes
Initiate level calculation
No level in cell j

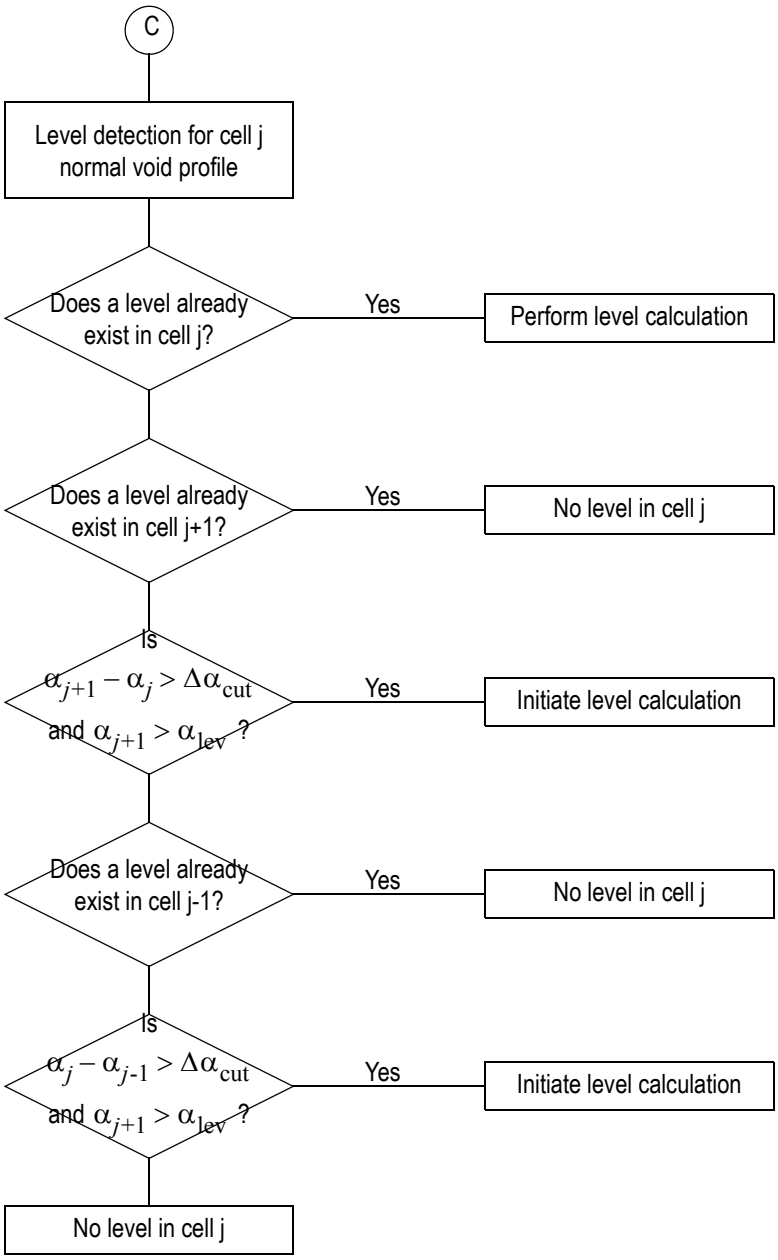
C
Level detection for cell j
normal void profile
Does a level already exist in cell j?
Yes
Perform level calculation
Does a level already exist in cell j+1?
Yes
No level in cell j
Is $\alpha_{j+1} - \alpha_j > \Delta\alpha_{cut}$ and $\alpha_{j+1} > \alpha_{lev}$?
Yes
Initiate level calculation
Does a level already exist in cell j-1?
Yes
No level in cell j
Is $\alpha_j - \alpha_{j-1} > \Delta\alpha_{cut}$ and $\alpha_{j+1} > \alpha_{lev}$?
Yes
Initiate level calculation
No level in cell j

VITA

Birol Aktas graduated in 1990 with a B.S. degree in Nuclear Engineering from Hacettepe University in Ankara, Turkey. He stayed another year at the same department as a research assistant working in a Nuclear Physics Laboratory equipped with a 400 KeV Tandem Van DeGraff particle accelerator. His duties included preparing experiments such as beta spectroscopy, slow/fast neutron coincidence experiments. He began his graduate studies at the Pennsylvania State University in the Fall of 1991. He has held both research and teaching assistantship positions within the Department of Nuclear Engineering at Penn State. Three years later, he earned a M.S. degree in Nuclear Engineering. After completing the course requirements for a Ph.D. degree, he joined Scientech (now Information Systems Laboratories, Inc), an engineering consulting company in Rockville, Maryland in 1996. He has worked on government research projects which included the development of a next generation reactor safety analysis code for the U.S. Nuclear Regulatory Commission. His current research interests are in the area of computational fluid mechanics and heat transfer with an emphasis on finite volume methods and their application to the transient analysis of nuclear reactors.